VOL.107 NO.ST4. APRIL 1981

JOURNAL OF THE STRUCTURAL DIVISION

PROCEEDINGS OF
THE AMERICAN SOCIETY
OF CIVIL ENGINEERS

VOL.107 NO.ST4. APRIL 1981

JOURNAL OF THE STRUCTURAL DIVISION

PROCEEDINGS OF THE AMERICAN SOCIETY OF CIVIL ENGINEERS

Copyright© 1981 by
American Society
of Civil Engineers
All Rights Reserved
ISSN 0044-8001

AMERICAN SOCIETY OF CIVIL ENGINEERS

BOARD OF DIRECTION

President
Irvan F. Mendenhall

Past President
Joseph S. Ward

President Elect
James R. Sims

Vice Presidents
Robert D. Bay
Francis J. Connell
Lyman R. Gillis
Albert A. Grant

Directors
Martin G. Abegg
Floyd A. Bishop
L. Gary Byrd
Larry J. Feeser
John A. Focht, Jr.
Sergio Gonzalez-Karg
James E. Humphrey, Jr.
Richard W. Karn
Leon D. Luck
Arthur R. McDaniel
Paul R. Munger
William R. Neuman
Leonard S. Oberman
John D. Parkhurst
Celestino R. Pennoni
Robert B. Rhode
S. Russell Stearns
William H. Taylor
Stafford E. Thornton
Robert E. Whiteside
Richard S. Woodruff

EXECUTIVE OFFICERS

Eugene Zwoyer, *Executive Director*
Julie E. Gibouleau, *Assistant to the Executive Director*
Louis L. Meier, *Washington Counsel/Assistant Secretary*
William H. Wisely, *Executive Director Emeritus*
Michael N. Salgo, *Treasurer*
Elmer B. Isaak, *Assistant Treasurer*

STAFF DIRECTORS

Donald A. Buzzell, *Managing Director for Education and Professional Affairs*
Robert A. Crist, Jr., *Managing Director for Publications and Technical Affairs*
Alexander Korwek, *Managing Director for Finance and Administrative Services*
Alexandra Bellow, *Director, Human Resources*
David Dresia, *Director, Publications Production and Marketing*
Barker D. Herr, *Director, Membership*
Richard A. Jeffers, *Controller*
Carl E. Nelson, *Director, Field Services*
Don P. Reynolds, *Director, Policy, Planning and Public Affairs*
Bruce Rickerson, *Director, Legislative Services*
James M. Shea, *Director, Public Communications*
Albert W. Turchick, *Director, Technical Services*
George K. Wadlin, *Director, Education Services*
R. Lawrence Whipple, *Director, Engineering Management Services*

COMMITTEE ON PUBLICATIONS

Stafford E. Thornton, *Chairman*
Martin G. Abegg
John A. Focht, Jr.
Richard W. Karn
Paul R. Munger
William R. Neuman

STRUCTURAL DIVISION

Executive Committee
John E. Bower, *Chairman*
Ronald G. Domer, *Vice Chairman*
Peter B. Cooper
Donald McDonald, *Secretary*
Frederick H. Sterbenz, *Management Group B Contact Member*
Joseph H. Appleton, *Management Group B Contact Member*
Roland L. Sharpe

Publications Committee
John E. Bower, ***Chairman and Exec. Comm. Contact Member***
Mihran S. Agbabian
Marvin E. Criswell
John T. DeWolf
Douglas Foutch
Ovadia E. Lev
Le-Wu Lu
Bruce E. Lyons
Walter Podolny
Emil Simiu
C. K. Wang
James T. P. Yao

PUBLICATIONS SERVICES DEPARTMENT

David Dresia, *Director, Publications Production and Marketing*

Technical and Professional Publications

Richard R. Torrens, *Manager*
Joseph P. Cerami, *Chief Copy Editor*
Linda Ellington, *Copy Editor*
Thea C. Feldman, *Copy Editor*
Meryl Mandle, *Copy Editor*
Joshua R. Spieler, *Copy Editor*
Shiela Menaker, *Production Co-ordinator*
Richard C. Scheblein, *Draftsman*

Information Services

Elan Garonzik, *Editor*

PERMISSION TO PHOTOCOPY JOURNAL PAPERS

Permission to photocopy for personal or internal reference beyond the limits in Sections 107 and 108 of the U.S. Copyright Law is granted by the American Society of Civil Engineers for libraries and other users registered with the Copyright Clearance Center, 21 Congress Street, Salem, Mass. 01970, provided the appropriate fee is paid to the CCC for all articles bearing the CCC code. Requests for special permission or bulk copying should be addressed to the Manager of Technical and Professional Publications, American Society of Civil Engineers.

CONTENTS

Nonlinear Finite Element Analysis of Pull-Out Test
by Niels Saabye Ottosen 591

Elastic-Plastic Large Displacement Analysis of Pipes
by A. F. Saleeb and W. F. Chen 605

Intermediate Stiffeners for Thin-Walled Members
by Thomas P. Desmond, Teoman Peköz, and George Winter 627

Proposed Steel Column Strength Criteria
by Dann H. Hall 649

Potentialities of Egyptian Gypsum for Housing
by Mahmoud A. Reda Youssef and Albert G. H. Dietz 671

Lateral-Torsional Buckling of Tapered I-Beams
by Thomas G. Brown 689

This Journal is published monthly by the American Society of Civil Engineers. Publications office is at 345 East 47th Street, New York, N.Y. 10017. Address all ASCE correspondence to the Editorial and General Offices at 345 East 47th Street, New York, N.Y. 10017. Allow six weeks for change of address to become effective. Subscription price to members is $22.50. Nonmember subscriptions available; prices obtainable on request. Second-class postage paid at New York, N.Y. and at additional mailing offices. ST.

The Society is not responsible for any statement made or opinion expressed in its publications.

TECHNICAL NOTES

Proc. Paper 16155

Wind-Excited Response of Buildings in Higher Modes
by Ahsan Kareem 701

DISCUSSION

Proc. Paper 16152

Limit Design of Extended End-Plate Connections, by Allan P. Mann and Linden J. Morris (Mar., 1979. Prior Discussion: Feb., 1980).
closure 709

Dome Effect in RC Slabs: Rigid-Plastic Analysis,* by Mikael W. Braestrup (June, 1980).
by Paul Regan 714

Dynamic Reduction of Structural Models,* by Charles A. Miller (Oct., 1980).
by Phillip L. Gould 716

Weibull Distributions and Extreme Wind Speeds, by Emil Simiu and James J. Filliben (Dec., 1980).
errata 716

INFORMATION RETRIEVAL

The key words, abstract, and reference "cards" for each article in this Journal represent part of the ASCE participation in the EJC information retrieval plan. The retrieval data are placed herein so that each can be cut out, placed on a 3 × 5 card and given an accession number for the user's file. The accession number is then entered on key word cards so that the user can subsequently match key words to choose the articles he wishes. Details of this program were given in an August, 1962 article in CIVIL ENGINEERING, reprints of which are available on request to ASCE headquarters.

*Discussion period closed for this paper. Any other discussion received during this discussion period will be published in subsequent Journals.

16197 ANALYSIS OF PULL-OUT TEST

KEY WORDS: Biaxial stresses; **Compression tests;** Compressive strength; **Concretes;** Cracking; **Failure (mechanics); Finite element method; Materials tests;** Mathematical models; Matrix methods; Mechanical properties; **Pull-out tests; Softening;** Strain hardening; **Strength; Stresses; Structural analysis;** Triaxial stresses

ABSTRACT: A specific pull-out test used to determine in-situ concrete compressive strength is analyzed. This test consists of a steel disc that is extracted from the structure. The finite element analysis considers cracking as well as strain hardening and softening in the pre- and post-failure region, respectively. The aim is to attain a clear insight into structural behavior. Special attention is given to the failure mode. Severe cracking occurs and the stress distribution is very inhomogeneous. However, large compressive forces run from the disc in a rather narrow band towards the support and this constitutes the load-carrying mechanism. The failure is caused by the crushing of the concrete in this region, and not by cracking.

REFERENCE: Ottosen, Niels Saabye, "Nonlinear Finite Element Analysis of Pull-Out Test," *Journal of the Structural Division,* ASCE, Vol. 107, No. ST4, **Proc. Paper 16197**, April, 1981, pp. 591-603

16199 LARGE DISPLACEMENT ANALYSIS OF PIPES

KEY WORDS: **Computer models;** Displacements; **Elastic-plastic analysis; Finite element method;** Friction; **Offshore structures; Pipes; Stiffness;** Strains; Stresses; **Tubes**

ABSTRACT: A numerical procedure based on the finite segment method has been presented and applied to large displacement analysis of pipe bending problems frequently encountered in offshore structural engineering applications. In this method, the pipe is treated as an assemblage of segments and the moment-curvature relation of the tubular cross section is approximated by simple mathematical expressions. Material and geometrical nonlinearities are treated using a modified incremental tangent stiffness approach. A number of numerical check problems are solved and compared with available "exact" solutions. Finally, the method is applied to an offshore pipe bending problem.

REFERENCE: Saleeb, A. F., and Chen, W. F., "Elastic-Plastic Large Displacement Analysis of Pipes," *Journal of the Structural Division,* ASCE, Vol. 107, No. ST4, **Proc. Paper 16199**, April, 1981, pp. 605-626

16194 INTERMEDIATE STIFFENERS FOR THIN-WALLED MEMBERS

KEY WORDS: Beams; Cold-rolled steel; Columns; Critical point; **Plates (structural members);** Rigidity; **Stability; Stiffeners;** Stiffness; **Strength of materials;** Thin-wall structures; **Ultimate strength**

ABSTRACT: An effective width approach is presented for predicting ultimate strengths of thin-walled compression elements with intermediate stiffeners. The study is limited to intermediately stiffened assemblies in which the stiffener is located in the center of the stiffened plate and is of relatively small width compared to the plate. In conjunction with procedures for predicting ultimate strength, a requirement for adequate stiffener rigidity is given. Stiffener adequacy is assessed as that rigidity for which the ultimate strength of each component plate element, one on either side of the stiffener, equals that of an element of similar dimensions and material properties, but supported by webs at both longitudinal edges. Critical and post-critical behavior are studied analytically and experimentally; however, the stiffener requirement is developed based primarily on the experimental results. Simple formulations for assessing the performance of the stiffener and plate elements are presented.

REFERENCE: Desmond, Thomas P., Pekoz, Teoman, and Winter, George, "Intermediate Stiffeners for Thin-Walled Members," *Journal of the Structural Division,* ASCE, Vol. 107, No. ST4, **Proc. Paper 16194**, April, 1981, pp. 627-648

16198 PROPOSED STEEL COLUMN STRENGTH CRITERIA

KEY WORDS: **Columns (supports); Elasticity;** Equations; Load factors; **Plasticity;** Regression analysis; **Steel; Strength;** Strength of materials; **Structural design**

ABSTRACT: The development of proposed design criteria is presented for pinned end columns for the load and resistance factor design provisions being developed for the American Institute of Steel Construction (AISC). Available test data have been examined by regression analysis to determine a practical column strength equation for design. The study resulted in the division of slenderness into three regions: a plastic region where slenderness does not effect column strength; an inelastic region where strength decreases linearly with increasing slenderness; and an elastic region where strength is defined by a hyperbola. Equations representing column strength in each of these regions are developed, and a resistance factor to be used with these equations is derived.

REFERENCE: Hall, Dann H., "Proposed Steel Column Strength Criteria," *Journal of the Structural Division,* ASCE, Vol. 107, No. ST4, **Proc. Paper 16198**, April, 1981, pp. 649-670

16205 EGYPTIAN GYPSUM FOR HOUSING

KEY WORDS: Composition; **Construction materials;** Density; **Egypt; Gypsum; Gypsum cements; Houses;** Retarders; Strength

ABSTRACT: Gypsum is one of the indigenous materials for housing being studied by Cairo University and the Massachusetts Institute of Technology under the Technology Adaptation Program. This program is supported by the Agency for International Development of the United States Department of State. Newly-found large deposits make gypsum attractive. Strength, density, retarders, optimum composition, and additives such as sawdust and foaming agents are examined. Solid and cored gypsum block, and the strength characteristics of walls made of such units, are compared with traditional red brick and sand-lime brick.

REFERENCE: Reda Youssef, Mahmoud A., and Dietz, Albert G.H., "Potentialities of Egyptian Gypsum for Housing," *Journal of the Structural Division,* ASCE, Vol. 107, No. ST4, **Proc. Paper 16205**, April, 1981, pp. 671-688

16211 LATERAL-TORSIONAL BUCKLING OF TAPERED I-BEAMS

KEY WORDS: **Buckling;** Computation; Energy methods; Finite difference theory; **I beams; Matrices (mathematics); Stability; Stability analysis**

ABSTRACT: The lateral-torsional buckling behavior of non-prismatic beams is not yet fully documented. Using the total change in potential energy during buckling, a fourth-order differential equation in the angle of twist, B, is obtained, in which the location of the transverse load with respect to the centroid is considered. Using central finite differences, this equation is transformed to a characteristic matrix eigenvalue equation. Solutions for a number of conventional tapered-beam problems are presented.

REFERENCE: Brown, Thomas G., "Lateral-Torsional Buckling of Tapered I-Beams," *Journal of the Structural Division,* ASCE, Vol. 107, No. ST4, **Proc. Paper 16211**, April, 1981, pp. 689-697

JOURNAL OF THE STRUCTURAL DIVISION

NONLINEAR FINITE ELEMENT ANALYSIS OF PULL-OUT TEST

By Niels Saabye Ottosen[1]

INTRODUCTION

A considerable interest is directed towards determining in-situ concrete properties, and various destructive as well as nondestructive methods are currently applied. Knowledge of the in-situ concrete compressive strength is of particular importance and pull-out tests have been proposed quite early for this purpose (14,15). Newer investigations within this field have been reported, e.g., by Malhotra (9), Clifton (1), and Mailhot, et al. (8). The importance of those pull-out tests, in which a circular steel disc is extracted from the structure using a cylindrical counter pressure, has manifested itself as a tentative standard, i.e., *ASTM-C900-78T*.

The present paper is devoted to nonlinear finite element analysis of such a pull-out test, namely the so-called Lok-Test proposed by Kierkegaard-Hansen (5). The aim of the analysis is to attain a clear insight into the structural behavior. The AXIPLANE program (13) is used for this purpose. In addition to the cracking of the concrete, this program considers the strain hardening and softening in the pre- and post-failure regions, respectively. The influence on the structural behavior of the uniaxial compressive strength, the ratio of tensile to compressive strength, different failure criteria, and post-failure behaviors are investigated. Moreover, because much dispute has been placed on the type of failure actually occurring in the concrete, special attention is given to the structural behavior and the failure mode. Finally, the predictions are compared with published experimental and theoretical results.

[1]Research Engr., Risø National Lab., Engrg. Dept., Postbox 49, DK-4000, Roskilde, Denmark.

Note.—Discussion open until September 1, 1981. To extend the closing date one month, a written request must be filed with the Manager of Technical and Professional Publications, ASCE. Manuscript was submitted for review for possible publication on April 3, 1980. This paper is part of the Journal of the Structural Division, Proceedings of the American Society of Civil Engineers, ©ASCE, Vol. 107, No. ST4, April, 1981. ISSN 0044-8001/81/0004-0591/$01.00.

The finite element program AXIPLANE described by the writer (13), and applicable for axisymmetric and plane structures, is applied. Only axisymmetric triangular elements with linear displacement functions are utilized in the present analysis.

In the numerical performance, the total load is considered, even though it is increased stepwise. However, for each load level, iterations are carried out until the constitutive equations for the concrete are in accordance with the total loading in question. To consider the effect of stress redistribution, small load increments, around 2%–4% of the ultimate load, are employed. The failure load is determined as that load in which a large number of iterations—i.e., 25—is insufficient to satisfy both the constitutive equations and the static equilibrium.

The constitution model of the concrete is quite simple to work with and is based on nonlinear elasticity, where the secant values of Young's modulus and Poisson's ratio are changed appropriately (11). This alternation is obtained through use of a nonlinearity index that relates the actual stress state to the failure surface.

Let σ_1, σ_2, and σ_3 denote the principal stresses, and let $\sigma_1 \geq \sigma_2 \geq \sigma_3$, in which tensile stress is considered positive; then if only compressive stresses are present, the nonlinearity index, β, is defined as

$$\beta = \frac{\sigma_3}{\sigma_{3f}} \quad \ldots \ldots \ldots \ldots \ldots \ldots \ldots \ldots \ldots \ldots \ldots \ldots \ldots \ldots \ldots \ldots \ldots \ldots \ldots \ldots \ldots \ldots \quad (1)$$

in which σ_3 = the actual, most compressive principal stress; and σ_{3f} = the corresponding failure value, provided that the other principal stresses, σ_1 and σ_2, are unchanged. Thus, $0 \leq \beta < 1$, $\beta = 1$, and $\beta > 1$ correspond to stress states located inside, on, and outside the failure surface, respectively. The nonlinearity index, given by Eq. 1, is proportional to the stress for uniaxial compressive loading, and it can therefore be considered an effective stress. When tensile stresses are present, we transform the actual stress state (σ_1, σ_2, σ_3), in which at least σ_1 = a tensile stress, by superposing the hydrostatic pressure, $-\sigma_1$, and obtaining the new stress state (σ_1', σ_2', σ_3') = (0, $\sigma_2 - \sigma_1$, $\sigma_3 - \sigma_1$), i.e., a biaxial compressive stress state. We then define β as

$$\beta = \frac{\sigma_3'}{\sigma_{3f}'} \quad \ldots \ldots \ldots \ldots \ldots \ldots \ldots \ldots \ldots \ldots \ldots \ldots \ldots \ldots \ldots \ldots \ldots \ldots \ldots \ldots \ldots \ldots \quad (2)$$

in which σ_{3f}' = the failure value of σ_3', provided that σ_1' and σ_2' are unchanged, i.e., the stress state (σ_1', σ_2', σ_{3f}') is to satisfy the failure criterion. When tensile stresses occur, the nonlinearity index as defined by Eq. 2 is less than unity even at failure.

In Eqs. 1 and 2, a failure criterion is involved and in the AXIPLANE program two options exist: (1) The simple and well-known modified Coulomb criterion proposed by Cowan (2); this criterion combines the Coulomb criterion—here with a friction angle equal to 37°—and a maximum tensile stress criterion; and (2) the more accurate, but also more complicated criterion proposed by the writer (10). This latter criterion contains all three stress components and

corresponds to a smooth, convex surface. A comparison of these two criteria with experimental data has been performed by the writer in Ref. 12.

Letting the secant values of Young's modulus and Poisson's ratio depend on the nonlinearity index, the constitutive model predicts the strain hardening before failure, and the failure itself and the strain softening in the post-failure region. Smooth stress-strain curves are obtained, different post-failure behaviors can easily be dealt with, and dilatation is simulated. Any failure criterion can be utilized, and the choice of an accurate criterion by itself assures accurate stress-strain curves. All stress states, including those where there are tensile stresses can be dealt with, as shown in Ref. 11, but path independency is inherent in the model. As described in Ref. 13, the applied implementation of the model in the finite element program results in a behavior corresponding to that of a fracturing solid. This greatly improves the unloading behavior as compared to that of strict nonlinear elasticity.

The model is calibrated to a given concrete by six parameters only, which are all derived from uniaxial tests. These parameters are: the initial elastic parameters, i.e., the initial Young modulus, E_i, and the initial Poisson ratio, ν_i; the strength parameters, i.e., the uniaxial compressive strength, $\sigma_c(\sigma_c > 0)$, and the uniaxial tensile strength, $\sigma_t(\sigma_t > 0)$; the ductility parameter, i.e., the strain, $\epsilon_c(\epsilon_c > 0)$, at uniaxial compressive failure; and finally the post-failure parameter, D, that determines the degree of strain softening when the crushing of the concrete occurs.

Through the maximum tensile stress criterion, the modified Coulomb criterion contains in itself a cracking criterion given by $\sigma_1 \geq \sigma_t$. The failure criterion of the writer (10) corresponds to a smooth surface in terms of one equation, and cracking is assumed to occur if: (1) The failure condition is violated; and (2) if $\sigma_1 \geq \sigma_t/2$ holds. This cracking criterion was proposed in Ref. 11, and its close agreement with experimental data is demonstrated in Ref. 12. The crack plane is assumed to be normal to the direction of the principal stress, σ_1, at the moment of cracking. Once a crack is developed, it is assumed to remain open with a fixed direction. The standard smeared cracking approach is utilized. The shear stiffness along the crack plane is reduced to ηG, in which G = the shear modulus of the concrete; and η = the shear retention factor, $0 \leq \eta \leq 1$. This factor is subject to much dispute, because in reality it is a complicated function of crack-width, relative displacement tangential to the crack plane and the nature of the crack surface. For simplicity, however, we consider the shear retention factor to be a fixed value, and $\eta = 0.01$ is utilized. The predictions obtained in Ref. 13 suggest this value to be sufficiently accurate. A detailed examination of these matters is also given there.

Lok-Test

The configuration of the specific pull-out test considered here, the Lok-Test proposed by Kierkegaard-Hansen (5), is shown in Fig. 1. During application, a test bolt, consisting of a stem and a circular steel disc, is mounted inside the form; see Fig. 1(*a*). After curing the concrete, the form is stripped, and the stem is unscrewed. At the time of testing, a rod having a slightly smaller diameter than the stem is screwed into the disc and a cylindrical counter pressure is mounted; see Fig. 1(*b*). The rod is loaded by a pull-out force until failure,

where a small piece of concrete can be punched out if sufficient displacement of the rod is applied. As shown in Figs. 1(*b*) and 2, this piece of concrete has the form of a frustrum of a cone. The meridians are almost straight lines that connect the outer periphery of the disc with the inner periphery of the cylindrical counter pressure.

Experimental data for the Lok-Test have shown a linear relation between the force required to extract the embedded steel disc, and the uniaxial compressive strength of the concrete. A general status of the various experimental investigations has been given recently by Kierkegaard-Hansen and Bickley (6).

Results

Fig. 3 shows the analyzed structure, as well as the axisymmetric finite element mesh consisting of 441 triangular elements. The elements that represent the steel disc appear in this figure. Perfect bond between the steel and the concrete is assumed. The pull-out force, as well as the boundary conditions at the location of the cylindrical counter pressure, are also indicated.

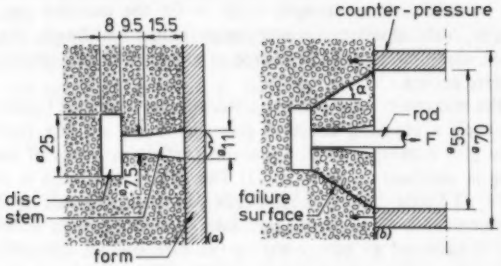

FIG. 1.—Application and Configuration of Lok-Test (All Dimensions Are in millimeters)

To begin with, some important aspects of the structural behavior of the Lok-Test will be illustrated. Special attention will be given to the failure mode. After that, the influence of some concrete material data will be investigated in detail. In the first place, the failure criterion of the writer (10) is utilized; later the effect of using the modified Coulomb criterion is evaluated.

To illustrate the structural behavior, we use concrete material data that can be considered as quite representative and realistic. For this purpose we approximate the behavior of a specific concrete tested by Kupfer (7). The constitutive model of this relatively strong concrete is calibrated by the following parameters, all in accordance with experimental data: $E_i = 3.24 \times 10^4$ MPa; $\nu_i = 0.2$; $\sigma_c = 31.8$ MPa; $\sigma_t/\sigma_c = 0.10$; $\epsilon_c = 2.17‰$; and $D = 0.2$. Using these data, the normalized stress-strain curve is shown in Fig. 4. The values $E = 2.05 \times 10^5$ MPa, and $\nu = 0.3$ were employed for the steel disc.

Let us first consider the predicted development of radial and circumferential cracks as the loading increases. This is shown in Fig. 5, where the loadings are expressed in relation to the predicted failure load. The analysis determines cracking in terms of cracked elements alone. Therefore, some arbitrariness is

necessarily involved when visualizing circumferential cracking as discrete cracks. However, cracking initiates as circumferential cracks behind the disc at 7% loading. This type of cracking appears in Fig. 5(*a*), and is caused directly by the pull-out force. At 18% loading, radial cracking initiates at the annulus near the outer concrete surface. These cracks are caused by flexure similar to the bending of plates. Such radial cracks appear in Fig. 5(*b*). With increased loading, the cracks shown there develop gradually. However, at 64% loading a considerable development of new circumferential cracks occur. As shown in Fig. 5(*c*), these new circumferential cracks extend from the outer part of the steel disc towards the support. It is of interest to note that even though the concrete is severely cracked, its carrying capacity is far from being exhausted. Therefore, it is obvious that only very little of the pull-out force is carried directly by tension in the concrete. Increased loading, in particular, causes the radial cracks to develop; the crack pattern just before predicted failure is shown in Fig. 5(*d*).

FIG. 2.—Punched-Out Piece of Concrete (Cracks Are Made Visible Using Pencil Tracing)

While the predicted circumferential cracks are supported by experimental evidence [compare Figs. 1(*b*) and 2], radial cracks have not been observed experimentally prior to the present study. However, whereas the region theoretically exposed to radial cracking is quite large, the corresponding crack widths are estimated to be quite small. If it is conservatively assumed that all tangential deformation is concentrated in only one radial crack, then just before failure this crack width is around 0.05 mm that is hardly visible. Moreover, the stresses are unloaded and crack widths reduced after failure, thereby supporting the conclusion that no radial cracks are directly visible on the punched-out piece of concrete. However, close inspection of such concrete specimens using a microscope reveals that clear radial cracking is indeed present. Such cracking is visualized on the specimen in Fig. 2 using pencil tracing.

To further illustrate the structural behavior of the Lok-Test, the stress

distribution of the three principal stresses is considered at 70% loading, i.e., the cracking is slightly more developed than indicated in Fig. 5(*c*). This stress distribution is shown in Fig. 6, in which isostress curves are shown and the directions of the principal stresses in the RZ plane are given at each nodal point. In accordance with the radial crack development, the distribution of the tangential stresses shows large regions where tension exists. Only at the support, and notably around the disc do compressive tangential stresses exist. The distribution of the maximum principal stress in the RZ plane also indicates large regions loaded in tension. Only in the vicinity of the disc, and notably at the support do small regions loaded in compression exist. The distribution of the minimum principal stress in the RZ plane is very interesting. Recalling

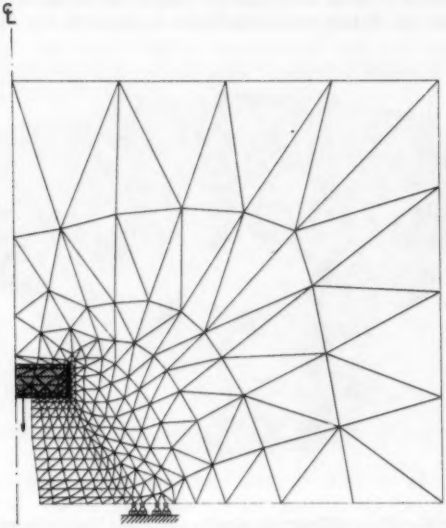

FIG. 3.—Axisymmetric Finite Element Mesh of Lok-Test

that the uniaxial compressive strength of the concrete is 31.8 MPa, and noting that the loading is 70% of the predicted failure load, it appears that large stresses are present at the annulus near the disc. In fact, triaxial compression exists here. Moreover, large compressive stresses are found at the outer periphery of the steel disc, and comparison with the preceding figures shows that biaxial compression occasionally superposed by a small tensile stress appears in this region. Noting the stress directions, it is apparent that large compressive forces run from the disc in a rather narrow band towards the support, where triaxial as well as biaxial compression exist. This carrying mechanism is supported by the crack pattern of Figs. 5(*c*) and 5(*d*). It is of interest to note that both the circumferential cracks and the stress directions describe curves that have

a slight curvature even though they are almost straight. This small curvature is also observed in practice; compare to Fig. 2.

In conclusion, Fig. 6 shows that the stress distribution is very inhomogeneous. At increasing loading, a considerable redistribution of stresses can therefore be expected. This suggests strain softening of the concrete in the post-failure region to be of importance for the failure load. Moreover, Fig. 6 shows that large compressive forces run from the disc in a rather narrow band towards the support, and this constitutes the load-carrying mechanism. The stress states in this band are primarily biaxial compression occasionally superposed by small tensile stresses.

As demonstrated previously in Ref. 13, the severity of the stress states is conveniently illustrated by means of the nonlinearity index, β, relating the actual stress state to the failure surface; compare Eqs. 1 and 2. For compressive loading, $0 \leq \beta < 1$, $\beta = 1$, and $\beta > 1$ correspond to stress states located inside, on, and outside the failure surface, respectively. Fig. 7 shows the

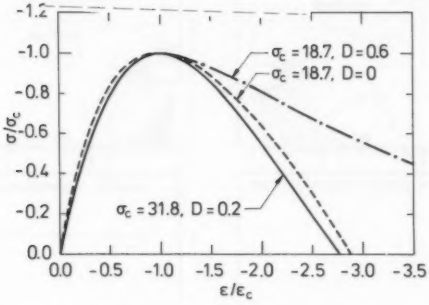

FIG. 4.—Normalized Stress-Strain Curves for Concretes Considered (Stengths Are Measured in megapascals)

development of the contour lines with increasing loading for the nonlinearity index, as a percentage. The distribution in Fig. 7(*b*) corresponds to the stress distribution given in Fig. 6. Fig. 7 supports the preceding observations that the region at the annulus adjacent to the disc is severely loaded, and this holds also for the region along the outer periphery of the disc. Moreover, the severely loaded narrow band running from the outer periphery of the disc towards the support is very apparent. It should be recalled that when tensile stresses are present, the nonlinearity index is less than unity even at failure; compare to Eq. 2. At 64% loading, strain softening initiates below the steel disc, both adjacent to the annulus and at the outer periphery of the disc. At 79% loading, strain softening develops from the outer periphery of the disc towards the support. This development is pronounced at 88% and also at 100% loading; the latter is the failure load, and the distribution given by Fig. 7(*d*) corresponds to the last iteration before the calculations were terminated. At the failure load, considerable strain softening occurs also at the disc adjacent to the annulus. This can be observed as a decrease in the nonlinearity index; compare Figs.

7(*c*) and 7(*d*). More important, however, is the strain softening occurring in the narrow region adjacent to the outer periphery of the disc, and running towards the support. This strain softening appears as a considerable drop of the nonlinearity index. This effect is very pronounced when comparing Fig. 7(*c*) with Fig. 7(*d*), but a comparison of Fig. 7(*b*) with Fig. 7(*c*) already shows this tendency. It is important to realize that this gradual decrease of the nonlinearity index due to strain softening in the post-failure region corresponds to the crushing of the concrete. Thus, even though small tensile stresses may exist in addition

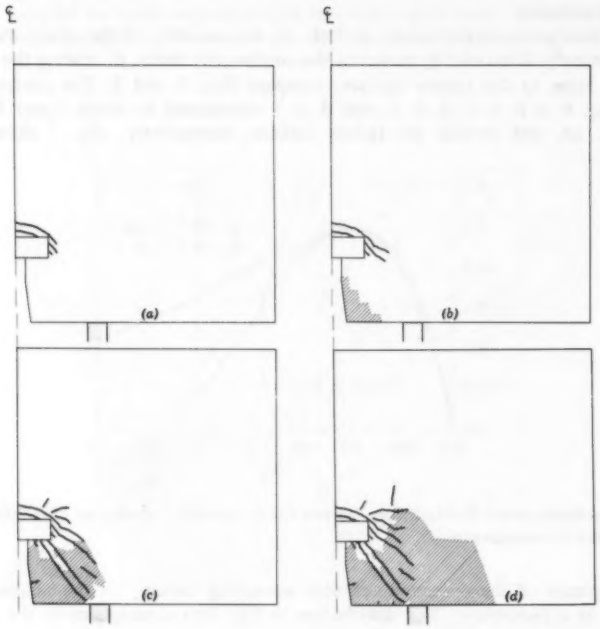

FIG. 5.—Crack Development with Increasing Loadings (Loading Is Expressed in Relation to Predicted Failure Load): (*a*) Loading = 15%; (*b*) Loading = 25%; (*c*) Loading = 64%; (*d*) Loading = 98%

to the primary biaxial compressive stress states, the failure is caused by the crushing of the concrete and not by cracking. This mechanism is in accordance with the experimentally observed ductile failure mode. Therefore, the force required to extract the embedded disc in a Lok-Test is directly dependent on the compressive strength of the concrete in question. However, the tensile strength may have some direct influence, as will be examined later on.

Let us now compare the predicted failure load with experimental data. Based on the results of different test series, including a total of 1,100 Lok-Tests, Kierkegaard-Hansen and Bickley (6) suggest the following linear relation between

pull-out force, F, and uniaxial compressive cylinder strength, σ_c: $F = 5 + 0.8\ \sigma_c$, in which F and σ_c are measured in kilonewtons and megapascals, respectively. This relation is shown in Fig. 8, and is based on concrete mixes, in which σ_c ranges from 6 MPa–53 MPa. The failure load resulting from the present calculation, in which $\sigma_c = 31.8$ MPa, is also indicated. The analysis underestimates the experimental failure load by only 1%.

To investigate the dependence of the σ_c value, a calculation was performed with data from another, weaker concrete. To ensure use of realistic concrete

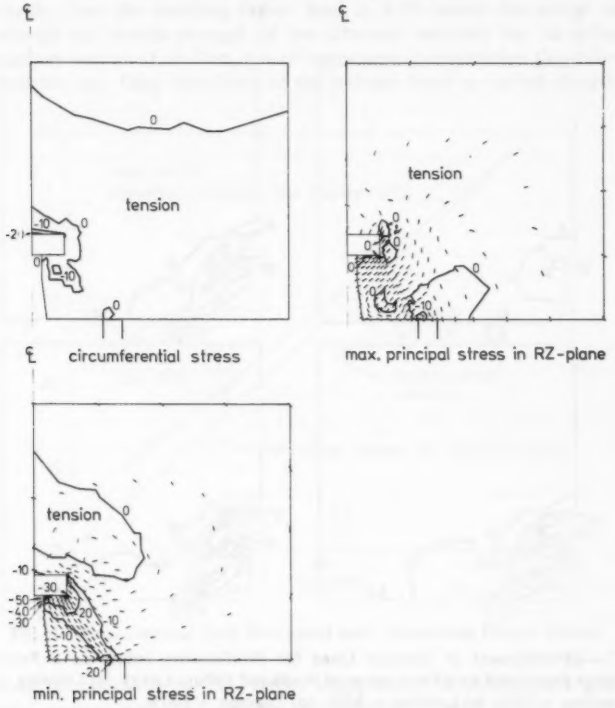

FIG. 6.—Isostress Curves and Directions of Three Principal Stresses at 70% Loading (Quantities Are in megapascals)

data, test results of Kupfer (7) were utilized again. In the constitutive model, the following parameters were applied: $E_i = 2.89 \times 10^4$ MPa; $\nu_i = 0.19$; $\sigma_c = 18.7$ MPa; $\sigma_t / \sigma_{ic} = 0.10$; $\epsilon_c = 1.87$ ‰; and $D = 0.6$. The close agreement of the resulting predictions with the experimental data of Kupfer (7) has previously been demonstrated in Ref. 11. In general, the weaker the concrete, the more ductile is its post-failure behavior; compare to, e.g., Hognestad, et al. (3). This suggests the use of $D = 0.6$ as is apparent from Fig. 4, in which the normalized

stress-strain curve from the aforementioned data is shown. The predicted failure load using these concrete parameters underestimates the actual failure load by only 3%, and is plotted in Fig. 8. Therefore, the calculations are in agreement with the experimental evidence, showing that within the considered variation of the σ_c values, a linear relation exists between pull-out force and compressive strength.

It is remarkable that the prolongation of the experimental line in Fig. 8 intersects the ordinate axis at some distance from the origin. However, two aspects of

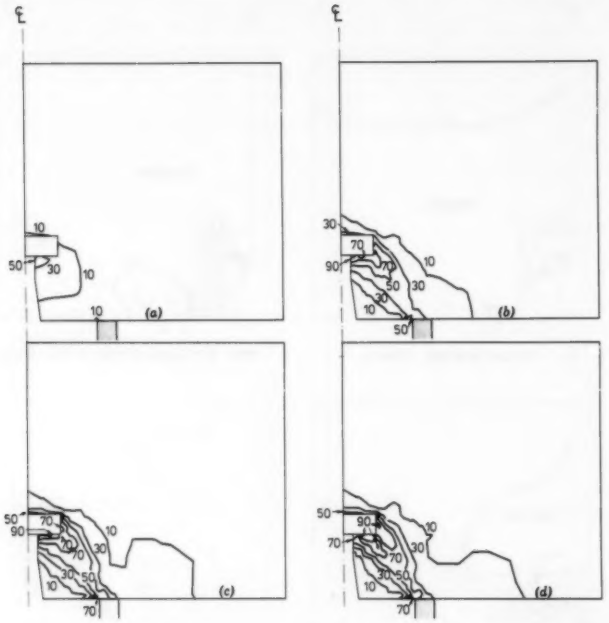

FIG. 7.—Development of Contour Lines for Nonlinearity Index, as a Percentage (Loadings Expressed as a Percentage of Predicted Failure Load): (*a*) Loading = 20%; (*b*) Loading = 70%; (*c*) Loading = 94%; (*d*) Loading = 100%

concrete behavior are dependent on compressive strength, namely the ductility and the ratio of tensile to compressive strength. As has already been touched upon, the weaker the concrete, the more ductile the post-failure behavior. To investigate the influence of minor variations in the post-failure behavior of the concrete, a calculation was performed using again the concrete having a strength of 18.7 MPa, and possessing unchanged properties except for a lesser ductility. Therefore, the value $D = 0$ was used instead of the more realistic one, $D = 0.6$; compare to Fig. 4. This in fact decreases the predicted failure load by 5%, as shown in Fig. 8. That the failure load depends on the particular

softening behavior of the concrete is indeed to be expected, considering the very inhomogeneous stress distribution.

In general, the weaker the concrete, the larger is the ratio of tensile to compressive strength; compare to, e.g., Wastiels (16). Let us investigate this effect using the concrete having $\sigma_c = 18.7$ MPa, and $D = 0.6$ again, but putting now $\sigma_t/\sigma_c = 0.12$, instead of $\sigma_t/\sigma_c = 0.10$. This increases the predicted failure load by 11%, as shown in Fig. 8. In reality, Kupfer (7) determined the σ_t/σ_c ratio to be 0.105 for the concrete considered, and if interpolation is performed between the two calculations having the σ_t/σ_c ratio equal to 0.10 and 0.12, respectively, then the resulting failure load is 0.7% below the actual value. Even though the tensile strength of the concrete certainly has an influence on the failure load of a Lok-Test, it is of importance to realize that this influence is an indirect one. Only very little of the pull-out force is carried directly by

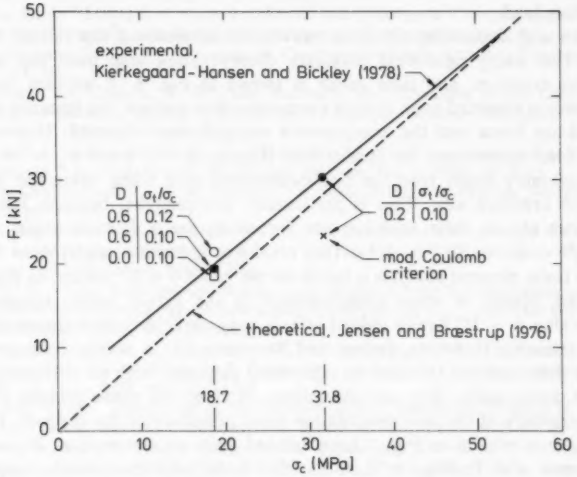

FIG. 8.—Experimental Data Compared with Theoretical Failure Values

tension in the concrete, but the regions where failure takes place are primarily in biaxial compression, occasionally superposed by small tensile stress. The failure is caused by crushing, but the existence of even a small tensile stress considerably decreases the failure strength.

The preceding analysis has demonstrated that the reason that the relation between pull-out force and compressive strength is linear and not proportional is a result of the increasing ductility and the increasing ratio of tensile to compressive strength, the weaker the concrete.

Let us now investigate the influence of different failure criteria. For this purpose we return to the concrete having $\sigma_c = 31.8$ MPa. All constitutive parameters are unchanged, but now the modified Coulomb criterion is applied. Compared to the previous analysis, this reduces the predicted failure load by

23%, as shown in Fig. 8. However, at failure, the critical regions are loaded primarily in biaxial compression, and the modified Coulomb criterion is known to underestimate the failure stresses for such stress states by 25%–30%.

It is of interest to observe that the decrease of failure load, when using the modified Coulomb criterion, is an accordance with the finding that the Lok-Test depends directly on the compressive strength of the concrete and not on its tensile strength. As demonstrated in Ref. 12, the modified Coulomb criterion, in general, underestimates the failure stresses, when concrete is loaded in compression, except when extremely large triaxial compressive stress states exist. Moreover, as shown there, this criterion, in general, overestimates the failure stresses when tensile stresses are present. Therefore, if the failure in a Lok-Test was caused by tensile cracking, then use of the modified Coulomb criterion would result in an increased failure load. However, in accordance with the preceding analysis, use of the modified Coulomb criterion decreases the failure load.

Jensen and Braæstrup (4) have previously determined the failure load for a Lok-Test using rigid-ideal plasticity theory. They also used the modified Coulomb criterion, and their result is shown in Fig. 8. It appears that close agreement is obtained even though proportionality and not just linearity between the pull-out force and the compressive strength was obtained. However, the failure load determined by Jensen and Braæstrup (4), when $\sigma_c = 31.8$ MPa, is considerably larger than the one determined here when using the modified Coulomb criterion also. This is particularly conspicuous, because Jensen and Braæstrup (4), in their analysis, are forced to use a friction angle equal to the angle α shown in Fig. 1(*b*). This results in a friction angle, $\phi = 31°$. The present finite element analysis is based on the value $\phi = 37°$ which, as previously examined, results in some underestimate of the actual failure stresses. Use of the value $\phi = 31°$ would indeed infer a considerable underestimate of actual failure stresses. However, Jensen and Braæstrup (4) in reality compensate for this, as their analysis is based on rigid-ideal plasticity with no softening effects at all. Consequently, they assume failure all along the plane running from the outer periphery of the disc towards the inner periphery of the support. Previous examinations related to Fig. 7 have refuted such an assumption. However, in accordance with findings in Ref. 13, this underlines the extreme importance of including a suitable strain softening behavior in constitutive modeling of concrete.

Conclusions

In the present paper, which takes advantage of Ref. 12, the structural behavior of a specific pull-out test, i.e., the Lok-Test, has been investigated in detail. Severe cracking occurs, and the stress distribution is very inhomogeneous. It has been shown that large compressive forces run from the disc in a rather narrow band towards the support, and this constitutes the load-carrying mechanism. Moreover, the failure in a Lok-Test is caused by the crushing the concrete and not by cracking. Therefore, the force required to extract the embedded steel disc is directly dependent on the compressive strength of the concrete in question. However, as the stress states, in which failure takes place, are primarily biaxial compressive occasionally superposed by small tensile stresses,

the tensile strength of the concrete has some indirect influence. The effect of strain softening in the post-failure region is important. In general, weak concrete compared to strong concrete has a relatively larger tensile strength and a higher ductility. This explains why the relation between the failure pull-out force and the compressive strength is linear and not proportional.

With respect to finite element modeling, it has been demonstrated that not only is use of an accurate failure criterion important, but modeling of the strain softening in the post-failure region turns out to be a mandatory prerequisite for realistic structural predictions.

APPENDIX.—REFERENCES

1. Clifton, J. R., "Nondestructive Tests to Determine Concrete Strength—A Status Report," *NBSIR 75729 (PB 246858)*, Materials and Composites Section, National Bureau of Standards, Washington, D.C., July, 1975.
2. Cowan, H. J., "Strength of Plain, Reinforced and Prestressed Concrete under Action of Combined Stresses, with Particular References to the Combined Bending and Torsion of Rectangular Sections," *Magazine of Concrete Research*, London, England, Vol. 5, No. 14, Dec., 1953, pp. 75–86.
3. Hognestad, E., Hanson, N. W., and McHenry, D., "Concrete Stress Distribution in Ultimate Strength Design," *Proceedings*, American Concrete Institute, Vol. 52, No. 4, Dec., 1955, pp. 455–479.
4. Jensen, B. C., and Bræstrup, H. W., "Lok-Tests Determine the Compressive Strength of Concrete," *Nordisk Betong*, Stockholm, Sweden, No. 2, 1976, pp. 9–11.
5. Kierkegaard-Hansen, P., "Lok-Strength," *Nordisk Betong*, Stockholm, Sweden, No. 3, 1975, pp. 19–28.
6. Kierkegaard-Hansen, P., and Bickley, J. A., "In-Situ Strength Evaluation of Concrete by the Lok-Test System," presented at the Oct. 29–Nov. 3, 1978, American Concrete Institute Fall Convention, held at Houston, Tex.
7. Kupfer, H., "Das Verhalten des Betons unter Mehrachsigen Kurzzeitbelastung unter besonderen Berücksichtigung der Zewiachsigen Beanspruchung," *Deutscher Ausschuss für Stahlbeton*, Berlin, West Germany, Vol. 229, 1973.
8. Mailhot, G., Bisaillon, A., Carette, G. G., and Malhotra, V. M., "In-Place Concrete Strength: New Pullout Methods," *Proceedings*, American Concrete Institute, Vol. 76, No. 12, Dec., 1979, pp. 1267–1282.
9. Malhotra, V. M., "Evaluation of the Pull-Out Test to Determine Strength of In-Situ Concrete," *Materials and Structures*, Vol. 8, No. 43, Jan.–Feb., 1975, pp. 19–31.
10. Ottosen, N. S., "A Failure Criterion for Concrete," *Journal of the Engineering Mechanics Division*, ASCE, Vol. 103, No. EM4, Proc. Paper 13111, Aug., 1977, pp. 527–535.
11. Ottosen, N. S., "Constitutive Model for Short-Time Loading of Concrete," *Journal of the Engineering Mechanics Division*, ASCE, Vol. 105, No. EM1, Proc. Paper 14375, Feb., 1979, pp. 127–141.
12. Ottosen, N. S., "Nonlinear Finite Element Analysis of Concrete Structures," thesis presented to the Technical University of Denmark, at Copenhagen, Denmark, in 1980, in partial fulfillment of the requirements for the degree of Doctor of Philosophy *Risø-R-411*, Risø National Laboratory, Roskilde, Denmark.
13. Ottosen, N. S., "Finite Element Analysis of Plane and Axisymmetric RC Structures," submitted for publication, Feb., 1980.
14. Skramtajew, B. G., "Determining Concrete Strength for Control of Concrete in Structures," *Proceedings*, American Concrete Institute, Vol. 34, Jan.–Feb., 1938, pp. 285–303.
15. Tremper, B., "The Measurement of Concrete Strength by Embedded Pull-Out Bars," *Proceedings*, American Society for Testing and Materials, June, 1944, pp. 880–887.
16. Wastiels, J., "Behaviour of Concrete under Multiaxial Stresses—A Review," *Cement and Concrete Research*, Vol. 9, Jan., 1979, pp. 35–44.

JOURNAL OF THE
STRUCTURAL DIVISION

ELASTIC-PLASTIC LARGE DISPLACEMENT ANALYSIS OF PIPES

By A. F. Saleeb[1] and W. F. Chen,[2] M. ASCE

INTRODUCTION

Large displacement analysis of elastic-plastic pipe bending problems is frequently encountered in many offshore structural engineering applications. One such application is the bend around of pipelines during a pull-in operation. In this case, a monotonically-increasing pulling force is applied at the tip of the pipeline in the sea, and is directed toward a fixed pull-in base point of offshore platform (located by the so-called "overlength and offset" distances, as shown in Fig. 1). The horizontal component of the pulling force (acting parallel to the original pipe position) will produce a large secondary bending moment (commonly called the P-Δ moment) in addition to the primary bending moment due to the vertical component of the pulling force (which acts perpendicular to the original pipe position). Thus, the additional P-Δ moment must be included in the analysis of the pipe bending problem.

It is obvious from the nature of the problem that the required final lateral deflection is very large (see Fig. 1). Therefore, the more exact expression for the curvature, Φ, and deflection, w, may have to be employed in the analysis of such a problem. This requires the use of the exact but nonlinear expression

$$\Phi = \frac{1}{R} = \frac{w''}{[1 + w'^2]^{3/2}} \quad \ldots \ldots \ldots

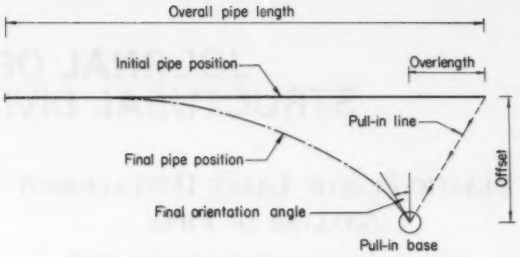

FIG. 1.—Plan View of Pipeline Being Pulled into Fixed Base and Definition of Offset and Overlength

in which R = the radius of curvature; $w' = dw/dx$; $w'' = d^2w/dx^2$; and x = the distance measured along the center line of the pipe.

To resort to formal mathematics in solving such a problem requires a rather complicated analysis which always leads to a nonlinear differential equation coupled with the displacement-dependent lateral frictional forces due to pipe-soil interaction. This nonlinear differential equation is often intractable even by the well-known numerical technique of the finite difference method. A more elegant approach would be to make physical idealizations of the pipe, coupled with a numerical procedure, in order to obtain solutions for practical use. This is the main objective of the present paper.

General Approach and Considerations

The problem of pipe bending analysis will be approached from the standpoint of beam-column theory with large displacement analysis, using the finite segment method and incremental tangent stiffness procedure (see chapter 11 of Ref. 6). More rigorous approaches, such as shell type of analysis is not considered here. It is believed that the pipe bending problem is essentially one-dimensional, and therefore can be best approached from this type of analysis.

The present work covers the in-plane behavior of the pipe under static loadings only. Pipe dynamics during pull-in will not be considered. The stress-strain relationship of the steel is assumed to be of the elastic-perfectly plastic type. In addition, torsional effects on the pipe tubular section are ignored because of the large torsional rigidity of the closed thin-walled tubular section.

As for the pipe-soil interaction model, only a simplified approach will be adopted here. In this approach, the pipe-soil interaction is simplified as a series of lumped concentrated friction loads at the nodal points along pipe length; each of these point friction loads follows the Coulomb friction relation with a single value of friction coefficient for both static and sliding friction.

The beam-column analysis of the pipe bending problem, as presented here, can be divided into three steps: (1) The moment-curvature behavior of a short segment; (2) the pipe-soil interaction modeling; and (3) the finite segment formulation, i.e., the segment stiffness matrices. These will be described briefly in the forthcoming.

Moment-Curvature (M-Φ) Relations.—The basic quantity required in any beam-column analysis is the value EI, which here can be considered as the slope of the relation curve between moment, M, and curvature, Φ. In the elastic range, this quantity is constant and therefore presents no difficulties. However, in the plastic range, this quantity is not constant since the moment-curvature response is nonlinear, and the instantaneous bending rigidity, EI, should be used. Even if the stress-strain relationship of the material is assumed to be an elastic-perfectly plastic type [see Fig. 2(*a*)], the generalized stress-strain or M-Φ relationship of the segment is seen to show an elastic strain hardening characteristic, as shown in Fig. 2(*b*). This is due to the fact that the section can be partially elastic and partially plastic.

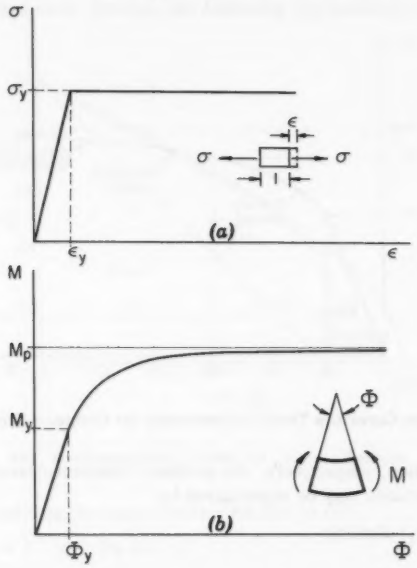

FIG. 2.—Stress-Strain and Moment-Curvature Relationships for Idealized Steel: (*a*) Idealized Stress-Strain Relationship (Elastic-Perfectly Plastic Type); (*b*) Typical Moment-Curvature Relationship

In the case of pipeline of fabricated tubular cross section, there are many factors which influence the M-Φ relations. These may be summarized in the following (see chapter 6 of Ref. 6; see also Refs. 7 and 9): (1) The intensity of axial load, P/P_y, in which P_y = the yield axial load of the cross section; (2) residual stresses in both longitudinal and circumferential directions due to the process of fabrication; (3) the initial out-of-roundness; and (4) the diameter to thickness ratio.

In order to obtain the moment-curvature relations which include the interactions between these factors, a computer subroutine has been developed and used

in Ref. 9 (using the tangent stiffness method). However, the use of this subroutine usually results in the most time-consuming part of the calculations. The computational time will be reduced significantly if closed-form moment-curvature expressions are developed to approximate the actual behavior of the cross section. A brief description of the method outlined by the second writer (3) for obtaining approximate expressions for the moment-curvature-thrust (M-Φ-P) relations, and their specific applications to fabricated tubular cross section, are given in the following.

The general M-Φ-P relation as shown in Fig. 3 can be divided into three regimes: (1) Elastic; (2) primary plastic; and (3) secondary plastic. Using the nondimensionalized quantities, $p = P/P_y$, $m = M/M_y$, and $\phi = \Phi/\Phi_y$, in which P_y, M_y, and Φ_y = the yield axial load, yield moment, and yield curvature

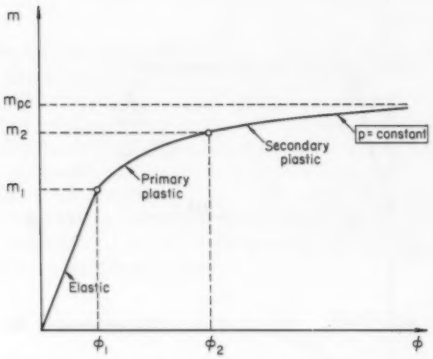

FIG. 3.—Moment-Curvature Thrust Relationship for Common Structural Section

of the cross section, respectively, the nonlinear moment-curvature relation for elastic-plastic sections may be represented by:

$$m = a\phi \quad (\phi \le \phi_1: \text{elastic});$$

$$m = b - \frac{c}{\sqrt{\phi}} \quad (\phi_1 < \phi \le \phi_2: \text{primary plastic});$$

$$m = m_{pc} - \frac{f}{\phi^2} \quad (\phi_2 < \phi: \text{secondary plastic}) \quad \ldots\ldots\ldots\ldots\ldots\ldots (3)$$

The parameters a, b, c, f, m_{pc}, ϕ_1, and ϕ_2 are functions of thrust, p, which are determined by test results or numerical computation for a particular shape of cross section. Once the values of m_1, m_2, m_{pc}, ϕ_1, and ϕ_2 are known, the parameters a, b, c, and f can easily be determined by solving the two sets of two simultaneous equations which arise if the particular values of ϕ_1 and ϕ_2 are inserted in the appropriate equations, i.e., Eq. 3, and the moments equated to the appropriate moments, m_1 and m_2. The results are given by (see chapter 5 of Ref. 5)

$$a = \frac{m_1}{\phi_1}; \quad b = \frac{m_2\sqrt{\phi_2} - m_1\sqrt{\phi_1}}{\sqrt{\phi_2} - \sqrt{\phi_1}};$$

$$c = \frac{m_2 - m_1}{\frac{1}{\sqrt{\phi_1}} - \frac{1}{\sqrt{\phi_2}}}; \quad f = (m_{pc} - m_2)\phi_2^2 \quad \ldots\ldots\ldots\ldots\ldots\ldots (4)$$

Approximate m-ϕ-p Expressions for Tubular Section.—Exact analytical expressions of m_1, m_2, m_{pc}, ϕ_1, and ϕ_2 for a tubular section subjected to axial load, P, and bending moment, M, have been developed, and used for plotting the interaction curves of Fig. 4. These expressions are very complicated and will not be included here. Instead, the following approximate expressions may

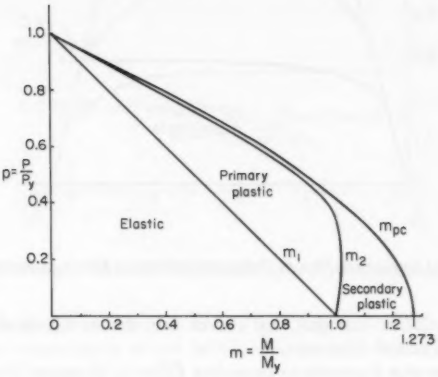

FIG. 4.—Interaction Curves for Tubular Section

be used to approximate the exact interaction curves (12):

$$m_1 = 1 - p, \ \phi_1 = 1 - p, \quad \text{for all} \quad p \quad \ldots\ldots\ldots\ldots\ldots\ldots (5a)$$

$$m_2 = 1 + 0.21\,p - 1.05\,p^2, \ \phi_2 = \frac{1}{1 - 1.395\,p + 1.206\,p^2},$$

$$\text{for} \quad 0 \le p \le 0.4; \quad m_2 = 1.528\,(1 - p), \ \phi_2 = 2.625\,(1 - p),$$

$$\text{for} \quad 0.4 \le p \le 1.0 \quad \ldots\ldots\ldots\ldots\ldots\ldots\ldots\ldots (5b)$$

$$m_{pc} = 1.273\,(1 - 1.18\,p^2), \quad \text{for} \quad 0 \le p \le 0.65;$$

$$m_{pc} = 1.82\,(1 - p), \quad \text{for} \quad 0.65 \le p \le 1.0 \quad \ldots\ldots\ldots\ldots\ldots\ldots (5c)$$

As an example of approximate m-ϕ-p relationships obtained using Eqs. 5*a*, 5*b*, and 5*c*, together with Eqs. 3 and 4, the approximate m-ϕ-p curves for the tubular cross section for four cases (p = 0, 0.4, 0.6, 0.8) are plotted in Fig. 5, in which actual m-ϕ-p relations, as reported in Ref. 9, are also included

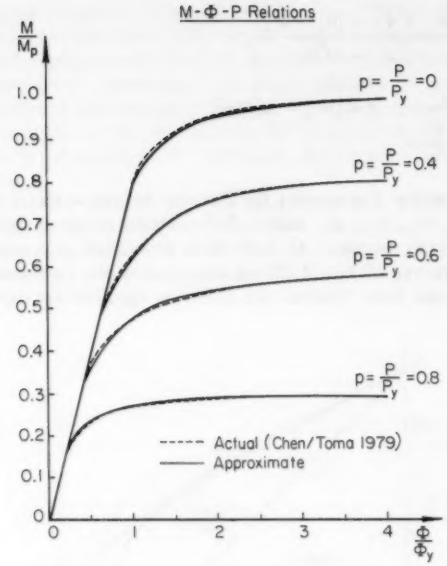

FIG. 5.—Moment-Curvature Thrust Relations (without Effect of Residual Stresses)

for comparison. It is seen that the curves are almost identical for both the approximate and actual relations.

Approximate m-ϕ-p Expressions Including Effect of Residual Stresses.—Based on the results obtained in Ref. 9, the approximate m-p-ϕ relations, including the residual stresses effect, can be derived. The details of the longitudinal and circumferential residual stress distributions considered are examined in Ref. 9. In this case, the values of m_1, m_2, m_{pc}, ϕ_1, and ϕ_2 can be closely approximated by:

$$m_1 = 0.893 - 1.305\,p + 0.796\,p^2,\ \phi_1 = 0.893 - 1.305\,p + 0.796\,p^2,$$

for $0 \le p \le 0.6$; $m_1 = 1.50 - 2.333\,p + 0.833\,p^2$, $\phi_1 = 1.50 - 2.333\,p + 0.833\,p^2$, for $0.6 \le p \le 1.0$ . . . . . (6*a*)

$$m_2 = 0.893 + 0.546\,p - 1.946\,p^2,\ \phi_2 = \frac{1}{1.12 - 2.491\,p + 4.308\,p^2},$$

for $0 \le p \le 0.6$; $m_2 = 1.375 - 1.50\,p + 0.125\,p^2$, $\phi_2 = 1.0 + 0.875\,p - 1.875\,p^2$, for $0.6 \le p \le 1.0$ . . . . . (6*b*)

$$m_{pc} = 1.273(1 - 1.18\,p^2), \text{ for } 0 \le p \le 0.65; \quad m_{pc} = 1.82(1 - p),$$

for $0.65 \le p \le 1$ . . . . . (6*c*)

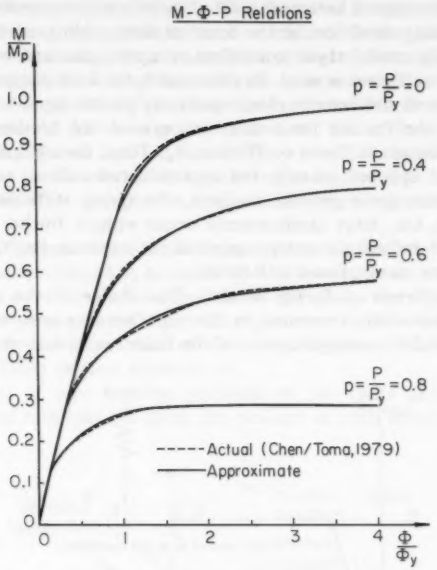

FIG. 6.—Moment-Curvature Thrust Relations (with Residual Stresses)

The corresponding curves are shown in Fig. 6, together with the actual relations (9). Again, the approximate m-ϕ-p relations agree well with the actual relationships.

Finally, similar approximate m-ϕ-p expressions, including the effects of residual stresses, out-of-roundness, and hydrostatic pressures can be developed. This is reported elsewhere (9,12).

Pipe-Soil Interaction Modeling.—As mentioned earlier, the pipe-soil interaction will be simplified as point friction nodal forces, each of which follows Coulomb friction relation. Although the coefficient of friction will have different static and dynamic values, a single value for both static and sliding friction will be used here.

The preceding is, of course, an extremely simplified approach for modeling the pipe-soil interaction behavior; nevertheless the general rigid-plastic type of load deflection behavior is valid and acceptable. In order to follow the actual load deflection behavior, it is necessary to conduct extensive experimental studies which will give the complete load deflection response from zero drag force upwards to sliding force, taking account of various directions of the pulling force. Thus, if this simplified drag force displacement relation is not acceptable, then a nonlinear or a piecewise linear relation must be developed using curve fitting techniques with experimental data, coupled with some simplified rigid-plastic type of analysis, such as limit analysis of soil plasticity (4). This is not considered in the present work.

The approach adopted here uses a set of constraints to impose approximately the rigid no sliding condition, or the constant force sliding conditions. In order to approximately model these conditions, a spring element with a relatively high stiffness coefficient is used. In this model, the load displacement relation of the spring is of the linearly elastic-perfectly plastic type, as shown in Fig. 7. As long as the friction force does not exceed the friction limit, F_0, the spring has a constant stiffness coefficient, k_0. Thus, the rigid no sliding (stick) condition is not imposed exactly, but approximated with an acceptable error. When the friction force exceeds its limit, the spring stiffness becomes zero and slip occurs, i.e., large displacements occur without further increase in the friction force. A refined alternative approach for implementing the friction stick or slip conditions can be found in Ref. 10.

Stiffness Coefficient of Spring Model.—The choice of the spring stiffness coefficient is extremely important in the pipe bending analysis, since it has been found that the convergence rate of the finite segment incremental solution

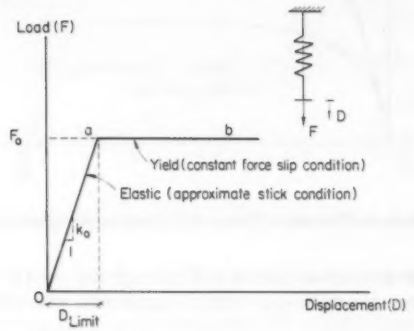

FIG. 7.—Simplified Load Displacement Relation for Elastic-Perfectly Plastic Spring Used for Friction Modeling

presented here is very sensitive to this choice. In fact, using too high stiffness coefficients causes the spring elements to dominate the solution excessively and produces a very large jump at slip. On the other hand, the use of too low stiffness causes an appreciable error in modeling the rigid no sliding (stick) condition. Therefore, a compromise is essential between accurate modeling of the stick condition and avoiding spurious effects of a too dominant stiffness and large jump at slip. Thus, the argument that has been used is to determine an acceptable tolerance in the stick condition approximation. Referring to Fig. 7, the stiffness coefficient, k_0, in the linear elastic range is given by

$$k_0 = \frac{F_o}{D_{\text{limit}}}; \quad F_0 = \mu N \ldots\ldots\ldots\ldots\ldots\ldots\ldots\ldots\ldots\ldots\ldots\ldots (7)$$

in which μ = the friction coefficient; N = total normal force; and D_{limit} = the "assumed" displacement limit. This displacement limit represents the assumed error in modeling the stick condition.

More Refined Friction Spring Model.—The change in direction of the friction force during pull-in of the pipeline is not considered in the previous model. To account for this change, a more refined spring model may be used. In this case, a spring model having two stiffness components is used, as shown in Fig. 8. The resultant frictional force is assumed to be in a direction perpendicular to the pipe segment at the nodal points. Therefore, the stiffness components, k_1' and k_2', in Fig. 8 are: $k_1 = k' \cos \psi$; $k_2' = k' \sin \psi$, in which k' = the resultant stiffness coefficient which has the value k_0 (see Eq. 7) in the linear elastic range; and ψ = the rotation angle of the pipe segment as shown in the figure.

Finite Segment Formulation.—In the finite segment method, the actual tubular pipeline is physically replaced by an assembly of finite segments, and the problem is formulated and solved approximately in terms of the behavior of these segments without recourse to complex differential equations. In this sense, the finite segment approach may be considered as a simplification of the more general approach of the finite element method (14).

In the analysis of pipe bending problems by the finite segment method, displacements and rotations are taken into account at each nodal cross section.

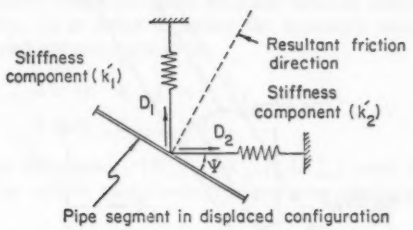

FIG. 8.—Refined Friction Model with Two Stiffness Components

In computation of the segment stiffness matrices, the direct stiffness method is utilized. Geometric and material nonlinearities are handled by application of a modified tangent stiffness approach. The details of the method and its application to solve biaxially-loaded beam-columns of wide flange shapes in elastic and plastic ranges are given in chapters 6 and 11 of Ref. 6 and also in Ref. 13.

In the case of in-plane analysis of pipe bending problems, the pipe will be treated as an assemblage of "cans" after segmentation. Only two displacements and one rotation are taken into account at each nodal cross section (see Fig. 9). The following assumptions are made in developing the segment stiffness matrices: (1) Segmental stiffnesses are based on undeformed straight segment behavior; (2) section properties for the tangent stiffness of a segment are invariants within the segment, and a segment tangent stiffness is calculated from the slope of the M-Φ relationship; (3) twisting effects are ignored; and (4) material stress-strain relation is linear elastic-perfectly plastic.

Segment Stiffness Matrices.—Consider an undeformed segment, AB, of length L, as shown in Fig. 9, with the local coordinate axes (ξ, η, ζ) defined as the

principal axes of the elastic portion of the cross section. At each nodal cross section, there are three nodal forces and three nodal displacements, namely, f_η, f_ζ, m_ξ, and u_η, u_ζ, θ_ξ, respectively. The segment stiffness matrix $[K(6 \times 6)]$ relates the six nodal forces, $\{f(6)\}$, to the corresponding six nodal displacements, $\{u(6)\}$; i.e.

$$\{f\} = [K(6 \times 6)]\{u\} \quad \ldots\ldots\ldots\ldots\ldots\ldots\ldots\ldots\ldots\ldots (8)$$

in which $\{f\}$ = the nodal force vector of components $f_{\eta A}$, $f_{\zeta A}$, $m_{\xi A}$, $f_{\eta B}$, $f_{\zeta B}$, and $m_{\xi B}$; and $\{u\}$ = the nodal displacement vector of components $u_{\eta A}$, $u_{\zeta A}$, $\theta_{\xi A}$, $u_{\eta B}$, $u_{\zeta B}$, and $\theta_{\xi B}$.

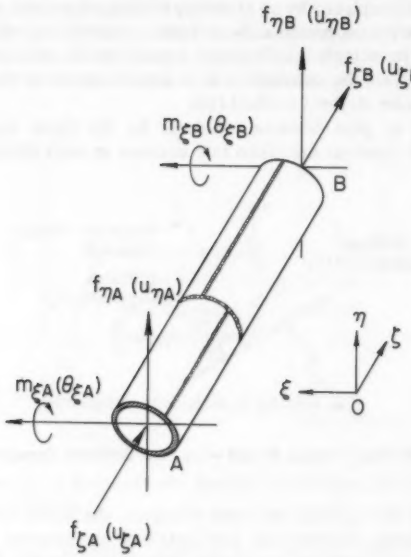

FIG. 9.—Forces and Displacements of Segment (Positive Directions for Forces and Displacements)

The segment stiffness matrix $[K(6 \times 6)]$ is computed, considering axial deformation and bending deformation separately. Further, the section properties are assumed to be constant within the segment. Thus, $[K(6 \times 6)]$ is derived by solving, separately, the axial and flexural problems, using the following force-displacement relations:

$$P = -EA\,u'_\zeta \quad \text{and} \quad m_\xi = -EI_\xi\,u''_\eta \quad \ldots\ldots\ldots\ldots\ldots\ldots\ldots\ldots (9)$$

and the governing differential equations (Ref. 6, chapter 11):

$$EA\,u''_\zeta = 0; \quad \text{and} \quad EI_\xi\,u''''_\eta + Pu''_\eta = 0 \quad \ldots\ldots\ldots\ldots\ldots\ldots (10)$$

in which the primes denote differentiation with respect to ζ. The first equation

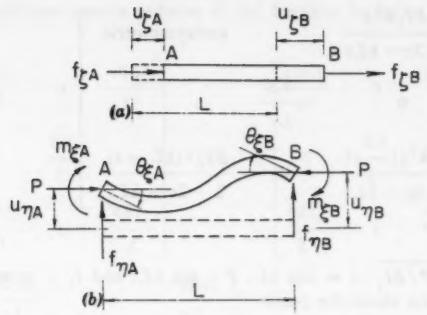

FIG. 10.—Independent Deformations of Segment: (*a*) Axial Deformations; (*b*) Bending and Shear Deformations

in Eq. 10 governs the problem of an axially-stressed segment, Fig. 10(*a*), while the second equation governs the flexure of a beam-column segment, Fig. 10(*b*). A set of six boundary conditions (three for each terminal cross section) should be attached to Eqs. 10 in order to define the boundary value problem. The final results obtained are summarized as:

$$[K(6\times 6)] = \begin{bmatrix} K_{AA}(3\times 3) & K_{AB}(3\times 3) \\ K_{BA}(3\times 3) & K_{BB}(3\times 3) \end{bmatrix} \quad \ldots\ldots\ldots\ldots\ldots\ldots (11)$$

Different forms of submatrices $[K_{AA}]$, $[K_{AB}]$, $[K_{BA}]$, and $[K_{BB}]$ are given in the following for various axial forces (compressive, tensile, and small):

1. For Axial Compressive Force: $(P = f_{\zeta A} = -f_{\zeta B})$

$$[K_{AA}] = \begin{bmatrix} \dfrac{EI_\xi k^3 s}{2-2c-kLs} & & \text{symmetric} \\ 0 & \dfrac{EA}{L} & \\ \dfrac{-EI_\xi k^2(1-c)}{2-2c-kLs} & 0 & \dfrac{EI_\xi k(s-kLc)}{2-2c-kLs} \end{bmatrix} \quad \ldots\ldots\ldots (12a)$$

$$[K_{BB}] = \begin{bmatrix} \dfrac{EI_\xi k^3 s}{2-2c-kLs} & & \text{symmetric} \\ 0 & \dfrac{EA}{L} & \\ \dfrac{EI_\xi k^2(1-c)}{2-2c-kLs} & 0 & \dfrac{EI_\xi k(s-kLc)}{2-2c-kLs} \end{bmatrix} \quad \ldots\ldots\ldots (12b)$$

$$[K_{AB}] = \begin{bmatrix} \dfrac{-EI_\xi k^3 s}{2-2c-kLs} & & \text{antisymmetric} \\ 0 & \dfrac{-EA}{L} & \\ \dfrac{EI_\xi k^2(1-c)}{2-2c-kLs} & 0 & \dfrac{EI_\xi k(kL-s)}{2-2c-kLs} \end{bmatrix} \quad \ldots\ldots\ldots (12c)$$

$$[K_{BA}] = [K_{AB}]^T \quad \ldots\ldots\ldots\ldots\ldots\ldots\ldots\ldots\ldots\ldots (12d)$$

in which $k = \sqrt{P/EI_\xi}$; $c = \cos kL$; $s = \sin kL$; and I_ξ = moment of inertia of the cross section about the ξ-axis.

2. For Axial Tensile Force: ($P = -f_{tA} = f_{tB}$)

$$[K_{AA}] = \begin{bmatrix} \dfrac{EI_\xi k^3 s'}{2-2c'+kLs'} & & \text{symmetric} \\ 0 & \dfrac{EA}{L} & \\ \dfrac{-EI_\xi k^2(c'-1)}{2-2c'+kLs'} & 0 & \dfrac{EI_\xi k(kLc'-s')}{2-2c'+kLs'} \end{bmatrix} \quad \ldots\ldots (13a)$$

$$[K_{BB}] = \begin{bmatrix} \dfrac{EI_\xi k^3 s'}{2-2c'+kLs'} & & \text{symmetric} \\ 0 & \dfrac{EA}{L} & \\ \dfrac{EI_\xi k^2(c'-1)}{2-2c'+kLs'} & 0 & \dfrac{EI_\xi k(kLc'-s')}{2-2c'+kLs'} \end{bmatrix} \quad \ldots\ldots (13b)$$

$$[K_{AB}] = \begin{bmatrix} \dfrac{EI_\xi k^3 s'}{2-2c'+kLs'} & & \text{antisymmetric} \\ 0 & \dfrac{EA}{L} & \\ \dfrac{EI_\xi k^2(c'-1)}{2-2c'+kLs} & 0 & \dfrac{EI_\xi k(s'-kL)}{2-2c'+kLs'} \end{bmatrix} \quad \ldots\ldots (13c)$$

$$[K_{BA}] = [K_{AB}]^T \quad \ldots\ldots\ldots\ldots\ldots\ldots\ldots\ldots\ldots\ldots (13d)$$

in which $c' = \cosh kL$; and $s' = \sinh kL$.

3. For Small Axial Force (Tensile or Compressive): The common factor ($2 - 2c - kLs$) or ($2 - 2c' + kLs'$) in the previous stiffness matrices approaches zero as the axial force becomes very small. In order to avoid numerical errors in such cases, an explicit form for the stiffness matrix is recommended. Using Taylor series expansions for the functions c, s, c', and s' for small values

of (kL), the stiffness matrix reduces to the familiar form for a beam segment, i.e.

$$[K_{AA}] = \begin{bmatrix} \frac{12EI_\xi}{L^3} & 0 & \frac{-6EI_\xi}{L^2} \\ 0 & \frac{EA}{L} & 0 \\ \frac{-6EI_\xi}{L^2} & 0 & \frac{4EI_\xi}{L} \end{bmatrix}; \quad [K_{BB}] = \begin{bmatrix} \frac{12EI_\xi}{L^3} & 0 & \frac{6EI_\xi}{L^2} \\ 0 & \frac{EA}{L} & 0 \\ \frac{6EI_\xi}{L^2} & 0 & \frac{4EI_\xi}{L} \end{bmatrix} \quad \ldots \quad (14a)$$

$$[K_{AB}] = \begin{bmatrix} \frac{-12EI_\xi}{L^3} & 0 & \frac{-6EI_\xi}{L^2} \\ 0 & \frac{-EA}{L} & 0 \\ \frac{6EI_\xi}{L^2} & 0 & \frac{2EI_\xi}{L} \end{bmatrix}; \quad [K_{BA}] = [K_{AB}]^T \quad \ldots \ldots \quad (14b)$$

Rotation Matrix and Structure Stiffness Matrix

The basic feature of a problem having geometric nonlinearity is that equilibrium equations must be written with respect to the deformed configuration, which is not known in advance. Therefore, the element-to-structure transformations are based on the deformed geometry of the element. Referring to Fig. 11, the local and global coordinate axes are ξ, η, ζ, and X, Y, Z, respectively. After the global total displacements, U_{YA}, U_{ZA}, U_{YB}, and U_{ZB}, have taken place, the undeformed configuration, A_0B_0, assumes the displaced position AB (see Fig. 11). The rotation angle, ψ, between the ζ- and Z-axes is

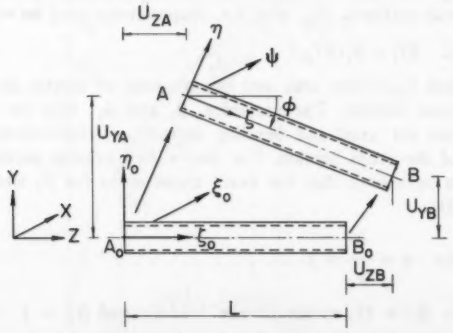

FIG. 11.—Displacements of Segment (In-Plane Behavior)

$$\psi = \tan^{-1} \frac{U_{YA} - U_{YB}}{L + U_{ZB} - U_{ZA}} \quad \ldots\ldots\ldots\ldots\ldots\ldots\ldots\ldots\ldots\ldots \quad (15)$$

in which ψ is positive if it is measured clockwise at the left end, B, of the segment. The global nodal forces, $\{F(6)\}$, and displacements, $\{U(6)\}$, are related to the corresponding local vectors, $\{f\}$ and $\{u\}$, through the relations:

$$\{U\} = [R]^T\{u\}; \quad \text{and} \quad \{F\} = [R]^T\{f\} \quad \ldots\ldots\ldots\ldots\ldots\ldots\ldots \quad (16)$$

in which $[R(6 \times 6)]^T$ = the transpose of the rotation matrix, $[R(6 \times 6)]$, which is given by:

$$[R(6 \times 6)] = \begin{bmatrix} [\bar{R}(3 \times 3)] & [0(3 \times 3)] \\ [0(3 \times 3)] & [\bar{R}(3 \times 3)] \end{bmatrix} \quad \ldots\ldots\ldots\ldots\ldots\ldots\ldots \quad (17a)$$

$$\text{in which} \quad [\bar{R}(3 \times 3)] = \begin{bmatrix} \cos\psi & \sin\psi & 0 \\ -\sin\psi & \cos\psi & 0 \\ 0 & 0 & 1 \end{bmatrix} \quad \ldots\ldots\ldots\ldots\ldots\ldots\ldots \quad (17b)$$

and $[0(3 \times 3)]$ is a 3×3 null matrix.

Finally, the structure stiffness matrix, $[S(N \times N)]$, is obtained from the relation

$$[S(N \times N)] = \Sigma\,[R]^T[K][R] \quad \ldots\ldots\ldots\ldots\ldots\ldots\ldots\ldots\ldots\ldots \quad (18)$$

in which N = total number of degrees-of-freedom in the structure.

Elastic-Plastic Section Properties

The value of the segment bending stiffness, EI, of the cross section can be easily determined from the slope of the nondimensionalized moment-curvature relations (by differentiating these relations which respect to the nondimensionalized curvature, ϕ). However, the segment axial stiffness, EA, must be determined by considering the elastic part of the cross section only (for linear elastic-perfectly plastic material). After partial plastification of the cross section, the instantaneous bending and axial stiffness, EI_ξ, and EA, respectively, may be written as

$$EA = \beta_1(EA_0); \quad EI_\xi = \beta_2(EI_{\xi 0}) \quad \ldots\ldots\ldots\ldots\ldots\ldots\ldots\ldots\ldots\ldots \quad (19)$$

in which A_0 and $I_{\xi 0}$ = the area and the moment of inertia about the ξ-axis of the *total* cross section. The variables, β_1 and β_2, may be considered as reduction factors for axial and bending stiffnesses, respectively, due to the plastification of the cross section. For thin-walled tubular section under pure bending, it can be shown that the exact expressions for β_1 and β_2 are given by (see Ref. 12):

$$\beta_1 = \beta_2 = 1 \quad \text{for} \quad \phi = \frac{\Phi}{\Phi_y} \leq 1 \quad \ldots\ldots\ldots\ldots\ldots\ldots\ldots\ldots\ldots\ldots \quad (20)$$

Variables $\beta_1 = \beta_2 + (1/\pi) \sin(2\cos^{-1} 1/\phi)$; and $\beta_2 = 1 - (2/\pi)\cos^{-1}(1/\phi) - (1/\pi)\sin(2\cos^{-1} 1/\phi)$, for $\phi > 1$ (compared to $\beta_1 = \sqrt[3]{\beta_2}$ for $\phi > 1$ for rectangular section).

For the general moment-curvature relations of Eqs. 3, β_2 is given by

$$\beta_2 = 1; \quad \phi \le \phi_1;$$

$$\beta_2 = \frac{1}{2} c \phi^{-3/2}; \quad \phi_1 < \phi \le \phi_2;$$

$$\beta_2 = 2 f \phi^{-3}; \quad \phi_2 < \phi \qquad (21)$$

and for small axial loads (as for pipe bending problems analyzed herein), β_1 can be approximately related to β_2 through the same relation for pure bending (see Eq. 20).

Incremental Modified Tangent Stiffness Approach

The problem to be solved now may be stated as follows: Given the state, A, at which a structure is subjected to forces $\{F_A\}$, and has displacements $\{U_A\}$, and tangent stiffness $[S_A]$, as shown in Fig. 12, it is required to find the displacements $\{U_B\}$, when forces are increased to $\{F_B\}$. Because of the nonlinearity of the system, the correct values of $\{U_B\}$ cannot be obtained directly. Herein a modified tangent stiffness approach is used (Ref. 6, chapter 11). The stiffness of the system during any loading increment is assumed to decrease monotonically. Therefore, the secant stiffness, $[\bar{S}]$, between the two states A and B, is bounded by $|S_B| \le |\bar{S}| \le |S_A|$. Using an averaging factor, α, the stiffness $[\bar{S}]$ may be expressed as:

$$[\bar{S}] = \alpha [S_A] + (1 - \alpha)[S_B] \qquad (22)$$

The procedure to obtain the displacements $\{U_B\}$, corresponding to the forces $\{F_B\}$, is summarized in the following steps (see Fig. 12).

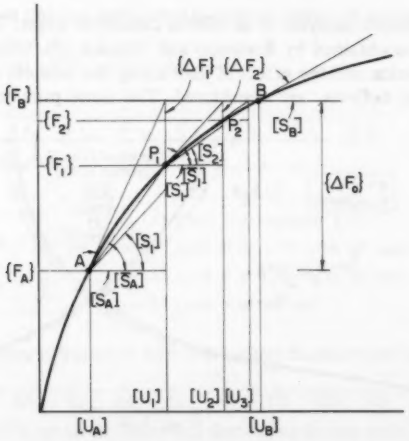

FIG. 12.—Modified Tangent Stiffness Procedure

1. Using the initial unbalanced force vector, $\{\Delta F_0\} = \{F_B\} - \{F_A\}$, and the current tangent stiffness at A, $[S_A]$, solve for the incremental displacement, $\{\Delta U_1\} = [S_A]^{-1}\{\Delta F_0\}$.

2. Calculate the new displacements, $\{U_1\} = \{U_A\} + \{\Delta U_1\}$.

3. From the updated displacements, $\{U_1\}$, the updated tangent stiffness, $[S_1]$, is obtained. The corresponding forces, $\{F_1\}$, are calculated using Eq. 22, i.e., $\{F_1\} = [\alpha S_A + (1 - \alpha) S_1]\{\Delta U_1\} + \{F_A\}$.

4. Calculate the unbalanced force vector, $\{\Delta F_1\} = \{F_B\} - \{F_1\}$, corresponding to point P_1 in Fig. 12.

5. Repeat the same procedure to obtain the new state represented by point P_2 in Fig. 12, i.e., $\{\Delta U_2\} = [S_1]^{-1}\{\Delta F_1\}$, $\{F_2\} = [\alpha S_1 + (1 - \alpha) S_2]\{\Delta U_2\} + \{F_1\}$, and $\{\Delta F_2\} = \{F_B\} - \{F_2\}$. Thus, after n cycles of iteration, we have $\{F_n\} = [\alpha S_{n-1} + (1 - \alpha) S_n]\{\Delta U_n\} + \{F_{n-1}\}$ and $\{\Delta F_n\} = \{F_B\} - \{F_n\}$.

6. After any cycle, n, check the equilibrium error, $\{\Delta F_n\}$. Stop if the unbalanced forces, $\{\Delta F_n\}$, become less than a prescribed tolerable limit.

Numerical Results

Based upon the aforementioned formulation, a computer program has been developed at Purdue University to provide numerical results. A number of sample (check) problems are solved to provide the necessary confirmation of the validity of the proposed numerical procedure. The results obtained are compared, whenever possible, with the available theoretically obtained solutions. Finally, as a practical case, the developed computer program is used to carry out the elastic analysis for a large displacement pipe bending problem. Some typical results are presented.

Check Problems.—The results obtained for some of the check problems are summarized in the following:

1. Large deflection analysis of an elastic cantilever beam: The exact solution of this problem is obtained by Bisshopp and Drucker (2), where both the exact curvature expression and the effect of shortening the moment arm as the loaded end of the beam deflects, are considered. The same problem is solved using

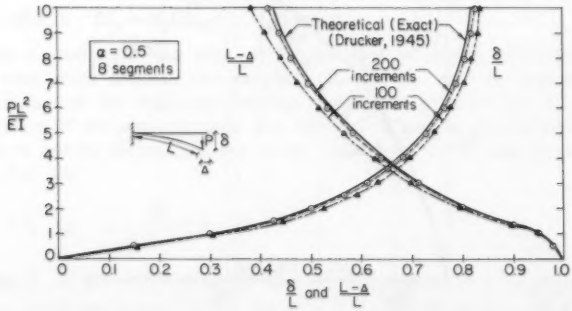

FIG. 13.—Large Deflection of Cantilever Beam: Effect of Load Steps

the developed computer program. Typical results are shown in Fig. 13 for the vertical and horizontal displacements, δ and Δ, respectively, of the free end. As can be seen, the finite segment solution agrees well with the theoretical results (2). The main conclusion drawn from this example is the justification

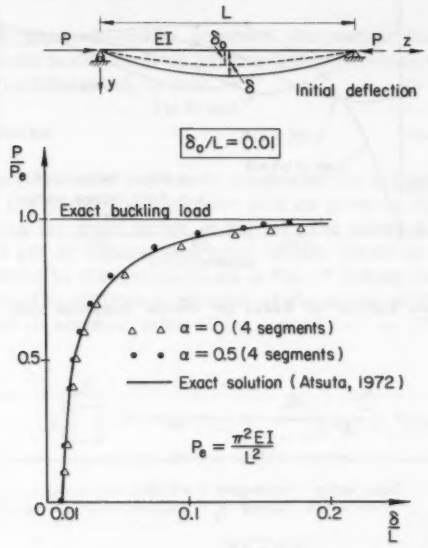

FIG. 14.—Pin-Ended Column with Initial Deflection (Effect of Averaging Factor α)

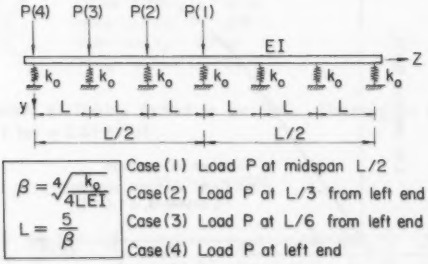

FIG. 15.—Beam on Elastic Supports with One Lateral Concentrated Load at Different Locations

of the assumption of a small displacement derivative during each load increment, which is the basis of deriving the governing differential equations (segment stiffness).

2. Elastic analysis of simply-supported column with sinusoidal initial imperfections (out-of-straightness): Typical results are shown in Fig. 14, where the exact solution of Ref. 1 is also plotted. A good agreement is observed.

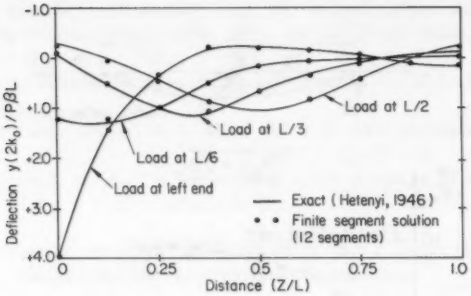

FIG. 16.—Deflection Curves for Beam on Elastic Supports with Different Load Locations

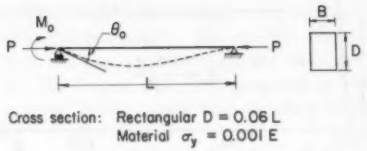

Cross section: Rectangular D = 0.06 L
Material σ_y = 0.001 E

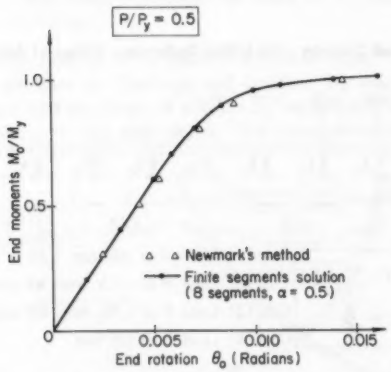

FIG. 17.—End Moment-End Rotation Relation for Beam-Column of Rectangular Cross Section Subjected to End Moments

3. Finite beam on elastic supports: For different locations of the load, *P*, on the beam (see Fig. 15), the calculated deflection curves are given in Fig.

16. Finite segment results are seen to be identical to those of the theoretical solutions (11).

4. Elastic-plastic analysis of beam-column with rectangular cross sections: The finite segments solutions and the results obtained using Newmark's method (5) are plotted in Fig. 17. Again, a good agreement is observed.

In short, the numerical results presented demonstrate the validity of the proposed computer model in solving different types of problems having geometrical, or material nonlinearities, or both.

Pipe Bending Problem

Herein, a more realistic problem is considered for a pipeline pulled in on the sea floor. The problem's descriptive data are given in Fig. 18. The tubing is modeled using the mesh shown in Fig. 19. The tubing-floor interaction is simulated as a set of concentrated point friction forces at the nodal points which are modeled by the springs shown in Fig. 19 (tubing weight = 19.5 lb/ft or 284.5 N/m). The stiffness coefficient of the spring models is determined on the basis of an assumed value of D_{limit} equal to 3 in. (76.2 mm). Several

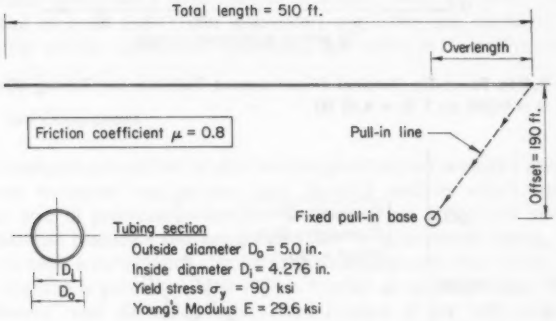

FIG. 18.—Top View of Tubing Pulled In on Floor: Dimensions and Properties (1 in. = 25.4 mm; 1 ksi = 6.89 MPa)

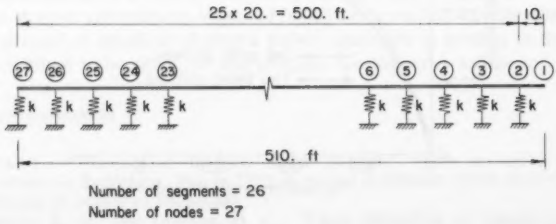

FIG. 19.—Finite Segments Discretization of Tubing (1 ft = 0.305 m)

trials were made before the final choice of this value.

In order to investigate the effect of friction modeling on the solution, two spring models are considered: the first model with one spring stiffness in the vertical direction, and the second model with two spring stiffnesses in the vertical and horizontal directions; each has the same friction force limit (extreme case of the proposed refined model).

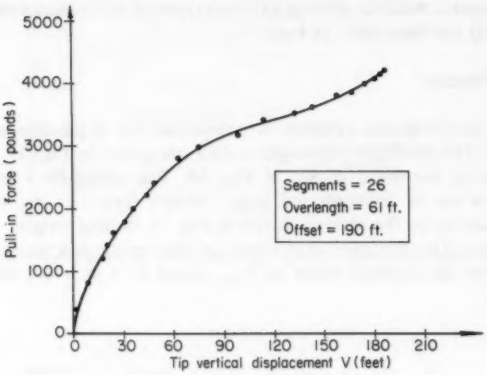

FIG. 20.—Pull-In Force-Tip Vertical Displacement Relation for Tubing (Overlength = 61 ft; 1 ft = 0.305 m; 1 lb = 4.45 N)

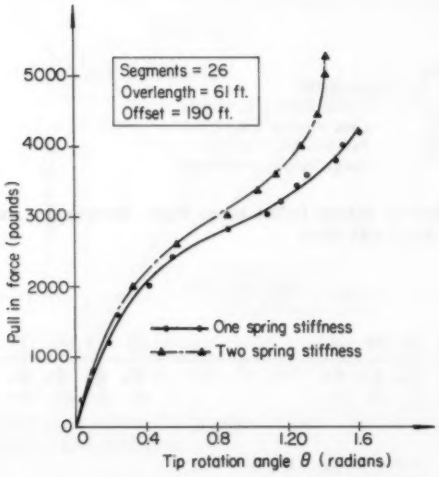

FIG. 21.—Pull-In Force-Tip Rotation Angle Relation for Tubing (Overlength = 61 ft; 1 ft = 0.305 m; 1 lb = 4.45 N)

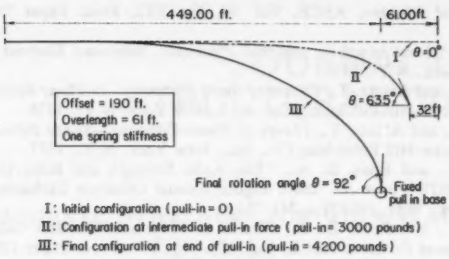

FIG. 22.—Tubing Configuration During Pull-In (Offset = 190 ft; Overlength = 61 ft; 1 ft = 0.305 m; 1 lb = 4.45 N)

Typical force-displacement responses of tubing obtained from the finite segment solution are shown in Figs. 20 and 21. Tubing configuration at final pull-in and at an intermediate value of pull-in force is given in Fig. 22.

The solutions obtained for all the cases investigated indicate that friction modeling has noticeable effects on the results. Numerical difficulties are encountered in some cases and a large number of loading steps are used. Therefore, a great deal of work and further studies are needed in this matter to achieve a reasonable specific conclusion concerning this effect in the analysis of actual cases.

Summary and Conclusions

Large displacement analysis of pipe bending problems is frequently encountered in offshore structural applications. Any rigorous analysis which attempts to solve this type of problems is destined to be complex, since both nonlinearity due to material plasticity and nonlinearity due to geometrical change must be included in such a formulation. Herein, the numerical procedure based on finite segment method is presented. The pipe is treated as an assemblage of "cans" or "segments" and the moment-curvature relation of the tube cross section is approximated by simple mathematical expressions. The segment stiffness relationships are computed using the direct stiffness method. Material and geometry nonlinearities are overcome by a modified tangent stiffness approach. Four numerical check problems are then presented and compared with "exact" solutions. A good agreement is observed for all cases studied. Finally, the problem of bend-around of pipelines during a pull-in operation is studied in detail. The method is found to be adequate and efficient for computer solutions.

Appendix.—References

1. Atsuta, T., "Analyses of Inelastic Beam-Columns," thesis presented to Lehigh University, at Bethlehem, Pa., in 1972, in partial fulfillment of the requirements for the degree of Doctor of Philosophy.
2. Bisshopp, K. E., and Drucker, D. C., "Large Deflection of Cantilever Beams," *Quarterly of Applied Mathematics*, Vol. 3, 1945, pp. 272–275.
3. Chen, W. F., "Further Studies of Inelastic Beam-Column Problems," *Journal of*

the Structural Division, ASCE, Vol. 97, No. ST2, Proc. Paper 7922, Feb., 1971, pp. 529–544.
4. Chen, W. F., *Limit Analysis and Soil Plasticity*, American Elsevier Publishing Co., Inc., New York, N.Y., 1975.
5. Chen, W. F., and Atsuta, T., *Theory of Beam-Columns—In-Plane Behavior and Design*, Vol. 1, McGraw-Hill Publishing Co., Inc., New York, N.Y., 1976.
6. Chen, W. F., and Atsuta, T., *Theory of Beam-Columns—Space Behavior and Design*, Vol. 2, McGraw-Hill Publishing Co., Inc., New York, N.Y., 1977.
7. Chen, W. F., and Ross, D. A., "The Axial Strength and Behavior of Cylindrical Columns," *OTC Paper No. 2683*, Eighth Annual Offshore Technology Conference, Houston, Tex., May, 1976, pp. 741–754.
8. Chen, W. F., and Ross, D. A., "Tests of Fabricated Tubular Columns," *Journal of the Structural Division*, ASCE, Vol. 103, No. ST3, Proc. Paper 12809, Mar., 1977, pp. 619–634.
9. Chen, W. F., and Toma, S., "Effect of External Pressure on the Axial Capacity of Fabricated Tubular Columns," report submitted to Exxon Production Research Company, Houston, Tex., Jan., 1979.
10. Herrman, L. R., "Finite Element Analysis of Contact Problems," *Journal of the Engineering Mechanics Division*, ASCE, Vol. 104, No. EM5, Proc. Paper 14055, Oct., 1978, pp. 1043–1057.
11. Hetenyi, M., *Beams on Elastic Foundation*, University of Michigan Press, Ann Arbor, Mich., 1946.
12. Saleeb, A. F., "Near-Bottom Bend of Flowlines," thesis presented to Purdue University, at West Lafayette, Inc., in May, 1974, in partial fulfillment of the requirements for the degree of Master of Science.
13. Santathadaporn, S., and Chen, W. F., "Tangent Stiffness Method for Biaxial Bending," *Journal of the Structural Division*, ASCE, Vol. 98, No. ST3, Proc. Paper 8637, Jan., 1972, pp. 153–163.
14. Zienkiewicz, O. C., *The Finite Element Method*, 3rd ed., McGraw-Hill Book Co., Inc., London, England, 1977.

JOURNAL OF THE STRUCTURAL DIVISION

INTERMEDIATE STIFFENERS FOR THIN-WALLED MEMBERS

By Thomas P. Desmond,[1] A. M. ASCE, Teoman Peköz,[2] M. ASCE, and George Winter,[3] Hon. M. ASCE

INTRODUCTION

This paper is the second of a two paper sequence describing the results of an investigation of the structural behavior of longitudinally stiffened compression elements of thin-walled members. The first paper (5) dealt with edge-stiffened elements, while the present paper deals with intermediately stiffened elements. In both cases, the stiffener is longitudinal, i.e., parallel to the direction of the applied in-plane compressive stresses. A detailed description of the complete investigation may be found in Ref. 4.

A typical component element of a thin-walled member is the stiffened element shown in Fig. 1(*a*). A stiffened plate element by definition is adequately supported on each longitudinal edge. Local plate buckling is a usual design consideration for thin-walled members. One way to increase the local buckling load and to enhance structural efficiency is by providing a secondary or intermediate stiffener between the main longitudinal stiffeners or webs. As shown in Fig. 1(*b*), the intermediate stiffener breaks up the wave-like pattern of the stiffened element of Fig. 1(*a*) such that the two plate strips, one on either side of the intermediate stiffener, behave as two stiffened elements.

The research described in this paper explored the structural behavior of intermediately stiffened elements analytically and experimentally. Based primarily on the experimental results, stiffener requirements were developed. Methods were also formulated for predicting ultimate strengths of elements that are supported by such stiffeners.

[1]Formerly, Research Asst., Cornell Univ., Ithaca, N.Y.

[2]Assoc. Prof. of Structural Engrg., Cornell Univ., School of Civ. and Environmental Engrg., Hollister Hall, Ithaca, N.Y. 14853.

[3]Prof. Emeritus, Cornell Univ., Ithaca, N.Y. 14853.

Note.—Discussion open until September 1, 1981. To extend the closing date one month, a written request must be filed with the Manager of Technical and Professional Publications, ASCE. Manuscript was submitted for review for possible publication on April 30, 1980. This paper is part of the Journal of the Structural Division, Proceedings of the American Society of Civil Engineers, ©ASCE, Vol. 107, No. ST4, April, 1981. ISSN 0044-8001/81/0004-0627/$01.00.

Buckling Behavior

Two distinct buckling modes characterize the buckling behavior of intermediately stiffened elements. One is the *stiffener buckling mode*, where the instability of the assembly is initiated by buckling of the flange-stiffener assembly direction perpendicular to the plane of the flange. Stiffener buckling will necessarily induce local buckling of the component plate elements. The second mode is the *local plate buckling mode*. Both buckling modes are shown schematically in Fig. 2.

An independent critical buckling analysis characterized the behavior of each buckling mode. For the stiffener buckling mode the buckling equation is given by Barbré (2), and for the local plate buckling mode the equation is given by Bryan (3). The detailed derivations of these equations are adequately documented in the cited references and are not given here.

Solutions to these buckling equations can be given as a relationship between the buckling coefficient k_b and the aspect ratio ϕ_b. The subscript b denotes that the buckling coefficient and aspect ratio are expressed as functions of b, the total width of the assembly. Alternatively, the buckling coefficient could

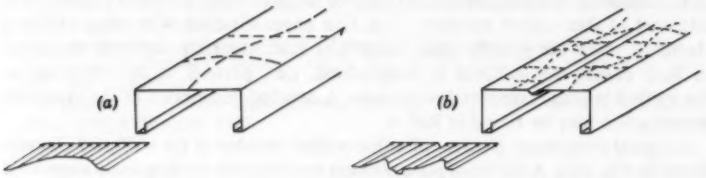

FIG. 1.—Thin-Walled Members: (*a*) Stiffened Element; (*b*) Intermediately Stiffened Element

also be expressed as a function of the flat width w, in which w is the width between the intermediate stiffener and the supported longitudinal edge, so that

$$k_b = \left(\frac{b}{w}\right)^2 k_w \quad \ldots \ldots \ldots

term A_s is the actual cross-sectional area of the stiffener, and A_s^* is the stiffener area which would lead to simultaneous stiffener and local plate buckling.

Experimental Investigation

The influence of the longitudinal stiffener rigidity on the performance of the intermediately stiffened plate assembly was studied by a series of tests. In this study, the depth of the longitudinal stiffener was systematically varied for each of several flat plate dimensions.

The investigation involved four beam test series with w/t ratios of 47, 70, 97, and 156, in which w is the flat width between the intermediate longitudinal stiffener and the supported edge of the compression flange. The specimens were hat sections with the stiffener cold-formed in the center of the compression flange, as shown in Fig. 5.

The stiffeners of each test series were designed such that the centroidal moment

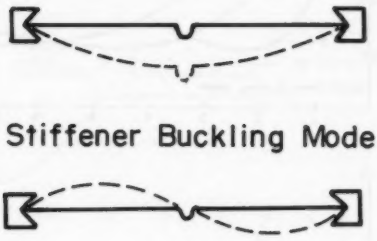

FIG. 2.—Critical Buckling Modes

of inertia of the stiffener for some of the specimens was above and for others below the minimum value currently required by the American Iron and Steel Institute (AISI) Specification (1). The specific stiffener centroidal moments of inertia are given in Table 1 along with the specimen dimensions. Table 2 gives the material properties, experimental ultimate moments, and buckling stress coefficients. The test setup is shown schematically in Fig. 6.

Strain gages were placed in the central region of the beams to establish the approximate stress distribution across the section and to determine when local or stiffener buckling occurred, or both.

The experimental buckling stress coefficients were obtained by the strain reversal method (8) and are compared to those obtained from the buckling analysis in Fig. 7. Buckling coefficients for test series I-47 are not shown in this figure since the compression flanges of these specimens either did not buckle or buckled inelastically. All but one experimental buckling coefficient, shown in the figure, exceeded the theoretical value for the local buckling mode.

A plausible reason for this is that the compression flanges were restrained rotationally by the webs. This was not accounted for in the buckling analysis. Nevertheless, agreement between experiment and theory is satisfactory.

By comparing the longitudinal strain at the stiffener-plate juncture with the strain at the web-plate juncture, the relative support provided by different stiffener rigidities could be assessed. The variation of strain at these locations is shown in Fig. 8 for a representative test series. It is apparent that the strain variations at the longitudinally supported edge and at the longitudinal stiffener are virtually the same for specimens with sufficiently large stiffeners. The strain variations of test I-97-313 (97 is the w/t ratio, and 313 is the nondimensional stiffener moment of inertia I_s/t^4) are representative of this type of behavior. In contrast,

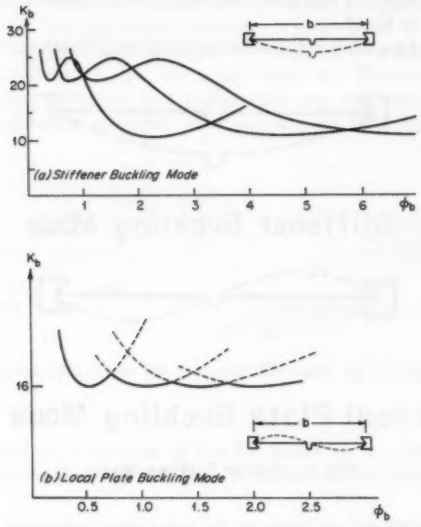

FIG. 3.—Critical Buckling Coefficient Curves

the strain at the longitudinal stiffener of a specimen with a relatively small stiffener shows a strain reversal tendency. This type of behavior, illustrated by test I-97-115, indicates a stiffener that buckles outwardly in a direction perpendicular to the plane of the plate.

Ultimate Strength Considerations

In this section, procedures are formulated for predicting ultimate strengths of elements that have stiffeners of adequate and inadequate rigidity. In a subsequent section, formulas will be developed for establishing required stiffener rigidities. In the following development, it will be apparent that procedures

for predicting ultimate strengths and for assessing adequate stiffener rigidities are interdependent.

An intermediate stiffener is defined as adequate if the intermediately stiffened plate can be treated as an assembly of two stiffened plate elements of width w, and a fully effective stiffener. When partially stiffened by an inadequate intermediate stiffener, the assembly can be treated as a partially stiffened plate of width b and a reduced or partially effective stiffener. Here b is the width between the supported edges of the intermediately stiffened plate and w is the width of each component plate. In the following development, it will be assumed that b is twice the width w. This is a valid assumption provided the width of the stiffener is small relative to b.

The ultimate strengths of the component plates will be predicted by an effective width approach. This is consistent with the design procedure developed in Ref. 5 for edge-stiffened elements. The effective width equation in the current AISI

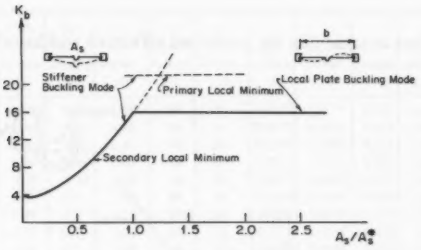

FIG. 4.—Minimum Critical Buckling Coefficients

specification (1) will be employed. The following is a generalization of that equation for a plate of width w

$$w_{\text{eff}} = 0.95t\sqrt{\frac{k_w E}{\sigma_y}}\left[1 - 0.209\left(\frac{t}{w}\right)\sqrt{\frac{k_w E}{\sigma_y}}\right] \quad \ldots\ldots\ldots\ldots (3a)$$

which is valid for:

$$\frac{w}{t} > 0.64\sqrt{\frac{k_w E}{\sigma_y}} \quad \ldots\ldots\ldots\ldots\ldots\ldots\ldots\ldots\ldots\ldots (3b)$$

The effective width of the total plate of width b can also be expressed as

$$b_{\text{eff}} = 0.95t\sqrt{\frac{k_b E}{\sigma_y}}\left[1 - 0.209\left(\frac{t}{b}\right)\sqrt{\frac{k_b E}{\sigma_y}}\right] \quad \ldots\ldots\ldots\ldots\ldots (4)$$

Depending upon the degree of support, the intermediately stiffened element is categorized as adequately stiffened, partially stiffened, or stiffened. The latter is the limiting case, where there is no intermediate stiffener and the plate is supported by two webs on its longitudinal edges. These categories are defined later, and the assumptions for buckling stress coefficients of each are given.

Adequately Stiffened Element.—An intermediately stiffened element is ade-

quately stiffened if the intermediate stiffener is of sufficient flexural rigidity so that the ultimate strength of each component plate element (of width w) equals that of an identical plate stiffened by webs on both longitudinal edges.

The effective width of each component plate is predicted by Eq. 3 with a buckling stress coefficient k_w equal to four. The intermediate stiffener is assumed to remain straight or unbuckled up to the ultimate failure load. Thus, it is assumed to remain fully effective for purposes of predicting its contribution to the ultimate strength of the assembly.

Alternatively, the ultimate strength of the total plate of width b can be predicted by Eq. 4 in which

$$b = 2\,w \quad \ldots \quad (5)$$

and $$k_b = 4\,k_w \quad \ldots \quad (6)$$

Substituting Eqs. 5 and 6 into Eq. 4

$$b_{\text{eff}} = 2\,w_{\text{eff}} \quad \ldots \quad (7)$$

which is equivalent to summing the predicted effective widths of each component element.

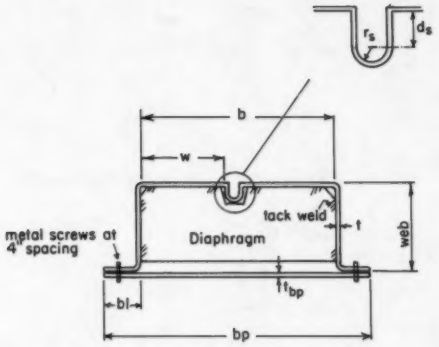

FIG. 5.—Cross-Sectional Geometry of Specimens

Effective widths of partially stiffened elements are considered later and will be based on the effective width equation expressed in terms of the total assembly width b.

Partially Stiffened Element.—An intermediately stiffened compression element is partially stiffened if the stiffener is inadequate; namely, if the flexural rigidity of the stiffener is insufficient to permit the ultimate strength of each component plate to equal that of an identical plate stiffened by webs on both longitudinal edges.

Intuitively, the ultimate strength of a partially stiffened element is bounded by two extreme cases: (1) A stiffened plate of width b with an adequate intermediate stiffener; and (2) a plate of similar dimensions but without an intermediate stiffener. Likewise, the buckling stress coefficient of a partially

stiffened element $(k_b)_{ps}$ is bounded by the buckling stress coefficient of an adequately stiffened element $(k_b)_{as}$ and by the coefficient of an element without an intermediate stiffener $(k_b)_{ns}$. The latter two buckling coefficients were shown to be 16 and 4 when expressed as functions of the total plate width.

Theoretical values for $(k_b)_{ps}$ require a detailed critical buckling analysis. However, for design purposes, $(k_b)_{ps}$ may be determined from the following expression, which is a close fit (Fig. 9) of the theoretical buckling stress coefficients obtained from a critical buckling analysis.

$$(k_b)_{ps} = \left(\frac{I_s}{I_s^*}\right)^{1/2} [(k_b)_{as} - (k_b)_{ns}] + (k_b)_{ns} \quad \ldots\ldots\ldots\ldots\ldots\ldots (8)$$

in which $(k_b)_{ps}$ = predicted buckling stress coefficient for partially stiffened

TABLE 1.—Dimensions of Intermediately Stiffened Beams[a]

Test series (1)	w/t (2)	b, in inches (3)	web, in inches (4)	bp, in inches (5)	bl, in inches (6)	L, in inches (7)	LS, in inches (8)	t, in inches (9)	t_{bp}, in inches (10)	r_s, in inches (11)	d_s, in inches (12)	I_s/t^4 (13)	A_s/t^2 (14)
I-47	48.0	6.10	5.00	9.35	1.50	88.	24.	0.0565	0.0575	0.210	0.145	60.0	16.3
	47.0	6.11	5.00	9.33	1.55	88.	24.	0.0575	0.0580	0.213	0.223	110.0	19.4
	47.4	6.10	5.00	9.35	1.55	88.	24.	0.0570	0.0588	0.217	0.259	142.	20.8
	47.0	6.10	5.00	9.38	1.54	88.	24.	0.0578	0.0572	0.209	0.350	217.	23.5
	46.8	6.00	5.00	9.38	1.50	88.	24.	0.0577	0.0590	0.215	0.535	499.	30.2
I-70	71.8	8.89	4.08	12.0	1.50	88.	24.	0.0564	0.0585	0.192	0.108	40.5	14.5
	70.4	8.83	4.09	12.0	1.50	88.	24.	0.0571	0.0585	0.213	0.230	118.	19.8
	70.1	8.80	4.00	12.0	1.50	88.	24.	0.0571	0.0593	0.213	0.230	118.	19.8
	69.5	8.95	4.10	12.0	1.30	112.	37.3	0.0590	0.0593	0.217	0.367	232.	24.0
	69.5	8.95	4.08	12.0	1.31	112.	37.3	0.0587	0.0592	0.224	0.458	367.	27.6
	69.8	8.95	4.10	12.0	1.34	112.	37.3	0.0587	0.0592	0.224	0.532	488.	30.1
	69.3	8.93	4.00	12.0	1.35	112.	37.3	0.0590	0.0598	0.230	1.150	2650.	51.2
I-97	96.4	11.7	5.50	15.0	1.56	88.	24.	0.0570	0.0690	0.219	0.226	115.	19.6
	97.5	11.8	5.45	15.0	1.58	88.	24.	0.0564	0.0690	0.214	0.263	150.	21.2
	79.3	11.7	5.50	15.0	1.30	88.	24.	0.0694	0.0698	0.236	0.359	153.	21.0
	79.5	11.7	5.50	15.0	1.50	88.	24.	0.0692	0.0697	0.224	0.545	313.	25.9
	80.7	11.7	5.50	15.0	1.55	88.	24.	0.0681	0.0695	0.228	0.681	527.	30.5
I-156	155.	18.6	5.50	21.9	1.55	88.	14.	0.0580	0.0595	0.217	0.218	107.	19.3
	156.	18.6	5.49	21.9	1.50	88.	14.	0.0580	0.0573	0.218	0.268	147.	21.0
	159.	18.7	5.50	21.8	1.54	88.	14.	0.0572	0.0575	0.218	0.350	235.	24.1
	157.	18.6	5.50	21.8	1.57	88.	14.	0.0573	0.0575	0.217	0.514	477.	29.8
	157.	18.6	5.50	21.9	1.58	88.	14.	0.0572	0.0571	0.218	1.130	2670.	51.3

[a]Refer to Figs. 5 and 6.
Note: 1 in. = 25.4 mm.

elements; I_s = moment of inertia of the stiffener about its centroidal axis parallel to the plate element; I_s^* = stiffener centroidal moment of inertia at which critical buckling of the assembly is initiated by simultaneous stiffener and local plate buckling; $(k_b)_{as} = 16$; and $(k_b)_{ns} = 4$. Eq. 8 was obtained by fitting a quadratic expression through the theoretical values for $(k_b)_{ps}$ at I_s/I_s^* equal to zero and one. The term I_s^* is the adequate stiffener rigidity based on a criterion of critical buckling; however, when the flat width ratio of the assembly exceeds some limiting value (to be determined in a following section), adequacy should be based on an ultimate strength criterion. Since the adequate stiffener rigidity for the latter criterion, $(I_s)_{adequate}$, can be considerably larger than I_s^* these

criteria are not identical. Consequently, it would not be appropriate to replace I_s^* with $(I_s)_{adequate}$.

For this reason, Eq. 8 is restated in terms of $(I_s)_{adequate}$ and an exponent $1/n$, in which n will be chosen such that the following equation is a close approximation of the theoretical buckling coefficients:

$$(k_b)_{ps} = \left[\frac{I_s}{(I_s)_{adequate}}\right]^{1/n} [(k_b)_{as} - (k_b)_{ns}] + (k_b)_{ns} \quad \ldots \ldots \ldots \ldots \ldots \quad (9)$$

The effective width of a partially stiffened element of width b is then determined

TABLE 2.—Material Properties and Test Results

Test series (1)	I_s/t^4 (2)	Material Properties: Yield stress, in kips per square inch (3)	Material Properties: Ultimate stress, in kips per square inch (4)	Test Results: M_{ult}, in kip-inches (5)	Test Results: k_b (6)
I-47	60.	45.9	51.4	92.4	10.2[a]
	110.	43.2	50.6	109.	10.2[a]
	142.	43.6	51.2	98.4	10.2[a]
	217.	43.0	50.2	102.	[b]
	499.	44.9	56.6	119.	10.3[a]
I-70	40.5	43.9	51.4	64.6	12.3
	118.	42.1	50.7	77.5	16.4
	118.	43.0	50.7	69.6	14.9
	232.	43.6	56.7	82.1	18.4
	367.	43.8	56.8	86.6	16.0
	488.	44.9	52.1	89.6	16.8
	2650.	42.6	56.3	87.7	16.7
I-97	115.	42.9	51.3	103.	12.3
	150.	44.5	51.5	108.	16.8
	153.	44.9	56.7	150.	15.3
	313.	44.0	57.2	159.	16.7
	527.	44.9	56.1	168.	18.4
I-156	107.	42.4	50.9	104.	10.6
	147.	42.5	49.6	104.	12.8
	235.	42.5	50.2	106.	11.3
	477.	42.2	51.2	123.	15.1
	2670.	40.0	50.4	127.	17.2

[a]Inelastic buckling stress coefficient.
[b]No observed stiffener or local plate buckling.
Note: 1 ksi = 6.9 Nm/m^2; 1 kip-in. = 111 Nm.

by Eq. 4 with $(k_b)_{ps}$ given by Eq. 9. The contribution of the partial intermediate stiffener to the ultimate strength of the assembly is covered in the following paragraphs.

The procedure for predicting the contribution of a partial or buckled stiffener to the ultimate strength of the assembly, is the same as outlined for edge-stiffened

elements in Ref. 5. The cross-sectional area of the partial stiffener is reduced by a simple linear expression to reflect its reduced effectiveness in resisting load:

$$(A_s)_{ps} = \frac{A_s I_s}{(I_s)_{adequate}} \quad \ldots\ldots\ldots\

Intermediate Stiffener Requirement

The definition of an adequate stiffener could be based on either a critical buckling criterion (CBC) or an ultimate strength criterion (USC). With the CBC, the adequate stiffener is defined as that stiffener rigidity at which instability is initiated by simultaneous stiffener buckling and local plate buckling. With the USC, the adequate stiffener rigidity is defined as the minimum rigidity at which the ultimate strength of each component plate on either side of the stiffener equals that of an identical plate stiffened by webs on both edges.

CBC.—To obtain a stiffener requirement based on a CBC, the stiffener buckling equation is solved for those stiffener dimensions for which the minimum buckling stress coefficient k_b equals 16. This is the stiffener dimension for which stiffener buckling and local plate buckling occur simultaneously for all aspect ratios ϕ_b. The requirement is shown in Fig. 11 as $(I_s/t^4)_{req}$, the required stiffener rigidity nondimensionalized with respect to the plate thickness t. Three requirements

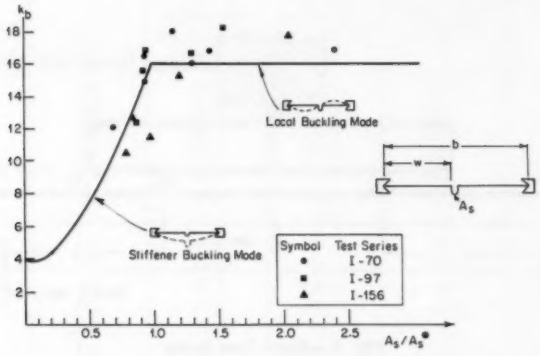

FIG. 7.—Comparison of Experimental and Analytical Buckling Coefficients

are shown in this figure. For the larger requirement, it is assumed that the neutral axis of bending of the stiffener coincides with its centroidal axis, and for the smaller it is assumed that the neutral axis of the stiffener coincides with the middle surface of the plate. Neither of these, however, is strictly correct. The stiffener attempts to bend about its centroidal axis, and the plate attempts to bend about its middle surface, as though each would buckle independently of the other. Because of compatibility of strains, shear stresses develop at the stiffener-plate juncture and the actual stiffener neutral axis is located somewhere between these two extremes. Based on a plane stress analysis, Seide (7) has derived an expression for the stiffener moment of inertia that reflects this change in neutral axis. The third stiffener requirement, shown in Fig. 11, is based on a stiffener moment of inertia due to the adjusted neutral axis. The stiffener requirement based on an adjusted neutral axis is not significantly different from that which assumes that the neutral axis is located at the plate's middle surface. Some design specifications (1) implicitly make

this assumption and for this case it appears to be valid. Nevertheless, the CBC stiffener requirement for intermediate stiffeners (and for edge stiffeners in Ref. 5) will be based on the adjusted neutral axis.

To assess the applicability of the CBC requirement, the observed ultimate strengths of several series of longitudinally stiffened elements are compared in Fig. 12. Each series consists of specimens with identical plate dimensions but different stiffener rigidities. An increase in stiffener rigidity beyond that required by the CBC increases the ultimate strength of the assembly to varying degrees. For test series I-47, I-70, I-97, and I-156, they are about 9%, 15%,

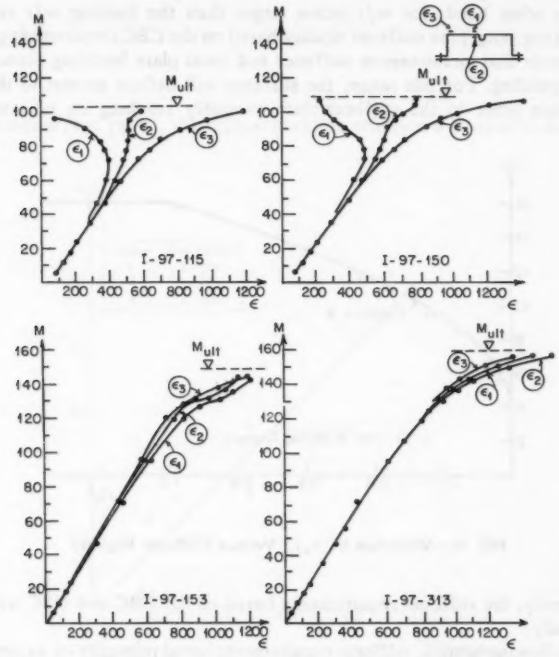

FIG. 8.--Post-Buckling Behavior of Intermediately Stiffened Assembly

12%, and 20%. Admittedly, an increase in the stiffener cross-sectional area contributes to some increase in ultimate strength; however, this increase amounts to a few percent at most. The significant increase in ultimate strength is attributed to the fact that stiffeners with larger rigidities retard the post-buckling deflections of the plate at the stiffener-plate juncture. This was demonstrated experimentally in Fig. 8 and was demonstrated analytically in Ref. 5 for edge-stiffened elements.

Also, it is apparent from Fig. 12 that for test series I-47 only small increases in ultimate strength are observed when the stiffener rigidity is increased beyond the CBC requirement. For such relatively small w/t ratios, this implies that

a stiffener requirement based on the CBC is not significantly different from one based on the USC; therefore, only for w/t ratios in the advanced post-buckling range is the CBC stiffener requirement excessively unconservative. The reason for this is covered later.

In the range of w/t ratios for which the component plate of width w remains fully effective (hereafter called the fully effective range), the stiffener rigidity based on the CBC requirement provides the minimum required support so that stiffener buckling occurs simultaneously with material yielding. Consequently, the stiffener remains unbuckled up to the ultimate failure load. The CBC and USC stiffener requirements are identical in this range.

On the other hand, for w/t ratios larger than the limiting w/t ratio (the post-buckling range) the stiffener rigidity based on the CBC requirement provides support such that simultaneous stiffener and local plate buckling occur before material yielding. For this range, the stiffener will deflect normal to the plane of the plate prior to the stiffener-plate assembly reaching its ultimate load.

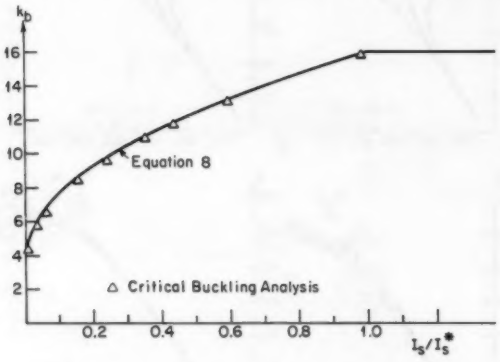

FIG. 9.—Variation of $(k_b)_{ps}$ Versus Stiffener Rigidity

Consequently, the stiffener requirements based on the CBC and USC will differ substantially.

In the following section, stiffener requirements based primarily on experimental results will be developed for the USC. It will be shown that for w/t ratios in the post-buckling range a stiffener requirement based on the CBC Requirement is insufficient for purposes of predicting ultimate strength.

USC.—In Ref. 5, the adequate edge stiffener requirement was expressed as a function of the w/t ratio normalized with respect to $(w/t)_a$, in which $(w/t)_a$ is the ratio below which the plate of width w is fully effective as an adequately stiffened element. For intermediate stiffeners, from Eq. 3(*b*):

$$\left(\frac{w}{t}\right)_a = 0.64\sqrt{\frac{k_w E}{\sigma_y}} \quad \ldots\ldots\ldots\

$$\left(\frac{w}{t}\right)_\alpha = \frac{221}{\sqrt{\sigma_y}} \quad \ldots\ldots\ldots\

$$\left(\frac{I_s}{t^4}\right)_{\text{adequate}} = \frac{100\left(\frac{w}{t}\right)}{\left(\frac{w}{t}\right)_\alpha} - 50 \quad \ldots\ldots\ldots\ldots\ldots\ldots\ldots\ldots\ldots\ldots \quad (16)$$

and is valid for

$$\left(\frac{w}{t}\right)_\beta < \left(\frac{w}{t}\right) \leq 1.5\left(\frac{w}{t}\right)_\alpha \quad \ldots\ldots\ldots\ldots\ldots\ldots\ldots\ldots\ldots\ldots \quad (17)$$

in which $(w/t)_\alpha$ is defined by Eq. 13, and $(w/t)_\beta$ is the flat width ratio below

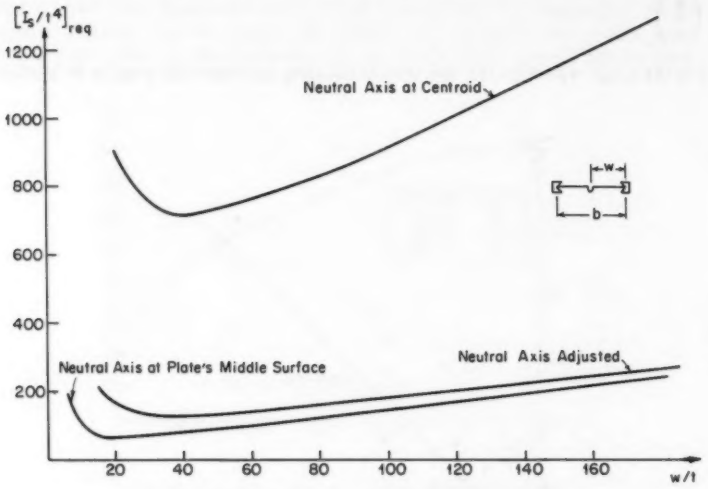

FIG. 11.—Stiffener Requirement Based on CBC

which a plate of width b (or $2w$) is fully effective without an intermediate stiffener.

$$\left(\frac{b}{t}\right)_\beta = \frac{221}{\sqrt{\sigma_y}} \quad \ldots\ldots\ldots\ldots\ldots\ldots\ldots\ldots\ldots\ldots\ldots\ldots \quad (18)$$

Eq. 18 can be expressed in terms of w if one substitutes $b = 2w$.

$$\left(\frac{w}{t}\right)_\beta = \frac{111}{\sqrt{\sigma_y}} \quad \ldots\ldots\ldots\ldots\ldots\ldots\ldots\ldots\ldots\ldots\ldots\ldots \quad (19)$$

For the range $w/t > 1.5\,(w/t)_\alpha$, a procedure similar to that for the edge-stiffened elements (5) is employed. Eight hypothetical stiffener requirements, A–H (in Fig. 13), will be compared to the test results. These requirements are arbitrarily drawn straight lines of increasing slope having a common origin at $(w/t)/(w/t)_\alpha$

equals 1.5. The requirement for which the predicted and experimental ultimate strengths are in best agreement will be suggested as a possible design requirement.

Comparison of Predicted and Experimental Ultimate Strengths

To facilitate a comparison of predicted and experimental ultimate strengths, two nondimensional ratios are used

$$R = \frac{(P_{ult})_1 - (P_{ult})_{ns}}{(P_{ult})_{as} - (P_{ult})_{ns}} \quad \ldots\ldots\ldots\ldots\ldots\ldots\ldots\ldots\ldots\ldots\ldots\ldots\ldots\ldots\ldots\ldots\ldots\ldots \quad (20)$$

and $$R_0 = \frac{(P_{ult})_t - (P_{ult})_{ns}}{(P_{ult})_{as} - (P_{ult})_{ns}} \quad \ldots\ldots\ldots\ldots\ldots\ldots\ldots\ldots\ldots\ldots\ldots\ldots\ldots\ldots\ldots\ldots\ldots\ldots \quad (21)$$

in which $(P_{ult})_1$ = predicted ultimate strength determined by the procedures

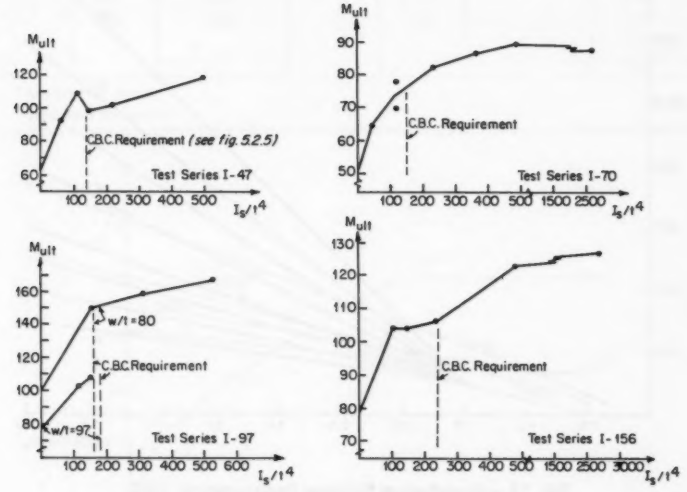

FIG. 12.—Variation of Ultimate Strength Versus Stiffener Rigidity

outlined for adequately or partially stiffened elements (whichever is appropriate); $(P_{ult})_t$ = experimental ultimate strength; and $(P_{ult})_{as}$ and $(P_{ult})_{ns}$ = predicted ultimate strengths for an adequately stiffened element and an element with no intermediate stiffener. All predicted ultimate strengths are determined by the effective width approach previously outlined.

These ratios normalize the predicted and experimental ultimate strengths such that they provide a measure of the degree to which the intermediate stiffener supports the flange. That is, if the ratios equal one, the ultimate strength of the intermediately stiffened flange equals that of an adequately stiffened flange; and if they equal zero, the ultimate strength equals that of a stiffened element

without an intermediate stiffener. In the following, experimental and predicted ultimate strengths are compared using the previously defined ratios.

Range $w/t_\beta < w/t \leq 1.5\ (w/t)_\alpha$.—For this range only one test series was conducted. For this series the ratios of experimental to predicted ultimate strengths R_0/R are given in Table 3 and are graphically compared in Fig. 14. In this range, the adequate stiffener requirement is given by Eq. 16, and $(k_b)_{ps}$ is determined from Eq. 9 with n equals 2.

Correlation between experimental and predicted ultimate strengths is satisfactory, which is to be expected since the required stiffener rigidity was adjusted based on this test series. It is noted, however, that the predicted ultimate strength of two adequately stiffened tests are overly conservative. This is attributed to the partial plastification of the webs of these beam specimens. It has been

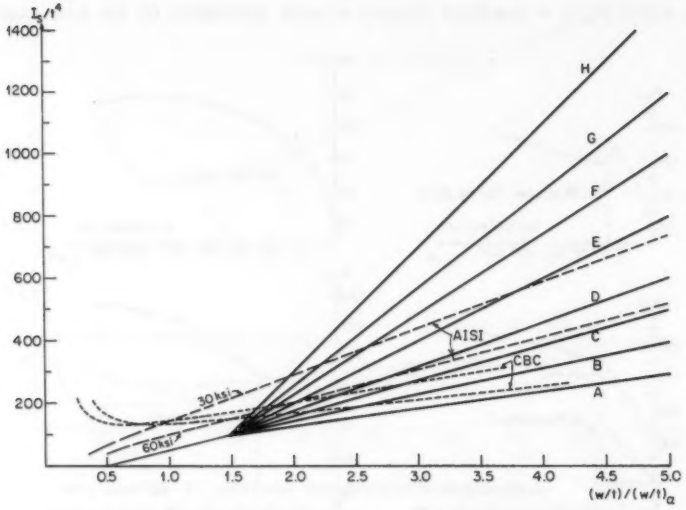

FIG. 13.—Hypothetical Stiffener Requirements: USC

shown (6) that compression flanges with w/t ratios of the order of, or significantly smaller than, $(w/t)_\alpha$ have an inelastic reserve capacity due to a partial plastification of the webs. Since this was not accounted for in the analysis, it is in all likelihood the reason for the predicted conservative ultimate strengths for several of these tests.

Range $w/t > 1.5\ (w/t)_\alpha$.—For this range, $(k_b)_{ps}$ is given by Eq. 9 as a function of $(I_s)_{adequate}$ and n. In the following comparisons of experimental and predicted ultimate strengths, eight hypothetical stiffener requirements are assumed for $(I_s)_{adequate}$ and several values for n (1–5) are considered. The comparisons of R_0 and R have been extended to determine both a satisfactory stiffener requirement and a good approximation of $(k_b)_{ps}$ for that requirement.

As in the comparison of ultimate strengths for the fully effective range, the ratios R_0/R are compared. To identify the value of n in these comparisons, R is subscripted by the appropriate integer n. Also, to determine the combination of buckling coefficient and stiffener requirement which best predicts the experi-

TABLE 3.—Intermediately Stiffened Elements: Comparison of Predicted and Experimental Ultimate Strengths in Range $(w/t)_\beta < w/t \leq 1.5\,(w/t)_\alpha$

w/t (1)	I_s/t^4 (2)	$I_s/(I_s)_{adequate}$ (3)	w/w_α (4)	R_0 (5)	Partially stiffened R_0/R (6)	Adequately stiffened R_0/R (7)
47.0	60.0	0.619	1.40	.853	1.09	
	110.	1.23		1.40		1.4
	142.	1.55		1.06		1.06
	217.	2.43		1.10		1.10
	499.	5.44		1.37		1.37
						1.23[a]
						0.177[b]

[a]Arithmetic mean.
[b]Standard deviation.

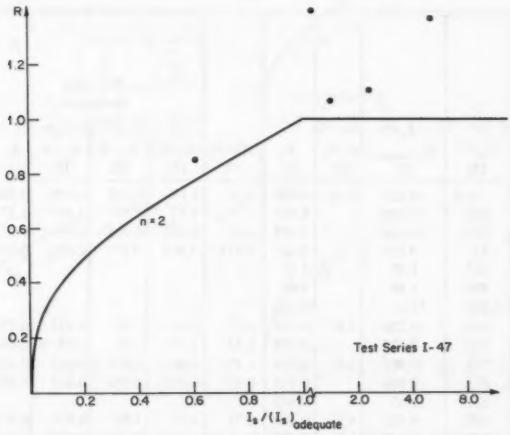

FIG. 14.—Comparisen of Experimental and Predicted Ultimate Strengths: $(w/t)_\beta < w/t \leq 1.5\,(w/t)_\alpha$

mental ultimate strengths, it is arbitrarily assumed that the predicted ultimate strength agrees satisfactorily with the experimental if

$$0.85 \leq \frac{R_0}{R} \leq 1.15 \quad \ldots\ldots\ldots\ldots\ldots\ldots\ldots\ldots\ldots\ldots\ldots\ldots\ldots\ldots\ldots\ldots\ldots\ldots \quad (22)$$

TABLE 4.—Number of Ultimate Strengths Accurately Predicted: Range $w/t \geq 1.5 (w/t)_o$

Stiffener requirement (1)	n				
	1 (2)	2 (3)	3 (4)	4 (5)	5 (6)
A	9	9	8	8	8
B	10	10	8	8	8
C	12	12	10	9	8
D	10	15	11	8	8
E	8	14	15	12	10
F	7	10	16[a]	16[a]	14
G	7	8	15	15	13
H	6	8	13	15	15

[a]The largest number of accurately predicted ultimate strengths.
Note: Sample = 17.

TABLE 5.—Comparison of Ultimate Strengths in Range $w/t \geq 1.5 (w/t)_o$: Intermediate Stiffener Requirement F

Test series (1)	w/t (2)	I_s/t^4 (3)	$I_s/(I_s)_{adequate}$ (4)	w/w_o (5)	R_0 (6)	R_0/R_1 (7)	Partially Stiffened: $I_s < (I_s)_{adequate}$ R_0/R_2 (8)	R_0/R_3 (9)	R_0/R_4 (10)	R_0/R_5 (11)	Adequately Stiffened: $I_s \geq (I_s)_{adequate}$ R_0/R (12)
I-70	70.	40.5	0.151	2.10	0.500	2.22	1.18	0.952	0.855	0.806	
		118.	0.480		0.993	1.75	1.43	1.34	1.30	1.27	
		118.	0.480		0.682	1.22	0.990	0.926	0.893	0.877	
		232.	0.937		0.887	0.935	0.917	0.917	0.909	0.909	
		367.	1.47		1.01						1.01
		488.	1.89		1.01						1.01
		2,650.	11.0		0.925						0.925
I-97	97.	115.	0.256	2.87	0.593	1.77	1.16	1.00	0.935	0.893	
		150.	0.320		0.689	1.72	1.22	1.09	1.03	1.00	
	80.	153.	0.461	2.37	0.704	1.29	1.04	0.971	0.935	0.917	
		313.	0.956		0.845	0.877	0.870	0.862	0.862	0.862	
		527.	1.53		0.962						0.962
I-156	156.	107.	0.121	4.57	0.500	2.73	1.35	1.06	0.935	0.870	
		147.	0.163		0.486	2.10	1.16	0.952	0.855	0.806	
		235.	0.256		0.563	1.70	1.12	0.971	0.901	0.862	
		477.	0.529		0.852	1.42	1.21	1.14	1.11	1.09	
		2,670.	3.06		0.900						0.900
						1.64[a]	1.14[a]	1.02[a]	0.960[a]	0.930[a]	0.961[a]
						0.539[b]	0.164[b]	0.129[b]	0.130[b]	0.133[b]	0.0495[b]

[a]Arithmetic mean.
[b]Standard deviation.

The number of tests that satisfies this inequality is given in Table 4 for each combination of stiffener requirement and n.

From this comparison, the experimental ultimate strengths are best predicted by requirement F, since the largest number of tests satisfies the foregoing inequality for this requirement. The requirement is expressed as

$$\left(\frac{I_s}{t^4}\right) = \frac{257\left(\frac{w}{t}\right)}{\left(\frac{w}{t}\right)_\alpha} - 285 \quad \ldots\ldots\ldots\ldots\ldots\ldots\ldots\ldots\ldots\ldots \quad (23a)$$

and is valid for

$$\frac{w}{t} > 1.5\left(\frac{w}{t}\right)_\alpha \quad \ldots\ldots\ldots\ldots\ldots\ldots\ldots\ldots\ldots\ldots \quad (23b)$$

In Table 5 the R_0/R ratios are given for stiffener requirement F. The arithmetic

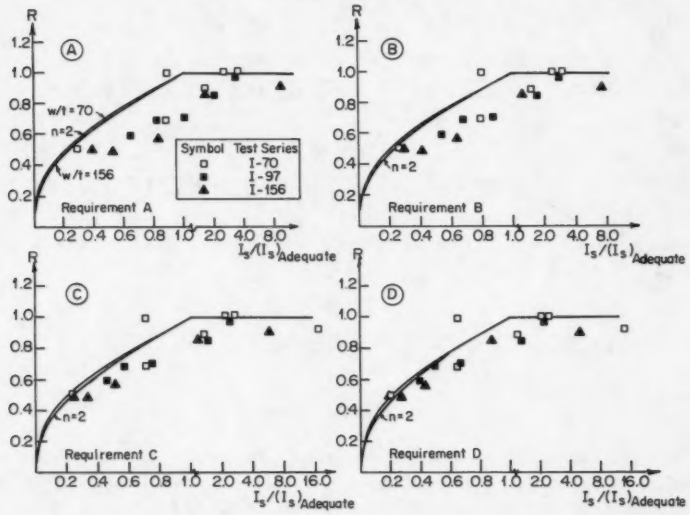

FIG. 15.—Comparison of Experimental and Predicted Ultimate Strengths: $w/t \geq 1.5\ (w/t)_\alpha$

mean and standard deviation of the ratios for adequately stiffened elements are 0.961 and 0.05. For partially stiffened elements, $n = 3$ is the best choice for n, since the predicted ultimate strengths are slightly more conservative for $n = 3$ compared to $n = 4$. The arithmetic mean and standard deviation for R_0/R_3 are 1.02 and 0.13, which are quite satisfactory.

The experimental and predicted R ratios are graphically compared for all

the stiffener requirements in Fig. 15, which confirms that the chosen requirement F is the most satisfactory of the eight. In each plot of Fig. 15, the upper curve is for $w/t = 70$ and the lower curve is for $w/t = 156$.

Limitations

The approach developed here is limited to intermediately stiffened elements whose stiffener width is small relative to the width of the assembly (i.e., w approx equals $b/2$ in Fig. 5). When w is considerably smaller than $b/2$ the equations for adequate stiffener rigidity and effective widths may be inappropriate. Two reasons are given for this:

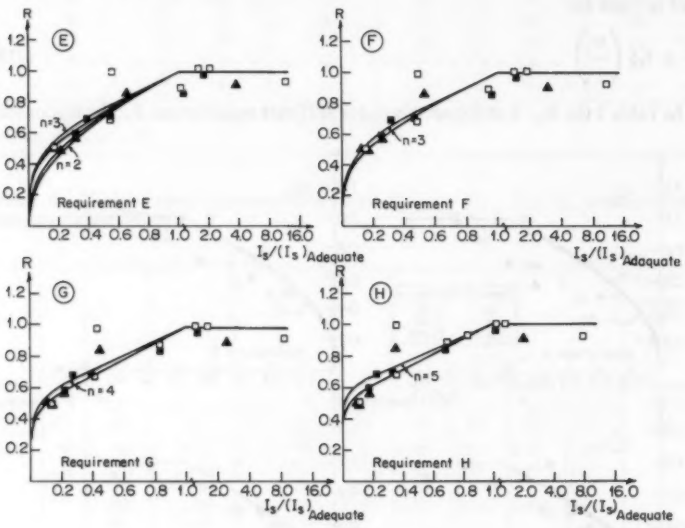

FIG. 15.—*Continued*

1. The critical buckling equation given in Ref. 2 for partially stiffened elements (and on which the aforementioned development is in part based) is not applicable to this case. In that derivation, it is assumed that w equals $b/2$.
2. The stiffener may itself be prone to local plate buckling, further complicating the behavior of the assembly.

These influences are currently under study at Cornell University with the objective of extending the approach developed here.

Summary and Conclusions

An approach has been presented for predicting effective widths of intermediately stiffened compression elements that are either adequately or partially

stiffened. A stiffener requirement that provides the minimum required stiffener rigidity to support these elements adequately is also presented.

Two criteria were considered for assessing the stiffener adequacy. For flanges which are in the range $(w/t)_\beta < w/t \leq 1.5\ (w/t)_\alpha$, a stiffener requirement based on a CBC appears satisfactory. For flanges having larger w/t ratios, a requirement based on an USC is necessary.

Acknowledgments

This research was sponsored at Cornell University by the AISI. The valuable cooperation of the Sheet Committees, and the cognizant task group is gratefully acknowledged.

Appendix I.—References

1. *Specification for the Design of Cold-Formed Steel Structural Members*, 1968 ed., American Iron and Steel Institute, New York, N.Y., 1968.
2. Barbré, R., "Buckling Stresses of Rectangular Plates with Longitudinal Stiffeners under Uniform Compression," *Der Bauingenieur*, Vol. 17, June, 1936 (in German); also, Translation #78, David Taylor Model Basin, Department of Navy, July, 1943.
3. Bryan, G. H., "On the Stability of a Plane Plate under Thrusts in its own Plane, with Applications to the Buckling of the Sides of a Ship," *Proceedings*, London Mathematical Society, Vol. 22, Dec., 1890, pp. 54–67.
4. Desmond, T. P., "The Behavior and Strength of Thin-Walled Compression Members with Longitudinal Stiffeners," *Department of Structural Engineering Report No. 369*, Cornell University, Ithaca, N.Y., Apr., 1977.
5. Desmond, T. P., Peköz, T., and Winter, G., "Edge Stiffeners for Thin-Walled Members," *Journal of the Structural Division*, ASCE, Vol. 107, No. ST2, Proc. Paper 16056, Feb., 1981, pp. 329–353.
6. Reck, H. P., Peköz, T., and Winter, G., "Inelastic Strength of Cold-Formed Steel Beams," *Journal of the Structural Division*, ASCE, Vol. 101, No. ST11, Proc. Paper 11713, Nov., 1975, pp. 2193–2203.
7. Seide, P., "The Effect of Longitudinal Stiffeners Located on One Side of a Plate on the Compressive Buckling Stress of the Plate-Stiffener Combination," *NACA Technical Note 2873*, National Advisory Committee for Aeronautics, Jan., 1953.
8. Stowell, E. Z., Heimerl, G. J., Libove, C., and Lundquist, E. E., "Buckling Stresses for Flat Plates and Sections," *Proceedings*, ASCE, Vol. 77, July, 1951, pp. 1–31.

Appendix II.—Notation

The following symbols are used in this paper:

A_s = cross-sectional area of intermediate stiffener;
A_s^* = characteristic stiffener cross-sectional area at which stiffener buckling and plate buckling occur simultaneously;
$(A_s)_{ps}$ = effective cross-sectional area of partial intermediate stiffener;
b = total width of intermediately stiffened assembly;
b_{eff} = effective width of plate components of intermediately stiffened assembly of width b;
b_α = limiting width of stiffened plate with adequate size intermediate stiffener below which it is fully effective;
b_β = limiting width of a simple stiffened plate (i.e., stiffened element with no intermediate stiffener) below which it is fully effective;

E = Young's modulus = 30,000 ksi (210,000 NM/m^2);
I_s = moment of inertia of edge stiffener taken about its centroidal axis parallel to flange;
I_s^* = characteristic stiffener centroidal moment of inertia at which local plate buckling of flange and stiffener buckling occur simultaneously;
$(I_s)_{adequate}$ = required minimum stiffener moment of inertia necessary to adequately support flange;
k_b = buckling coefficient for plate of width b;
$(k_b)_{as}$ = buckling coefficient of intermediately stiffened assembly that is adequately stiffened;
$(k_b)_{ps}$ = buckling coefficient of intermediately stiffened assembly that is partially stiffened;
$(k_b)_{ns}$ = buckling coefficient of simple stiffened element of width b;
k_w = buckling coefficient for plate of width w;
L = supported length of beam specimens;
LS = distance from concentrated load to support in beam tests;
M_{ult} = experimental ultimate bending moment of beam specimens;
n = integer;
$(P_{ult})_{as}$ = predicted ultimate strength of intermediately stiffened assembly with adequate size stiffener;
$(P_{ult})_1$ = predicted ultimate strength of adequately, partially, or simple stiffened element (whichever is appropriate);
$(P_{ult})_{ns}$ = predicted ultimate strength of simple stiffened element (i.e., stiffened element with no intermediate stiffener);
$(P_{ult})_t$ = experimental ultimate strength;
R = normalized predicted ultimate strength;
R_0 = normalized experimental ultimate strength;
t = thickness;
w = width of component plate of intermediately stiffened assembly;
w_{eff} = effective width of plate of width w;
w_a = limiting width of flange below which it is fully effective as stiffened element of width w;
ν = Poisson's ratio;
σ_{cr} = $k_w \pi^2 E/12(1-\nu^2)(w/t)^2$ = critical buckling stress;
σ_y = material yield stress, in kips per square inch (1 ksi = 6.9 NM/m^2); and
ϕ_b = flange aspect ratio.

JOURNAL OF THE STRUCTURAL DIVISION

PROPOSED STEEL COLUMN STRENGTH CRITERIA

By Dann H. Hall,[1] M. ASCE

INTRODUCTION

For 200 yr the strength of metal columns has received considerable attention. The Euler formula derived for elastic columns has been shown by tests to give an upper bound for rather slender columns. The inelastic range of column slenderness has proven much more elusive to quantify. Strength of such columns depends strongly on at least two parameters, residual stresses and crookedness, not quantifiable by the designer. Accordingly, it is not surprising that the scatter in the inelastic range of column strength is larger than that for most other structural members.

It was not until the 1940s that Shanley explained the inelastic column failure mechanism as we presently understand it (19). This mathematical solution for column strength is iterative and best handled by computer (1,2). Shanley's model has been used to accurately predict the strength of many column tests if sufficient detailed information is provided. Because of the lack of a closed solution at this time and the large scatter in strength, column design equations must be empirical in the inelastic range of slenderness. The basis of the equations is either physical tests or theoretically calculated column strengths.

This paper presents the development of empirical column strength criteria based on physical tests of steel columns. These tests are the only sound evidence that includes all of the variables in real steel columns. However, most of the tests have pinned ends; thus, the tests do not simulate an actual column in a building with end restraints.

The test data can be fitted with the Euler hyperbola in the elastic range. The inelastic range of column strength can be represented by a sloping straight line from the Euler curve to a horizontal plateau in the lowest slenderness. The column data are further examined to provide a compression resistance factor, Φ_c, which can be used in the load and resistance factor design (LRFD)

[1]Consulting Engr., Technical Services Div., Engrg. Dept., Bethlehem Steel Corp., Bethlehem, Pa. 18016.

Note.—Discussion open until September 1, 1981. To extend the closing date one month, a written request must be filed with the Manager of Technical and Professional Publications, ASCE. Manuscript was submitted for review for possible publication on August 13, 1980. This paper is part of the Journal of the Structural Division, Proceedings of the American Society of Civil Engineers, ©ASCE, Vol. 107, No. ST4, April, 1981. ISSN 0044-8001/81/0004-0649/$01.00.

of steel buildings. The resistance factor is a measure of the reliability that can be assigned to the nominal strength predictor. The smaller the scatter of test results, the closer to 1.0 is the resistance factor.

Column Behavior

The most common shapes of steel columns have a cross-sectional configuration which generally buckles in the pure flexural mode. These sections include rolled I-shapes, rectangular boxes, and solid and hollow rounds. Other shapes, such as angles, are subject to flexural-torsional buckling and are not considered. Also, sections which have critical local buckling of elements of the cross section are not considered in this study.

Flexural buckling of columns can be divided into three regions of slenderness. The lowest slenderness columns fail by yielding in compression. The strength of these stub sections is a function of cross-sectional area, compressive yield stress, and strain hardening. Columns in the intermediate range of slenderness have strengths dependent on a number of additional variables, including slenderness, initial straightness, tensile yield stress, elastic modulus, moment of inertia, residual stresses, and end conditions. Columns with large slenderness fail by elastic buckling where slenderness, end conditions, initial straightness, elastic modulus, and moment of inertia are the determinant variables.

Curve Fitting of Test Data

The test data used in these statistical studies were collected from many aggregations of tests performed over the past 30 yr by various investigators. Much of these data were cataloged and reported in Ref. 12.

Column test data may be examined by plotting the average compression stress at failure versus slenderness as the independent variable. In order to compare columns having different yield stress, it is common to nondimensionalize the strength and slenderness by the yield stress. The compressive stress at failure is divided by the yield stress. Slenderness is transferred to λ, in which $\lambda = (l/r)\sqrt{F_y/(\pi^2 E)}$. The transformation of slenderness is derived from the elastic buckling equation. In this study, the test data were nondimensionalized in this manner using laboratory-measured tensile yield stresses.

Table 1 gives a breakdown, by column type, of the 393 tests included in the data base. The rolled H-shapes in parentheses were part of a single major test effort. The scatter in these data was less than in the remaining data, indicating that test methods may have introduced some of the observed scatter.

The data were divided into two categories—columns with l/r less than 110, and those with slenderness of 110 or greater. The more slender columns were assumed to behave as elastic members and fit a hyperbola. A plot of the data in Fig. 1 indicates this to be true. The less slender columns exhibited greater scatter, and the best curve type was not apparent.

In order to select an appropriate curve for the inelastic range, test data of shapes with the maximum residual stress reported were selected from the 393 values. Forty-four such column tests were identified. Appendix I shows a summary of a statistical analysis of 15 various combinations of four parameters: nondimensional slenderness, measured yield stress, maximum measured compressive

residual stress, and shape of the cross section. Based on these results, a simple straight line relationship between strength and nondimensional slenderness was selected because it was statistically as good as the others, and from the designer's point of view it was the simplest.

TABLE 1.—Column Data Base

Type of shape (1)	Welded H[a] (2)	Rolled H (European)[b] (3)	Riveted[c] (4)	Welded box[d] (5)	Solid rounds[e] (6)	Coverplated H[f] (7)	Totals[g] (8)
			(*a*) Material				
Flame cut	14			4			18
As-rolled	5	321 (269)	9	10		2	347
Anneal		2					2
Cold straightened		1			22		23
Sheared edge	3						3
			(*b*) Axis				
X	3	6	2				11
Y	19	318 (269)	7	10		2	356
Not applicable				4	22		26
			(*c*) Steel Grade				
A7	6	26	3	10		2	47
A36	6	23	6				35
A242		4					4
T1	10	2		4	22		38
ESSC (F'_Y = 34 KSI)		(269)					269
			(*d*) Test Condition				
Pinned	22	324 (269)	9	14		2	371
Other					22		22
			(*e*) Slenderness				
<40	7	7	6	5	11		36
40≤ $KL/\bar{R}$ < 110	15	237 (190)	3	9	11	2	277
≥110		80 (79)					80

[a]22 tests were plotted; information taken from Refs. 4, 6, 13, 14, 17, 21, and 22.
[b]324 (269) tests were plotted; in formation taken from Refs. 5, 11, 16, 17, 18, 22, 23, 24, and 26.
[c]9 tests were plotted; information taken from Refs. 17 and 26.
[d]14 tests were plotted; information taken from Refs. 4, 14, and 26.
[e]22 tests were plotted; information taken from Refs. 7, 9, 15, and 25.
[f]2 tests were plotted; information taken from Ref. 16.
[g]393 tests were plotted.
Note: Ref. 12 was used as the basic reference to build this data base.

The nondimensionalized data were further divided into two categories of yield stress: column tests with nominal yield stress between 33 ksi and 36 ksi (227.7 mPa and 248.4 mPa), and column tests with nominal yield stress of 100 ksi

(690 mPa). No columns were tested with slenderness greater than 110 for 100 ksi (690 mPa) yield stress; so there were three groups of tests to curve fit. This division by yield stress was made to investigate the possible effect of yield stress not accounted for correctly in the nondimensionalization process. The laboratory tensile yield stress was used to nondimensionalize each test result.

Table 2 gives pertinent statistics from the regression analysis. The following

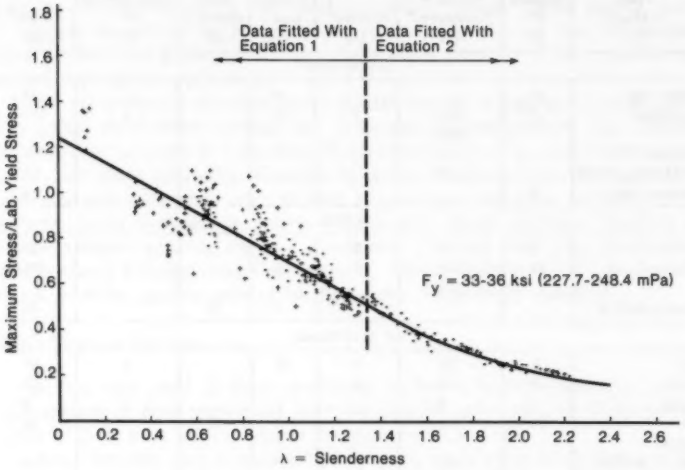

FIG. 1.—Test Data and Regression Equations

are the regression equations from nondimensional test data for the three fitted curves:

$$\frac{F_{ult}}{F_y'} = 1.24 - 0.53\lambda \quad \ldots\ldots (1)$$

$$\frac{F_{ult}}{F_y'} = \frac{0.937}{\lambda^2} \quad \ldots\ldots (2)$$

$$\frac{F_{ult}}{F_y'} = 1.20 - 0.45\lambda \quad \ldots\ldots (3)$$

Eq. 1, with a coefficient of determination, R^2, of 0.74, explains 74% of the observed variation, which is better than any of the equations reported in Appendix I. One reason for the improvement is that Eq. 1 is based on a number of tests with many replications, whereas the equations in Appendix I were based on unreplicated data. The largest error reported for Eq. 1 was 45%. The largest errors were associated with test specimens of low yield stress. Some of these specimens had reported laboratory yield stress as low as 28 ksi. This is not

representative of modern structural steel grades.

Eq. 2 is a hyperbola very similar to the Euler equation. The coefficient of determination is 0.96. This increase over the R^2 for the inelastic region is to be expected because elastic buckling, which is dominant in this region of slenderness, has fewer parameters affecting strength. Also, calculation of λ is theoretically correct in the elastic region, whereas, the use of lambda in the inelastic region may introduce scatter. Eqs. 1 and 2 are plotted with the data used in their development in Fig. 1.

Eq. 3 is for columns of material with nominal yield stress equal to 100 ksi (690 mPa). There were 36 data points in this category. The coefficient of determination is 0.77, which is similar to that for Eq. 1. However, the largest error has been reduced to 23%, from 45% for Eq. 1. This reduction is, in

TABLE 2.—Regression Equations from Nondimensional Test Data

Equation number (1)	Nominal yield stress, in kips per square inch (2)	R^2, adjusted (3)	Correlation coefficient (4)	Largest error, as a percentage (5)
1	33–36	0.74	−0.86	45
2	33–36	0.96	−0.98	21
3	100	0.77	−0.88	23

*6.9 ksi = 1 mPa.

part, due to the smaller scatter in yield stress. Eq. 3 is plotted with the data used in its development in Fig. 2.

Nominal Strength Equations

The similarity between Eqs. 1 and 3 leads to the decision to combine columns of nominal yield stress material from 33 ksi–100 ksi (227.7 mPa–690 mPa) into a single equation. This combination results in Eq. 4.

$$\frac{F_{ult}}{F'_y} = 1.3 - 0.57\lambda' \quad \ldots\ldots\ldots\ldots\ldots\ldots\ldots\ldots\ldots\ldots\ldots\ldots\ldots\ldots\ldots\ldots (4)$$

in which $\lambda' = (l/r)\sqrt{F'_y/\pi^2 E}$. Eq. 4 represents the nominal strength of columns of both levels of yield stress 33 ksi–36 ksi and 100 ksi (227.7 mPa–248.4 mPa and 690 mPa) in the inelastic range of slenderness. Eq. 4 is tangent to the Euler hyperbola at $\lambda = 1.53$. It has been modified to account for a 7% difference between actual average yield stress and minimum specified yield stress. This modification is shown in Appendix III. For slenderness greater than 1.53, the Euler hyperbola represents column strength. The fitted hyperbola in the elastic range is modified to coincide with the Euler curve. The mathematics of this modification is shown in Appendix II. For slenderness greater than 1.53, the Euler hyperbola represents the nominal column strength.

A further modification is made in the low slenderness range because Eq.

4 predicts a column strength of 1.3 times the yield strength when $\lambda = 0$. Although tests indicate the strength of some columns may be this high, it is doubtful that such a high value represents typical behavior. Local buckling limits in the code are based on yield point. Galambos (10) reports that the mean value of the average measured static tensile yield stress in steel cross sections is 7% above the nominal yield stress. The range of static tensile yield stress values is lower than the scatter of column strengths in the low slenderness range. This difference is likely due to strain hardening and possibly higher compression yield stress. A plateau has been placed at $1.10F_y$ for steels with nominal yield stress of 65 ksi or less to recognize some benefit for overrun of yield stress and strain hardening. Steels with nominal yield stress over 65 ksi do not exhibit the same overrun in yield stress. Therefore, the plateau for these steels has

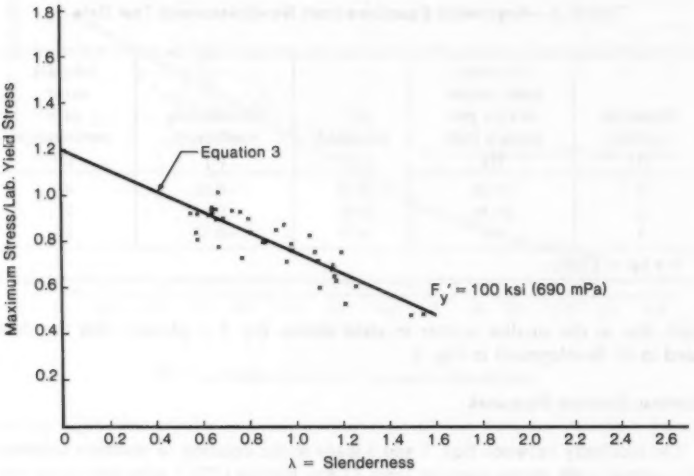

FIG. 2.—Test Data and Regression Equations

been placed at $1.0F_y'$. The following are the nominal column strength equations:

$$R_{nc} = 1.1QF_y'A_g, \quad 0 \le \lambda \le 0.35 \quad \text{for} \quad F_y' \le 65 \text{ ksi};$$

$$R_{nc} = 1.0QF_y'A_g, \quad 0 \le \lambda \le 0.53 \quad \text{for} \quad F_y' > 65 \text{ ksi} \quad \ldots\ldots\ldots\ldots\ldots (5)$$

$$R_{nc} = \left[1.3 - 0.57\left(\frac{kl}{r}\right)\sqrt{\frac{QF_y'}{\pi^2 E}}\right] QF_y'A_g, \quad 0.35 \le \lambda \le 1.53 \quad \ldots\ldots\ldots (6)$$

$$R_{nc} = \frac{\pi^2 EA_g}{\left(\frac{kl}{r}\right)^2}, \quad \lambda > 1.53 \quad \ldots\ldots\ldots\ldots\ldots\ldots\ldots\ldots\ldots (7)$$

in which Q = a shape factor which accounts for certain cross section proportions

and is equal to 1.0 for the shapes tested. Refs. 20 and 27 cover Q. Because these equations are intended for design use, they are written in terms of the minimum specified yield stress, F_y'. The term R_{nc} is the nominal resistance of compression members.

Resistance Factor

The LRFD model employed by Galambos and Ravindra (10) utilizes the coefficient of variation (COV). The COV is determined by dividing the standard deviation by the mean value, σ/μ. In many instances, the variance is constant over the range and the mean differs. The result is that the COV is not constant. In the column case, the mean value decreases with increasing slenderness. Thus, the COV becomes larger with increasing slenderness if standard deviation is constant over the range. This problem is evident in Table 3 which presents a summary of calculations used to determine a weighted COV for the column data based on the fitted curve. Calculated mean values of strength at midrange

TABLE 3.—Coefficient of Variation from Test Data in Inelastic Range

$\lambda_{segment}$ (1)	λ_{mean} (2)	F_{ult}/F_y (3)	σ (4)	Segmented COV (5)	n (6)	Weighted COV[a] (7)
0.35–0.55	0.45	1.0435	0.013	0.012	26	0.313
0.56–0.75	0.65	0.930	0.092	0.099	54	5.346
0.76–0.95	0.85	0.816	0.081	0.100	59	5.900
0.96–1.05	1.0	0.730	0.098	0.134	20	2.680
1.06–1.25	1.10	0.673	0.056	0.087	77	6.699
1.26–1.55	1.35	0.531	0.060	0.119	22	2.618
					258[b]	23.556[b]

[a]Weighted COV = 23.556/258 = 0.0913.
[b]Total.

λ are used as the mean for each λ segment. The standard error of the estimate has been used as an estimate of the standard deviation as done by Galambos. Comparison of the weighted COV indicates it is a fair representation of the segmented COV values in Col. 5.

The compressive resistance factor, Φ_c, is calculated in Appendix II for the entire range of slenderness. The COV in the elastic range is smaller than that determined in Table 3 for the inelastic range. As a result, the resistance factor, Φ_c, is larger. For the sake of simplicity, the hyperbola has been shifted upward to coincide with the Euler curve, as previously mentioned, and the resistance factor has been reduced a like amount. The result is a constant resistance factor of 0.78 over the entire slenderness range.

Comparison of Results to Data

The regression analysis has combined all column types. Each type of column included in the set will be compared to the nominal strength curve and this curve reduced by the compression resistance factor, Φ_c.

ROLLED SHAPES

The results of 324 rolled shape column tests shown on Fig. 3 are compared to a plot of the proposed nominal column strength, and Φ_c times the nominal column strength. The data plotted in Fig. 3 include seven tests of W12 × 161 and 16 tests of their European counterpart, HEM 340. The slenderness of these 23 columns is either 50 or 95. Their laboratory measured tensile yield stress was between 27 ksi and 35 ksi. The results of all tests of rolled shapes, except five W12 × 61 tests at $l/r = 50$, fall above the $\Phi_c(R_{nc})$ curve. The points below the $\Phi_c(R_{nc})$ curve were tests performed on American shapes that were not straightened. Some of the columns were too crooked to meet American Society of Testing and Materials (ASTM) A6 straightness requirements, and could not have been sold for structural members.

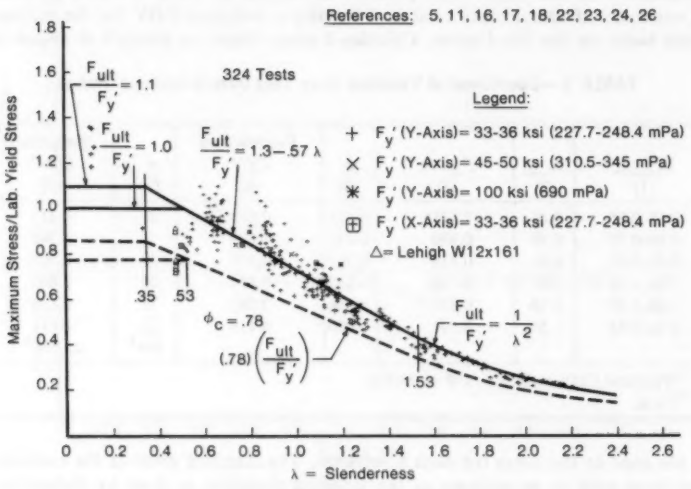

FIG. 3.—Rolled H Test Data

Fig. 4 shows test values of the W12 × 161 sections with $l/r = 50$ plotted against maximum initial crookedness. These tests were performed using two different loading methods. The earlier tests were performed by centering the member in the end fixtures so that nearly equal strains were generated at the midheight of the column for low loads. This method of loading is called the "old Lehigh method." The more recent tests were performed with the loads applied at the geometric center at the ends of the column. The figure dramatically demonstrates the effect of both initial crookedness and test method on column strength. Those specimens tested by geometrically centering the load at the ends of the column are further divided between dynamic and static tests. Test values determined at both testing rates were nondimensionalized by the same laboratory determined static tensile yield stress.

Figs. 5 and 6 show measured residual stresses in the American W12 × 161 section which has not been straightened and the similar European section, HEM 340, which may have been straightened and thus is representative of normal practice. The HEM 340 sections all had test strengths greater than $\Phi_c(R_{nc})$. These HEM 340 sections were tested with the load applied to the geometric center of the cross section at each end of the column.

Literature provides little specific information concerning the effect of cold straightening on the strength of columns, although crookedness has long been identified as a contributor to premature column failure. Cold straightening has two beneficial effects. First, the straightened column is subjected to smaller initial bending moments due to crookedness. Second, cold straightening tends to reduce any longitudinal residual stresses due to differential cooling during rolling or welding, or due to cold forming.

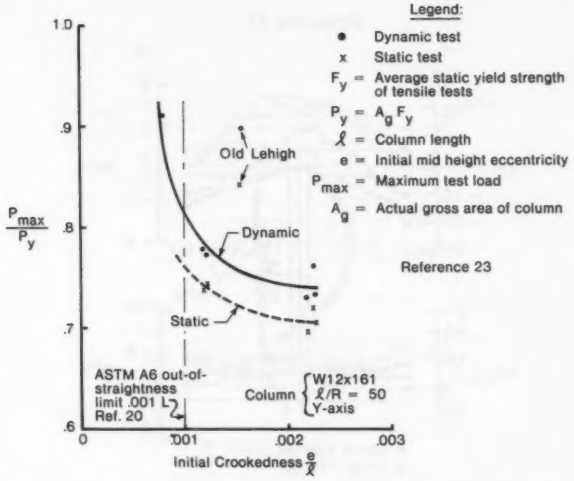

FIG. 4.—Column Strength Versus Initial Crookedness

Columns are straightened in several ways. Rotary straightening of rolled shapes is performed on the majority of steel product less than 100 lbs/ft (149 kg/m) and 18 in. (457 mm) deep, although the capability to straighten different shapes varies between mills. Rotary straighteners bend the section back and forth over a sharp radius, causing plastic deformations which obliterate previous residual stresses. This is a continuous process affecting the entire length of product. The residual stresses resulting from this process are reported to be rather small.

The gag press is used to straighten large sections that cannot be rotary straightened. Gag straightening is done intermittently, and the effect on residual stresses is rather unpredictable, except it is unlikely to induce residual stresses greater than half of the yield stress.

Small sections are sometimes straightened by stretching, which also eliminates

residual stresses. This process is most often used on aluminum sections.

The tests of rolled shapes, except the excessively crooked atypical W12 × 161 sections, confirm that the proposed design criterion is safe. The unstraightened shapes confirm the rationale of limiting crookedness of steel compression members, even in the rather low range of slenderness.

Welded Box-Shapes and H-Shapes

Tests of 22 welded H-shapes and 14 welded box shapes are plotted with the R_{nc} and $\Phi_c(R_{nc})$ curves on Figs. 7 and 8, respectively. These test data, except for three points, lie above the $\Phi_c(R_{nc})$ curve with the central tendency somewhat below the R_{nc} curve. This plot confirms that the design criteria are compatible with the physical evidence of welded column shapes, except for

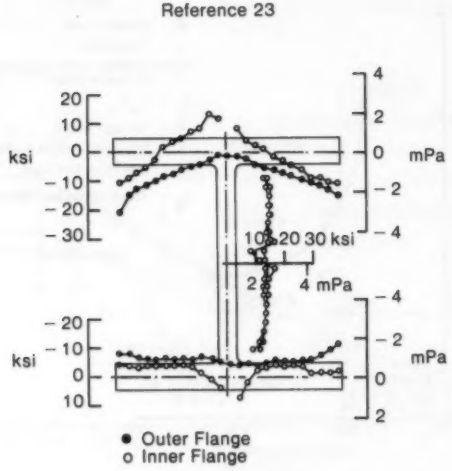

FIG. 5.—Residual Stresses in W12 × 161

the three low values for tests of H-shapes which deserve further investigation.

The three low points were tests of the shape shown in Fig. 9. These tests were performed in the mid 1950s when structural welding was in its infancy and A7 steel was the common structural grade. The welding was done semiautomatically, using the submerged arc process. Wire size was 5/64 in.; voltage was 30 V; amperage was 375 amps; and welding speed was about 20 in./min. The relatively low heat input probably deposited considerably less weld, and provided less fusion than would be acceptable by today's standards. More heat input would most likely have caused distortion of the section, resulting in subsequent straightening which would have modified residual stress patterns. The actual specimens were reported to be very straight, with maximum initial crookedness less than 0.001l. Modern welded H-shapes would have higher yield

stress, thus reducing the effect of residual stresses.

Although there were three low values for some of the earliest welded columns, the proposed criteria safely represent the strength of modern welded columns evidenced by tests.

Riveted Shapes and Coverplated H-Shapes

The test data for nine riveted columns shown in Fig. 10 fall around the nominal strength. The scatter, although substantial, seems to be less than that of the welded columns. This may be due to the smaller variation of residual stresses, straightness, or yield strength. The only two tests of rolled H-shapes with welded

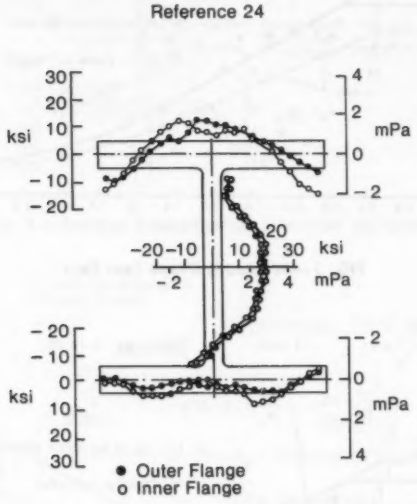

FIG. 6.—Residual Stresses in HEM 340 (Italy)

coverplates reported are also shown in Fig. 10. These types of columns may also be safely represented by the proposed criteria.

Solid Round Shapes

Tests of 22 solid round bars are presented in Fig. 11. All tests are of 100-ksi (690-mPa) yield stress material. Unlike the other column tests with pinned ends, these tests were made on flat end specimens. Strain gages were used to determine the inflection points so that effective slenderness could be determined. The effective slenderness was used to plot points on Fig. 11. These points are well-distributed about the fitted line, indicating that the strength of this column type can be represented by Eq. 3.

Comparisons of Results to Other Models

Fig. 12 compares the $\Phi_c(R_{nc})$ curve developed in this work with the $\Phi_c(R_{nc})$ curve proposed by Galambos (8) and the Canadian limit state specification (3).

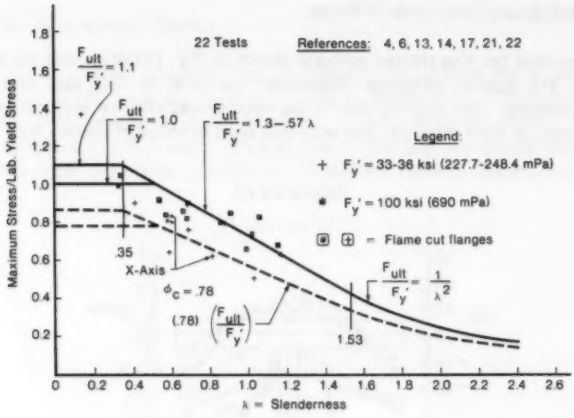

FIG. 7.—Welded H-Shape Test Data

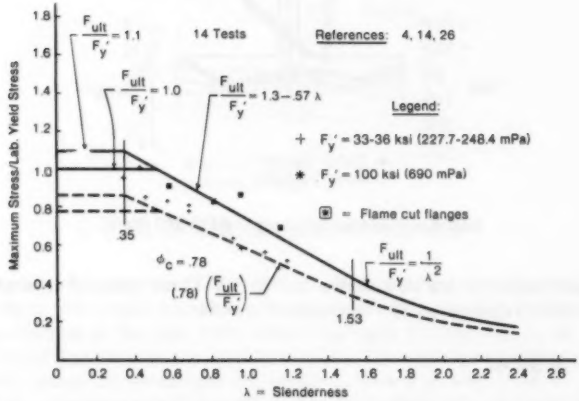

FIG. 8.—Welded Box Test Data

Additional abscissas of l/r for F_y equal 36 ksi and 50 ksi (248.4 mPa and 345 mPa) are also shown. The proposal by Galambos results in nearly a straight line which lies somewhat below this proposal. The Canadian limit state criterion crosses the proposed curve several times, but closely parallels it over the entire

slenderness range. The proposal by Galambos, which was based on a theoretical model of column behavior rather than test results, indicates that a straight line is a reasonable representation of column strength. Among the reasons why

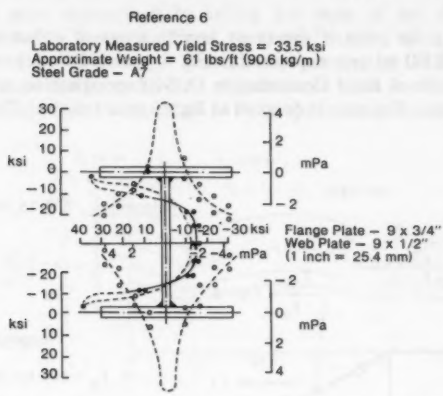
Reference 6
Laboratory Measured Yield Stress = 33.5 ksi
Approximate Weight = 61 lbs/ft (90.6 kg/m)
Steel Grade – A7
ksi
mPa
40 30 20 10 10 20 30 ksi
4 2 2 4 mPa
Flange Plate – 9 x 3/4"
Web Plate – 9 x 1/2"
(1 inch = 25.4 mm)

FIG. 9.—Residual Stress Pattern in Welded Member

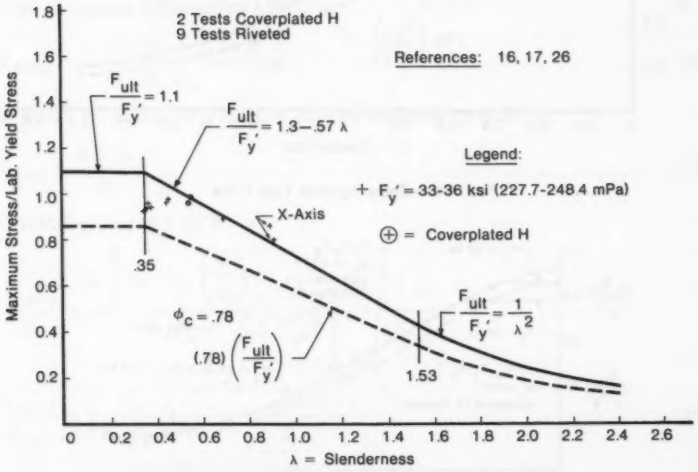

FIG. 10.—Coverplated H and Riveted Test Data

the Galambos curve is lower is the fact that this model was not adjusted for the actual yield stress of columns which is reported to be about 7% higher than minimum specified for hot-rolled shapes. A second reason is that it is

based on the conservative assumption of all columns having the maximum allowable initial curvature.

Comparison of Proposal to American Institute of Steel Construction

Fig. 13 shows the ratio of the cross section areas of columns designed by the proposed LRFD criteria expressed in Eq. 8 (which follows) and the present American Institute of Steel Construction (AISC) specification as expressed in Eq. 9 (also follows). The ratio is denoted as Eq. 10 (also follows). This comparison

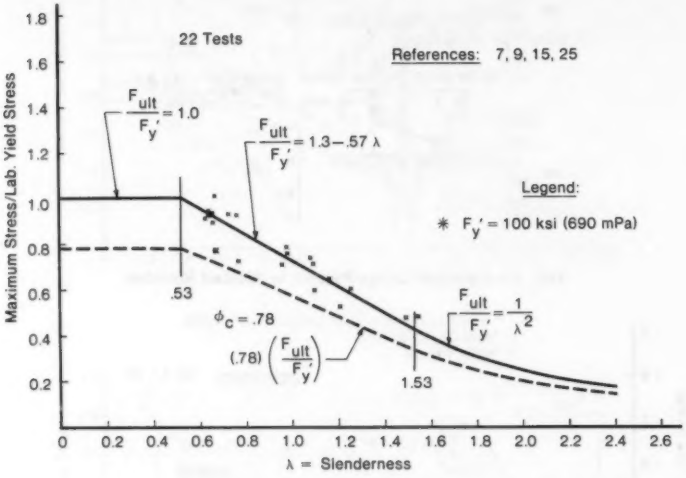

FIG. 11.—Solid Rounds Test Data

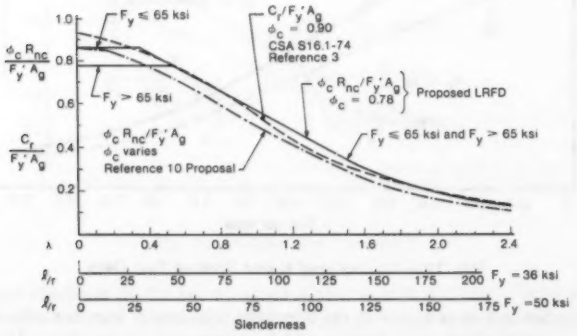

FIG. 12.—Comparison of Three Column Criteria

assumes that the slenderness, l/r of the two columns being compared is constant. The comparison is made for different ratios of live and dead load to demonstrate the dissimilarity due to varying load factors applied to dead and live loads. Three Φ_c values are presented on the ordinate.

The curves were determined by taking the ratio of the AISC allowable compressive stress to the stress found by multiplying Φ_c by F_{nc}, in which F_{nc} is the stress corresponding to R_{nc}. This ratio is corrected by the ratio of factored loads in load factor design to the ratio of unfactored loads used in AISC working stress design (20). This relationship is developed as shown in the following.

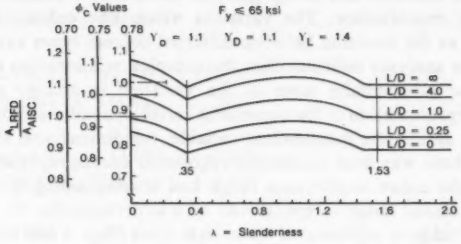

FIG. 13.—Comparison of Column Areas: Proposed LRFD and AISC

Area of column designed by LRFD is:

$$A_{LRFD} = \frac{\gamma_o [\gamma_D(D) + \gamma_L(L)]}{\Phi_c F_{nc}} \quad \ldots\ldots\ldots\ldots\ldots\ldots\ldots\ldots\ldots\ldots (8)$$

in which $F_{nc} = R_{nc}/A_g$. Area of column designed by AISC is:

$$A_{AISC} = \frac{D + L}{F_a} \quad \ldots\ldots\ldots\ldots\ldots\ldots\ldots\ldots\ldots\ldots\ldots\ldots\ldots\ldots (9)$$

Divide Eqs. 8 and 9 by D:

$$\frac{A_{LRFD}}{D} = \frac{\gamma_o \left[\gamma_D - \gamma_L \left(\frac{L}{D}\right)\right]}{\Phi_c F_{nc}}; \quad \frac{A_{AISC}}{D} = \frac{1 + \frac{L}{D}}{F_a};$$

$$\frac{A_{LRFD}}{A_{AISC}} = \left(\frac{F_a}{\Phi_c F_{nc}}\right) \frac{\gamma_o \left[\gamma_D + \gamma_L \left(\frac{L}{D}\right)\right]}{1 + \frac{L}{D}}; \quad \ldots\ldots\ldots\ldots\ldots (10)$$

The proposed design criteria will provide some economy over the entire range of slenderness when the live and dead loads are equal ($L/D = 1.0$). When live load is greater than dead load ($L/D > 1.0$), the proposed criteria may require larger columns. If there is only live load, this difference in column size can be nearly 10%.

Conclusions

1. Unlike many structural elements, the strength of steel compression members is significantly affected by several factors not quantifiable by the designer.
2. All column design equations are empirical in that they represent a range of column strengths. However, they cannot be derived from column theory as it is presently understood.
3. Data from 393 tests indicate that there is a large scatter of column strengths when plotted against slenderness. The variation is due to variables within a group of similar columns and to the inherent difference between column types and method of manufacture. The variation within one column type appears nearly as large as the variation between different column types examined.
4. Regression analyses indicates that the complex relationships examined did not account for substantially more of the variation in column strength than a straight line representation of the dependent variable, nondimensional maximum average stress, against the independent variable, nondimensional slenderness.
5. The data base was used to develop regression curves representing column strength over the entire slenderness range and corresponding Φ_c values. The strength in the elastic range is represented by a hyperbola (Eq. 7). The strength in the inelastic range is represented by straight lines (Eqs. 5 and 6).
6. The proposed design criteria are very similar to the Canadian Limit State criterion. They are slightly less conservative than the criteria proposed by Galambos. They provide for columns slightly larger than present AISC if all the load is live load. As the portion of dead load increases, this proposal provides designs increasingly less conservative than present AISC until the load is all dead load, and the reduction is 15%–20% in column area compared to AISC.

Appendix I.—Regression Equations Using Various Independent Variables

The 15 regression equations presented in the following were developed to ascertain whether the inclusion of more parameters or a parabola, or both, would provide a better fit for column strength than a straight line. The investigation was limited to the inelastic range.

Fortyfour column tests were used to develop the following regression equations. Only those tests which considered maximum compressive residual stresses (σ_r), shape of the cross section (K), laboratory yield stress (F_y), and slenderness (λ) are included.

The following 15 equations are selected combinations of the foregoing variables. The selections are not exhaustive, but are meant to represent combinations likely to maximize the explained variation.

There are t statistics reported for each coefficient. Generally, t should exceed 2.0 for the corresponding coefficient to be significantly different from zero. The coefficient of determination (R^2) has been adjusted for degrees of freedom. It is a measure of the portion of the total variability of the data explained by the particular equation. The difference between 1 and R^2, $(1 - R^2)$, is the unexplained variation. In all 15 cases $(1 - R^2)$ exceeds 40%.

This study implies that an increase in complexity of the regression model would not provide any improvement in reducing the unexplained variation.

Regression Equations for F_{ult}/F_y

The t statistic for each coefficient given in parentheses and the first number in each equation equals R^2

$$0.57\frac{F_{ult}}{F_y} = \overset{(0.868)}{0.084\lambda} + \overset{(0.951)}{0.007\sigma_{rs}} + \overset{(2.33)}{0.128K} + \overset{(1.42)}{0.014\lambda^2\sigma_{rs}} - \overset{(-0.59)}{0.009\lambda\sigma_{rs}} + \overset{(9.87)}{0.832} \quad \ldots\ldots\ldots\ldots\ldots\ldots\ldots\ldots\ldots\ldots (11)$$

$$0.38\frac{F_{ult}}{F_y} = \overset{(-5.11)}{-0.283\lambda} + \overset{(22.4)}{1.007} \quad \ldots\ldots\ldots\ldots\ldots\ldots\ldots\ldots\ldots\ldots (12)$$

$$0.44\frac{F_{ult}}{F_y} = \overset{(-5.46)}{-0.288\lambda} + \overset{(2.31)}{0.004\sigma_{rs}} + \overset{(21.3)}{1.068} \quad \ldots\ldots\ldots\ldots\ldots\ldots\ldots\ldots\ldots\ldots (13)$$

$$0.49\frac{F_{ult}}{F_y} = \overset{(-3.51)}{-0.200\lambda} + \overset{(3.07)}{0.005\lambda\sigma_{rs}} + \overset{(24.6)}{1.008} \quad \ldots\ldots\ldots\ldots\ldots\ldots\ldots\ldots\ldots\ldots (14)$$

$$0.56\frac{F_{ult}}{F_y} = \overset{(-1.06)}{-0.102\lambda} + \overset{(0.036)}{0.0002\sigma_{rs}} + \overset{(2.42)}{0.134K} + \overset{(2.33)}{0.012\lambda\sigma_{rs}} + \overset{(10.0)}{0.837} \quad \ldots\ldots\ldots\ldots (15)$$

$$0.38\frac{F_{ult}}{F_y} = \overset{(-5.09)}{-0.283\lambda} - \overset{(-0.825)}{0.026K} + \overset{(17.1)}{1.041} \quad \ldots\ldots\ldots\ldots\ldots\ldots\ldots\ldots\ldots\ldots (16)$$

$$0.56\frac{F_{ult}}{F_y} = \overset{(1.49)}{0.409\lambda} - \overset{(-1.75)}{0.318\lambda^2} + \overset{(1.39)}{0.010\lambda^2\sigma_{rs}} - \overset{(-0.639)}{0.005\lambda\sigma_{rs}} + \overset{(6.99)}{0.734} \quad \ldots\ldots\ldots\ldots (17)$$

$$0.56\frac{F_{ult}}{F_y} = \overset{(1.64)}{0.440\lambda} - \overset{(-2.19)}{0.364\lambda^2} + \overset{(3.52)}{0.006\lambda^2\sigma_{rs}} + \overset{(7.40)}{0.750} \quad \ldots\ldots\ldots\ldots\ldots\ldots\ldots\ldots (18)$$

$$0.44\frac{F_{ult}}{F_y} = \overset{(1.32)}{0.400\lambda} - \overset{(-2.29)}{0.427\lambda^2} + \overset{(6.68)}{0.764} \quad \ldots\ldots\ldots\ldots\ldots\ldots\ldots\ldots\ldots\ldots (19)$$

$$0.43\frac{F_{ult}}{F_y} = \overset{(-5.63)}{-0.185\lambda^2} + \overset{(35.5)}{9.11} \quad \ldots\ldots\ldots\ldots\ldots\ldots\ldots\ldots\ldots\ldots (20)$$

$$0.54\frac{F_{ult}}{F_y} = \overset{(-2.54)}{-0.0099\lambda^2} + \overset{(3.38)}{0.006\lambda^2\sigma_{rs}} + \overset{(39.7)}{0.912} \quad \ldots\ldots\ldots\ldots\ldots\ldots\ldots\ldots (21)$$

$$0.54\frac{F_{ult}}{F_y} = \overset{(4.31)}{0.018\lambda^2\sigma_{rs}} - \overset{(-2.48)}{0.012\lambda\sigma_{rs}} + \overset{(32.82)}{0.831} \quad \ldots\ldots\ldots\ldots\ldots\ldots\ldots\ldots (22)$$

$$0.52\frac{F_{ult}}{F_y} = \overset{(-4.05)}{-0.137\lambda^2} + \overset{(3.03)}{0.005\lambda\sigma_{rs}} + \overset{(37.0)}{0.941} \quad \ldots\ldots\ldots\ldots\ldots\ldots\ldots\ldots\ldots\ldots (23)$$

$$0.35\frac{F_{ult}}{F_y} = \underset{(4.74)}{0.008\lambda\sigma_{rs}} + \underset{(34.74)}{0.889} \quad \ldots\ldots\ldots\ldots\ldots\ldots\ldots\ldots\ldots\ldots \quad (24)$$

$$0.48\frac{F_{ult}}{F_y} = \underset{(6.28)}{0.008\lambda^2\sigma_{rs}} + \underset{(46.1)}{0.875} \quad \ldots\ldots\ldots\ldots\ldots\ldots\ldots\ldots\ldots\ldots \quad (25)$$

in which F_{ult} = maximum average column stress; F_y = laboratory tensile test yield strength of column; σ_{rs} = maximum residual compressive stress; and K = shape constant = 1 if H-shape and 2 if box-shape.

Appendix II.—Determination of Resistance Factor for Columns

The column resistance factor, Φ_c, is considered by Galambos and Ravindra (10). In essence, it is a measure of reliability within which the true strength of a particular element should lie. The mathematics of this determination is not pure, so the result should be re-examined against actual test data. In the LRFD model, Φ is assumed to be a function of the designer's knowledge about the member behavior (professional factor, P), its material properties (material factor, M), and the member's fabrication tolerances and accuracy of manufacture (fabrication factor, F).

If the three factors (P, M, and F) are multiplicative in the strength relationship, such as $R = f(P) \times f(M) \times f(F)$, the total coefficient of variation, V_R, can be expressed as

$$V_R = \sqrt{V_P^2 + V_M^2 + V_F^2} \quad \ldots\ldots\ldots\ldots\ldots\ldots\ldots\ldots\ldots\ldots \quad (26)$$

in which V = coefficient of variation = σ/μ; σ = standard deviation, estimated by the standard error of the estimate; μ = mean value; P = professional factor of error which includes engineering assumptions not considered in the equation, such as crookedness and residual stress; M = material factor of error which includes variation in yield strength and elastic modulus; F = fabrication factor of error which includes geometric variations; and R = resistance.

However, the multiplicative assumption is not appropriate in the case of columns without some corrections. For example, yield strength of the shape is very important in short columns, and of little consequence in slender columns. The elastic column strength, in fact, is independent of yield strength. If the error due to material properties is a function only of yield strength variation, V_M will be nil for elastic columns. In Eq. 6, $R_{nc} = (1.3 - 0.57\lambda)A_g QF_y'$, we find that the constant term contains F_y', and the term with lambda contains F_y'. Thus the resistance, R_{nc}, is related to F_y' in this range. However, in the elastic range, where $R_{nc} = (1/\lambda^2)\, A_g QF_y'$, F_y' cancels, and thus does not affect R_{nc}.

The segregation of the three factors in Eq. 26 is not compatible with the column data as analyzed. The result is potential double counting of some of the variability comprising each of the factors. The test data treat variation in fabrication such as initial crookedness, straightening methods, and type of column. The professional factor also treats variation in material properties such as elastic modulus, which is assumed constant. Yield stress is also included in the variability of the test data in that F_y is used to determine the slenderness, λ, and the

nondimensional strength. By using the measured yield stress to nondimensionalize the data, much of the effect of yield stress may be removed from the data set. However, it is known that the nondimensionalization process introduces some error which is biased in an unknown manner. The error may increase or reduce the scatter of the nondimensional test data.

The addition of a coefficient of variation for fabrication and one for material properties may be double counting, in that the most important variables affecting column strength are evidenced in the variety of columns composing the data base. Nonetheless, the same V_F and V_M values that were used by Galambos are added. The V_F term accounts for variation in area of the cross section which is not accounted for in the data because measured column dimensions were used to determine area. The V_M term accounts for the variation in yield stress which has remained unaccounted for previously.

Since the equation is fitted to the data, the average value of $(P_{\text{test}}/P_{\text{prediction}})$ is 1.0. The coefficients of variation for material and fabrication have been reported in Ref. 10 as follows: $V_M = 0.10$; $V_F = 0.05$.

Using the weighted COV determined in Table 3, we find $V_P = 0.10$ for the inelastic range.

The general formulation given in Ref. 10 for the resistance factor, Φ, is written for compression members as Eq. 27:

$$\Phi_c = \left(\frac{P_{\text{test}}}{P_{\text{prediction}}}\right) \exp\left(-\alpha\beta V_R\right) \quad \ldots \quad (27)$$

in which $\alpha = 0.55$; and $\beta = 3.0$ (10). First, V_R is found using Eq. 26. For the inelastic range, $V_R = \sqrt{0.10^2 + 0.10^2 + 0.05^2}$ and $V_R = 0.15$. Then, Φ_c can be determined using Eq. 27: $\Phi_c = 1 \times \exp(-0.55 \times 3.0 \times 0.15) = 0.78$.

For the elastic range, $V_R = \sqrt{0.06^2 + 0.10^2 + 0.05^2} = 0.13$; $\Phi_c = 1 \times \exp(-0.55 \times 3.0 \times 0.13) = 0.82$.

The strength in the elastic range is predicted by Eq. 2: $R_{\text{nc}} = (0.937/\lambda^2) A_g Q F'_y$. If we increase the coefficient such that Eq. 2 becomes $R_{\text{nc}} = (1/\lambda^2) A_g Q F'_y$, or the Euler curve, the $(P_{\text{test}}/P_{\text{prediction}})$ term becomes $0.937/1.0$. In order to maintain the position of the $\Phi_c R_{\text{nc}}$ curve in the elastic region of slenderness, Φ_c must be reduced $0.937/1.0 \times 0.82 \approx 0.78$. Thus, Φ_c is constant over the entire range of slenderness.

Appendix III.—Correction for Difference between Minimum Specified Yield Strength and Average Yield Strength

Assume that the effect of yield strength decreases linearly with λ from a maximum of 7% at $\lambda = 0$ to nil at $\lambda = 1.5$.

$$\frac{F_{\text{ym}}}{F'_y} = 1.07 - 0.07\frac{\lambda}{1.5} = 1.07 - 0.05\lambda; \quad 0 < \lambda \leq 1.5 \quad \ldots \quad (28)$$

$$F_{\text{ym}} = F'_y; \quad \lambda > 1.5 \quad \ldots \quad (29)$$

in which F_{ym} = mean yield stress, in kips per square inch; F'_y = minimum specified yield stress, in kips per square inch. Including the yield stress correction given in Eq. 28 directly in the column strength prediction, Eqs. 1 and 3 can

be combined and modified as follows:

$$\frac{F_{ult}}{F'_y} = (1.2 - 0.5\lambda)(1.07 - 0.05\lambda) = 1.28 - 0.535\lambda - 0.06\lambda + 0.025\lambda^2$$

$$= 1.28 - 0.59\lambda + 0.025\lambda^2; \quad \lambda < 1.5 \quad \ldots\ldots\ldots\ldots\ldots\ldots\ldots\ldots \quad (30)$$

At $\lambda = 1.5$, $F_{ult}/F'_y = 0.44$.

The λ^2 term introduces a minor nonlinearity. A straight line through the end points of the relevant range $F_{ult}/F'_y = 1.28$ at $\lambda = 0$ and $F_{ult}/F'_y = 0.44$ at $\lambda = 1.5$ is an appropriate linear replacement. The slope of this line is $(1.28 - 0.44)/(1.5 - 0.0) = 0.563$. The regression line after adjustment for yield stress in the inelastic range and rounding is

$$\frac{F_{ult}}{F'_y} = 1.3 - 0.57\lambda; \quad \lambda < 1.53 \quad \ldots\ldots\ldots\ldots\ldots\ldots\ldots\ldots \quad (31)$$

Appendix IV.—References

1. Batterman, R. H., and Johnston, B. G., "Behavior and Maximum Strength of Metal Columns," *Journal of the Structural Division*, ASCE, Vol. 93, No. ST2, Proc. Paper 5190, Apr. 1967, pp. 205–230.
2. Bjorhovde, R., "Deterministic and Probabilistic Approaches to the Strength of Steel Columns," dissertation presented to Lehigh University, at Bethlehem, Pa., in 1972, in partial fulfillment of the requirements for the degree of Doctor of Philosophy.
3. "Steel Structures for Buildings—Limit States Design," *CSA Standard S16-1974*, Canadian Standards Association, Rexdale, Ontario, Canada, 1974.
4. Estuar, F. R., and Tall, L., "Experimental Investigation of Welded Build-up Columns," *Fritz Engineering Laboratory Report 249.13*, Lehigh University, Bethlehem, Pa., Aug., 1962.
5. Feder, D. K., and Lee, G. C., "Residual Stresses in High Strength Steel," *Fritz Engineering Laboratory Report 269.2*, Lehigh University, Bethlehem, Pa., Apr., 1959.
6. Fujita, Y., "Built-up Column Strength," dissertation presented to Lehigh University, at Bethlehem, Pa., in 1956, in partial fulfillment of the requirements for the degree of Doctor of Philosophy.
7. Fujita, Y., and Driscoll, G. C., Jr., "Strength of Round Columns," *Journal of the Structural Division*, ASCE, Vol. 88, No. ST2, Proc. Paper 3090, Apr., 1962, pp. 43–59.
8. Galambos, T. V., "Proposed Criteria for Load and Resistance Factor Design of Steel Building Structures," *Bulletin No. 27*, American Iron and Steel Institute, Washington, D.C., Jan., 1978.
9. Galambos, T. V., "Strength of Round Steel Columns," *Journal of the Structural Division*, ASCE, Vol. 91, No. ST1, Proc. Paper 4219, Feb., 1965, pp. 71–99.
10. Galambos, T. V., and Ravindra, M. K., "Tentative Load and Resistance Factor Design Criteria for Steel Buildings," *Research Report 18*, Civil Engineering Dept., Washington University, St. Louis, Mo., Sept., 1973.
11. Huber, A. W., and Beedle, L. S., "Residual Stress and the Compressive Strength of Steel," *Fritz Laboratory Report 220A.9*, Lehigh University, Bethlehem, Pa., Dec., 1953.
12. Lenz, J. C., "Reliability Based Design Rules for Column Buckling," thesis presented to Washington University, at St. Louis, Mo., in 1972, in partial fulfillment of the requirements for the degree of Master of Science.
13. McFalls, R. K., and Tall, L., "A Study of Welded Columns Manufactured from Flame-cut Plates," *Welding Journal*, Vol. 48, Apr., 1969.
14. Nishino, F., and Tall, L., "Experimental Investigation of the Strength of T-1 Steel Columns," *Fritz Laboratory Report 290.9*, Lehigh University, Bethlehem, Pa., May, 1970.

15. Nitta, A., Ketter, R. L., and Thurlimann, B., "Strength of Round Columns of USS 'T-1 Steel'," *Fritz Laboratory Report 272.1,* Lehigh University, Bethlehem, Pa., Oct., 1959.
16. Rao, N. R. N., and Tall, L., "Columns Reinforced Under Load," *Fritz Laboratory Report 286.1,* Lehigh University, Bethlehem, Pa., Apr., 1962.
17. Rao, N. R. N., Marek, P., and Tall, L., "Hybrid Steel Columns," *Fritz Laboratory Report 305.2,* Lehigh University, Bethlehem, Pa., May, 1969.
18. Rokach, A. J., "A Statistical Study of the Strength of Steel Columns," thesis presented to Massachusetts Institute of Technology, at Cambridge, Mass., in 1970, in partial fulfillment of the requirements for the degree of Master of Science.
19. Shanley, R. F., "Inelastic Column Theory," *Journal of Aeronautical Sciences,* Vol. 14, No. 5, May, 1947, pp. 261–267.
20. *Specification for the Design, Fabrication and Erection of Structural Steel for Buildings,* American Institute of Steel Construction, New York, N.Y., Nov., 1978.
21. Tall, L., "Recent Developments in the Study of Column Behavior," *Journal of the Institution of Engineers,* Vol. 36, No. 12, Australia, Dec., 1964.
22. Tamarao, G. J., Jr., "Column Curve for Low Slenderness Ratios," thesis presented to Lehigh University, at Bethlehem, Pa., in 1961, in partial fulfillment of the requirements for the degree of Master of Science.
23. Tebedge, N., Marek, P., and Tall, L., "Comparison of Testing Methods for Heavy Columns," *Fritz Laboratory Report 351.2,* Lehigh University, Bethlehem, Pa., Oct., 1969.
24. Tebedge, N., Chen, W. F., and Tall, L., "Experimental Studies on Column Strength of European Heavy Shapes," *Fritz Laboratory Report 351.7,* Lehigh University, Bethlehem, Pa., Nov., 1972.
25. Ueda, Y., and Galambos, T. V., "Column Tests on 7-1/2 Inch Round Steel Bars," *Fritz Laboratory Report 272.4,* Lehigh University, Bethlehem, Pa., June, 1961.
26. Wilson, W. M., and Brown, R. L., "The Effect of Residual Longitudinal Stresses Upon the Load-Carrying Capacity of Steel Columns," *Engineering Experiment Station Bulletin No. 280,* University of Illinois, Nov., 1935.
27. Winter, G., *Commentary on the 1968 Edition of the Specification for the Design of Cold-formed Steel Structural Members,* American Iron and Steel Institute, New York, N.Y., 1970.

APPENDIX V.—NOTATION

The following symbols are used in this paper:

A = area of column;
C = Canadian Standards Association (CSA) S16.1-74 column strength;
D = dead load;
E = modulus of elasticity;
e = maximum initial out-of-straightness of column;
F = stress;
K = shape factor;
k = effective length factor;
L = live load;
l = column length;
P = load on column;
Q = effective area $Q_s Q_A$ as defined by AISC;
R = resistance of element;
R^2 = coefficient of determination;
r = radius of gyration;
t = student's statistic;
V = coefficient of variation;

α = separation factor;
β = safety index;
γ = load factor;
λ = slenderness parameter;
μ = mean value;
σ = standard deviation estimated by standard error of estimate; and
Φ = resistance factor.

Subscripts

a = axial according to AISC;
c = compression;
D = dead load;
F = fabrication factor;
g = gross;
L = live load;
M = material factor;
n = nominal;
o = engineering analysis;
P = professional factor;
R = resistance;
r = CSA resistance;
rs = maximum compressive residual;
ult = ultimate strength;
Y = yield; and
ym = mean yield stress.

Superscripts

= minimum specified.

JOURNAL OF THE STRUCTURAL DIVISION

POTENTIALITIES OF EGYPTIAN GYPSUM FOR HOUSING[a]

By Mahmoud A. Reda Youssef[1] and Albert G. H. Dietz,[2] Hon. M. ASCE

INTRODUCTION

Egypt has had a long and illustrious history of construction, stretching back at least 5,000 yr to the great era of pyramid building, and encompassing the equally great temples and tombs of later periods. That construction was based upon local indigenous materials, including stone, soil, silt-based brick, fibers, reeds, and gypsum, with its crystalline counterpart, alabaster.

The rapidly-expanding Egyptian population, accompanied by large-scale shifts, such as rural-urban migration, is placing massive demands upon the Egyptian building industry, especially upon its ability to produce housing. This, in turn, requires immense amounts of materials which must be low in cost, and therefore, they must be largely, if not wholly, indigenous. Recognizing these needs, the Technology Adaptation Program carried out by the joint collaboration of Cairo University and the Massachusetts Institute of Technology under the auspices of the Agency for International Development of the United States Department of State has concentrated on indigenous materials in the portion of its program, devoted to housing to meet the needs of the Egyptian Ministry of Housing and the Ministry of Development and New Communities.

Among the materials considered are soil and soil stabilization, low-cost cement, lightweight aggregates, and concrete, brick, fibers, and gypsum. Gypsum is an attractive, now little-used indigenous material. This paper examines strength and related properties of gypsum blocks and panels with various additives and a foaming agent.

Gypsum was chosen because, after the loss of the Sinai Peninsula and its gypsum deposits, explorations in the western desert revealed large deposits

[a]Presented at the April 14–18, 1980, ASCE Annual Convention and Exposition, held at Portland, Oreg.

[1]Assoc. Prof., Struct. Engrg. Dept., Cairo Univ., Cairo, Egypt.

[2]Prof. Emeritus of Building Engrg., Dept. of Architecture, Massachusetts Inst. of Tech., Cambridge, Mass. 02139.

Note.—Discussion open until September 1, 1981. To extend the closing date one month, a written request must be filed with the Manager of Technical and Professional Publications, ASCE. Manuscript was submitted for review for possible publication on March 11, 1980. This paper is part of the Journal of the Structural Division, Proceedings of the American Society of Civil Engineers, ©ASCE, Vol. 107, No. ST4, April, 1981. ISSN 0044-8001/81/0004-0671/$01.00.

of high-grade gypsum. It appeared possible, therefore, that gypsum might well be used for more diverse building purposes than its traditional role as plaster only, and might therefore help to relieve the pressure on tight supplies of portland cement concrete products and dwindling supplies of the traditional red brick derived from Nile silt, declining because the Nile no longer overflows. This paper presents some aspects of the work on gypsum as an item of possible value to others interested in materials, especially indigenous materials, for construction in general, and housing in particular.

Experimental Program

An extensive experimental program was undertaken at Cairo University to study the different characteristics and potentialities of locally-produced gypsum for use in various components for walls and roofs in housing units of different cost standards.

TABLE 1.—Physical and Mechanical Characteristics of Locally-Produced Gypsum[a]

Property (1)	Test results (2)
Fineness	Percentage retained on sieve No. 14 = 0.0; percentage retained on sieve No. 100 = 20.0
Normal consistency:	
without keratin	Water/plaster ratio by weight = 0.60
with 0.1% keratin (ASTM-C472)	Water/plaster ratio by weight = 0.48
Setting time (water/gypsum = 0.48, no keratin) (ASTM-C472)	10 min
Compressive strength (water/gypsum = 0.48, no keratin) (ASTM-C472)	145 kg/cm^2
Flexural strength (water/gypsum = 0.48, no keratin)	42.2 kg/cm^2
Tensile strength (water/gypsum = 0.48, no keratin)	24.6 kg/cm^2

[a]All results are based on the average of five tests; (maximum deviation within ±10% of average value).

The program was divided into three main parts dealing with plain gypsum, gypsum masonry blocks, and reinforced gypsum components. This paper presents the work on plain gypsum and gypsum blocks.

Program on Plain Gypsum.—This part of the program was undertaken on locally-produced plain gypsum to determine its physical and mechanical properties, and assess its resulting modified characteristics as affected by the percentage of mixing water, the degree of compaction, the method of drying, the amount of setting retarder, the addition of sand, the presence of sawdust, and the amount of sodium bicarbonate added to foam gypsum.

Physical and Mechanical Characteristics.—Locally-produced hemihydrate beta gypsum was used in all tests, which complied with standards of the American Society for Testing and Materials. This included: fineness, time of setting; and

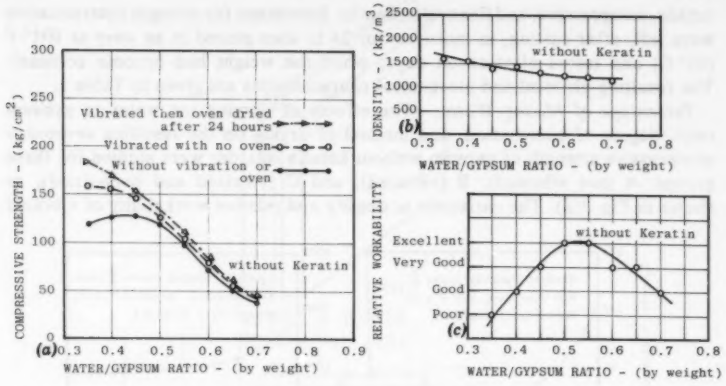

FIG. 1.—Effect of Water/Gypsum Ratio on: (*a*) Compressive Strength; (*b*) Density of Gypsum; (*c*) Relative Workability of Gypsum Mix

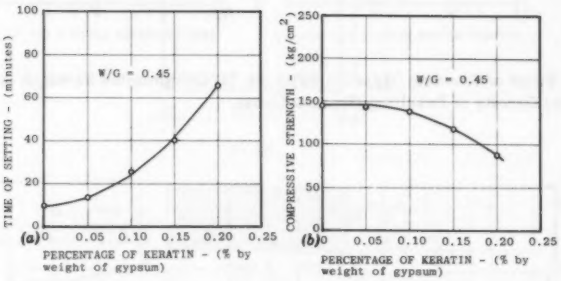
TIME OF SETTING - (minutes)
W/G = 0.45
(a)
PERCENTAGE OF KERATIN - (% by weight of gypsum)
COMPRESSIVE STRENGTH - (kg/cm²)
W/G = 0.45
(b)
PERCENTAGE OF KERATIN - (% by weight of gypsum)

FIG. 2.—Effect of Keratin Percentage on: (*a*) Gypsum Time of Setting; (*b*) Compressive Strength of Gypsum

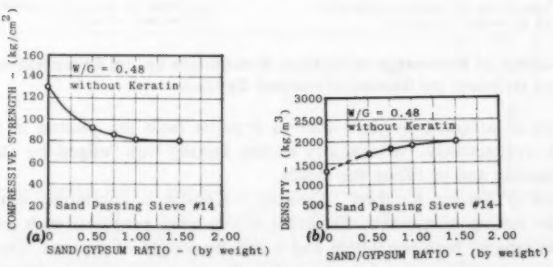

FIG. 3.—Effect of Sand/Gypsum Ratio on: (*a*) Compressive Strength of Gypsum; (*b*) Density of Gypsum

tensile, compressive, and flexural strengths. Specimens for strength determination were left, after casting, in moist air for 24 h, then placed in an over at 104° F (40° C) and tested after seven days, when the weight had become constant. The resulting physical and mechanical characteristics are given in Table 1.

Percentage of Mixing Water.—The effects of varying the water to gypsum ratio, degree of compaction, and method of drying on the resulting seven-day compressive strength of gypsum without keratin retarder were studied for three groups: A (not vibrated), B (vibrated), and C (vibrated and oven-dried), as shown in Fig. 1(*a*). The variations in density and relative workability of vibrated

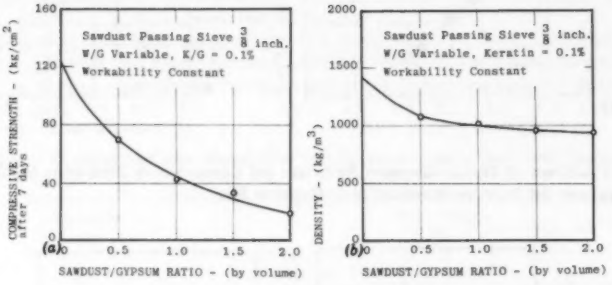

FIG. 4.—Effect of Sawdust/Gypsum Ratio on: (*a*) Compressive Strength of Gypsum Cubes; (*b*) Density of Resulting Gypsum Cubes

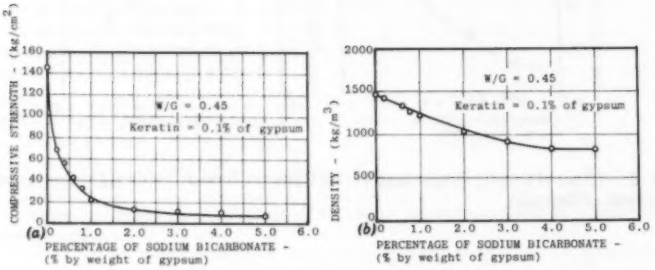
COMPRESSIVE STRENGTH - (kg/cm²)
W/G = 0.45
Keratin = 0.1% of gypsum
(a)
PERCENTAGE OF SODIUM BICARBONATE - (% by weight of gypsum)
DENSITY - (kg/m³)
W/G = 0.45
Keratin = 0.1% of gypsum
(b)
PERCENTAGE OF SODIUM BICARBONATE - (% by weight of gypsum)

FIG. 5.—Effect of Percentage of Sodium Bicarbonate on: (*a*) Compressive Strength of Foamed Gypsum; (*b*) Density of Foamed Gypsum

specimens as affected by the water to gypsum ratio are plotted in Figs. 1(*b*) and 1(*c*), respectively. Workability during mixing was judged by the relative ease of mixing and of filling the molds.

Amount of Setting Retarder (Keratin).—Keratin is commonly employed to retard the setting of gypsum. Different mixes were prepared with percentages of keratin ranging between 0.05% and 0.20% by weight of gypsum. The resulting setting times and compressive strengths after seven days are plotted in Figs. 2(*a*) and 2(*b*), respectively.

Effect of Adding Sand.—Sand passing a No. 14 sieve was added to gypsum

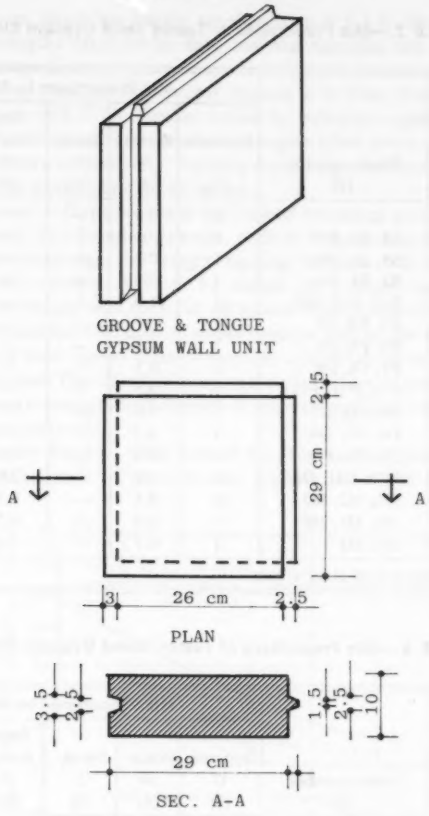

FIG. 6.—Gypsum Wall Unit Provided with Grooves and Tongues

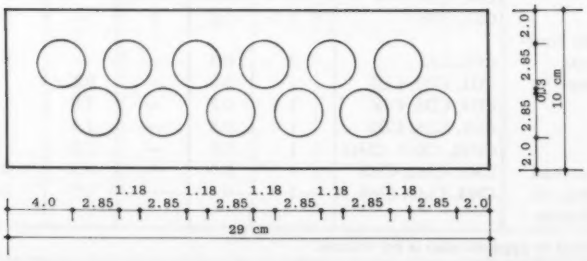

FIG. 7.—Cross Section of 29 cm × 29 cm × 10 cm Cored Wall Block

TABLE 2.—Mix Proportions of Tested Solid Gypsum Blocks

Filler material or additive (1)	Block number (2)	Mix Proportions by Weight				
		Gypsum, *G* (3)	Water, *W* (4)	Sand, *S* (5)	Sawdust,* *D* (6)	Sodium bicarbonate, *N* (7)
None	1, 2, 3	1	0.5	—	—	—
Sand	S1, S2, S3	1	0.7	2	—	—
	S4, S5, S6	1	0.8	3	—	—
	S7, S8, S9	1	0.9	4	—	—
	S10, S11, S12	1	1.0	5	—	—
Sodium bicarbonate	F1, F2, F3	1	0.5	—	—	0.006
	F4, F5, F6	1	0.5	—	—	0.010
	F7, F8, F9	1	0.5	—	—	0.015
	F10, F11, F12	1	0.5	—	—	0.020
Sawdust	D1, D2, D3	1	0.6	—	0.5	—
	D4, D5, D6	1	0.7	—	1.0	—
	D7, D8, D9	1	0.8	—	1.5	—
	D10, D11, D12	1	0.9	—	2.0	—
Sodium bicarbonate and sawdust	M1, M2, M3	1	0.6	—	0.5	0.006
	M4, M5, M6	1	0.6	—	0.5	0.010
	M7, M8	1	0.7	—	1.0	0.010

*Sawdust to gypsum ratio is by volume.

TABLE 3.—Mix Proportions of Tested Cored Gypsum Blocks

Filler material or additive (1)	Block number (2)	Mix Proportions by Weight				
		Gypsum, *G* (3)	Water, *W* (4)	Sand, *S* (5)	Sawdust,* *D* (6)	Sodium bicarbonate, *N* (7)
None	C1, C2, C3	1	0.5	—	—	—
Sand	CS1, CS2, CS3	1	0.7	2	—	—
	CS4, CS5, CS6	1	0.8	3	—	—
	CS7, CS8	1	1.0	5	—	—
Sodium bicarbonate	CF1, CF2	1	0.5	—	—	0.101
Sawdust	CD1, CD2, CD3	1	0.6	—	0.5	—
	CD4, CD5, CD6	1	0.7	—	1.0	—
	CD7, CD8, CD9	1	0.8	—	1.5	—
	CD10, CD11, CD12	1	0.9	—	2.0	—
Sawdust and sodium bicarbonate	CM1, CM2, CM3	1	0.0	—	0.3	0.006
	CM4, CM5, CM6	1	0.6	—	0.5	0.010

*Sawdust to gypsum ratio is by volume.

without keratin in ratios by weight ranging from 0.5–1.5. The corresponding compressive strengths after seven days and the densities are plotted in Figs. 3(*a*) and 3(*b*), respectively.

Effect of Adding Sawdust.—Sawdust passing a 3/8-in. (0.95-cm) sieve was added to gypsum with 0.1% keratin ratios by volume ranging from 0.5–2.0. The resulting densities and compressive strengths after seven days are plotted in Figs. 4(*a*) and 4(*b*), respectively. Varying water to gypsum ratios were adopted to attain excellent workability for all mixes.

Foamed Gypsum.—Gypsum might be foamed to reduce weight and increase thermal insulation. For foaming gypsum, sodium bicarbonate was added to the dry gypsum in percentages by weight ranging between 0.2–5.0. Keratin was added to the dry mixture as 0.1% by weight of gypsum, and the water to gypsum ratio by weight was 0.45 for all mixes. Compression test cubes were cast without mechanical vibration to avoid losing a part of the foam.

The cast cubes were tested after 14 days in laboratory air when their weight had become constant. The effects of varying the percentage of sodium bicarbonate on the compressive strength and density of foamed gypsum are plotted in Figs. 5(*a*) and 5(*b*), respectively.

Gypsum Masonry Blocks.—This part of the program was intended to develop masonry wall units made of unreinforced gypsum, to which a filler might be

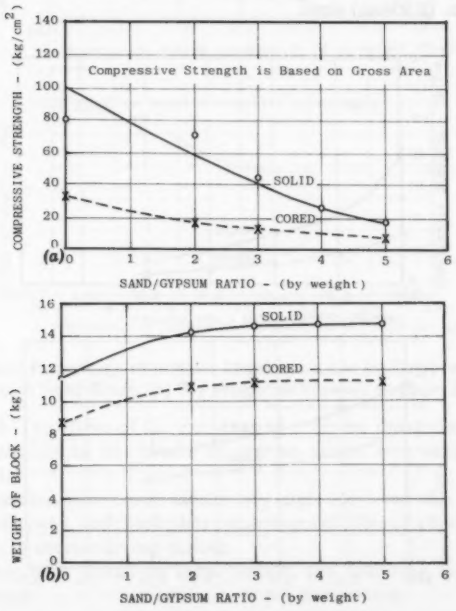

FIG. 8.—Effect of Sand/Gypsum Ratio on: (*a*) Compressive Strength of Solid and Cored Gypsum Blocks; (*b*) Dry Weight of Solid and Cored Gypsum Blocks

added, if needed, to decrease weight, cost, or both.

The dimensions of wall units had to give a thickness allowing the grip of the hand, and at the same time give a reasonable stiffness and impact resistance to the plain gypsum wall unit. The overall size had to be as large as possible to decrease handling labor during construction and the quantity of mortar required. Yet the size was limited by weight, allowing the unit to be lifted by one or two hands. Taking the preceding into account, a wall unit with overall dimensions, 11.42 in. × 11.42 in. × 3.94 in. (29 cm × 29 cm × 10 cm) was chosen, satisfying a module of 11.81 in. (30 cm) and allowing for 0.39-in. (1-cm) thick mortar joints.

Manufacturing of Gypsum Wall Units.—Gypsum wall units were case in aluminum forms consisting of a base and four sides connected by quick-release bolts. Three types of forms were used. The first gave a tongue-and-groove type block as shown in Fig. 6; the second gave a block with flat sides; and the third had flat sides containing circular openings in two opposite sides through which plastic pipes could be inserted and removed, giving a cored gypsum block as shown in Fig. 7.

Sand, sawdust, and sodium bicarbonate were tried as fillers or additives to gypsum for producing both solid and cored gypsum wall units. The mix proportions are recorded in Tables 2 and 3. In all mixes, the percentage of setting retarder (keratin) to gypsum was 0.1% by weight. Sand passed a No. 14 and sawdust passed a 3/8-in. (0.95-cm) sieve.

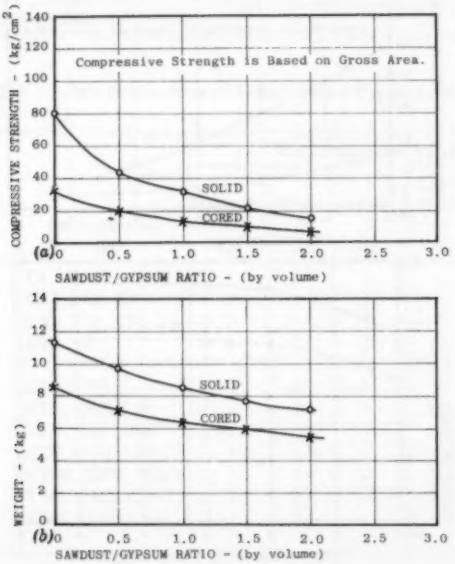

FIG. 9.—Effect of Sawdust/Gypsum Ratio on: (*a*) Compressive Strength of Solid and Cored Gypsum Blocks; (*b*) Dry Weight of Solid and Cored Gypsum Blocks

The cast gypsum blocks could be demolded 30 min–45 min after casting.

Test Procedure.—The gypsum blocks were weighed just afer demolding and placed in relatively high humidity for 24 h, then removed to the open air and weighed every day until completely dry. All types of solid and cored gypsum blocks were then tested in compression up to ultimate failure. Blocks with tongue and groove were first prepared by trimming the protruding tongue, and filling the groove on the opposite side with appropriate mortar.

Test Results.—The effects of type and percentage of additive on the resulting compressive strength and dry weight of solid and cored gypsum blocks are plotted in Figs. 8–10. The resulting material cost of solid and cored gypsum block as affected by the added percentage of sand or sawdust is plotted in

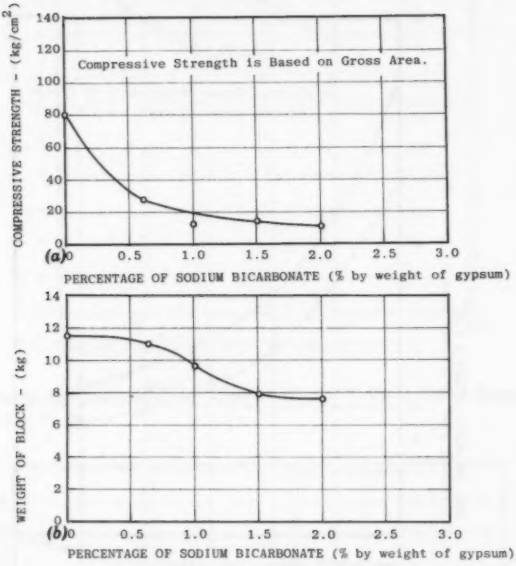
COMPRESSIVE STRENGTH - (kg/cm²)
Compressive Strength is Based on Gross Area.
(a)
PERCENTAGE OF SODIUM BICARBONATE (% by weight of gypsum)
WEIGHT OF BLOCK - (kg)
(b)
PERCENTAGE OF SODIUM BICARBONATE (% by weight of gypsum)

FIG. 10.—Effect of Percentage of Sodium Bicarbonate on: (*a*) Compressive Strength of Foamed Gypsum Solid Block; (*b*) Dry Weight of Foamed Gypsum Solid Blocks

Figs. 11 and 12. The effect of the existence of cores on the drying time needed for pure gypsum blocks and blocks of gypsum mixed with sand is shown in Figs. 13 and 14.

The tests indicate that cored blocks dry eight days–ten days earlier than equivalent solid blocks, and that higher percentages of filler or additive, especially sawdust, result in shorter drying periods.

Recommendations.—Based on these results, the following types of blocks are recommended.

1. Solid blocks with a sand filler, where the sand to gypsum ratio by weight is 2.8, are recommended for load-bearing walls; as their expected compressive

strength is about 639 psi (45 kg/cm^2) and their weight is about 32 lb/block (14.50 kg/block), whereas the cost is about 0.063 L.E./block ($0.09/block). The required water to gypsum ratio is 0.77 by weight to give excellent workability. The value of the Egyptian pound was about $1.45 at the time this report was written.

2. Cored blocks with sawdust as a filler and sawdust to gypsum ratio of 0.8 by volume may be used as nonbearing wall units as their compressive strength is only about 213 psi (15 kg/cm^2; 1,469 kPa). The corresponding weight is about 15.4 lb/block (7.0 kg/block), and the cost is nearly 0.078 L.E./block ($0.11/block). The required water to gypsum ratio by weight is 0.66 to give excellent workability.

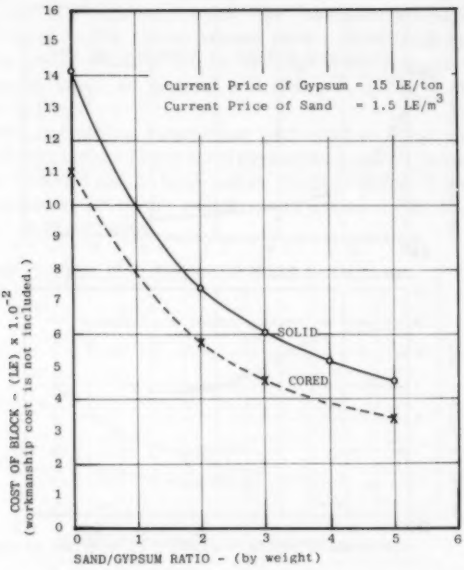

FIG. 11.—Effect of Sand/Gypsum Ratio on Cost of Solid and Cored Gypsum Blocks 29 cm × 29 cm × 10 cm

3. Whenever weight is not a problem, a lower cost can be obtained by using cored blocks for nonbearing walls with a sand to gypsum ratio by weight of 2.5 giving an approximate cost per block of only 0.05 L.E. ($0.07). The corresponding weight is 24.2 lb/block (11.0 kg/block), and the compressive strength about 213 psi (15 kg/cm^2; 1,469 kPa). The water to gypsum ratio by weight is 0.75.

The cost of all the preceding recommended blocks compares quite well with the cost of an equivalent wall area of traditional red bricks, which would be not less than 0.15 L.E. ($0.21).

Mortar for Suggested Gypsum Blocks.—In an effort to study the type of

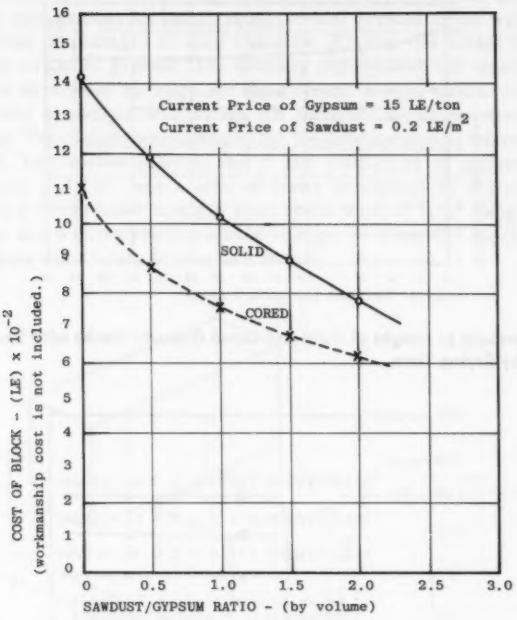

FIG. 12.—Effect of Sawdust/Gypsum Ratio on Cost of Solid or Cored Gypsum Block 29 cm × 29 cm × 10 cm

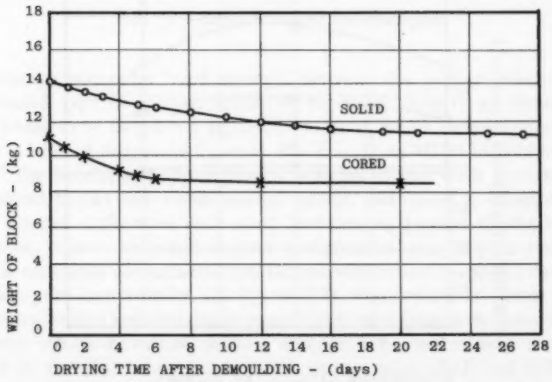

FIG. 13.—Decrease in Weight of Solid and Cored Pure Gypsum Blocks with Drying Time

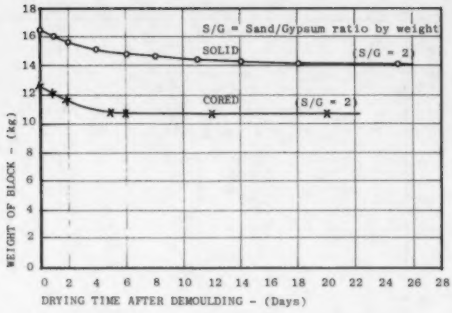

FIG. 14.—Decrease in Weight of Solid and Cored Gypsum Blocks with Sand as Filler as Affected by Drying Time

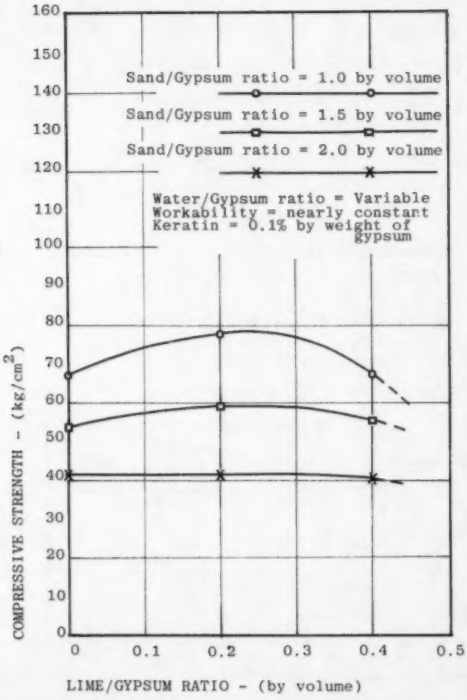
Sand/Gypsum ratio = 1.0 by volume
Sand/Gypsum ratio = 1.5 by volume
Sand/Gypsum ratio = 2.0 by volume
Water/Gypsum ratio = Variable
Workability = nearly constant
Keratin = 0.1% by weight of gypsum
COMPRESSIVE STRENGTH - (kg/cm²)
LIME/GYPSUM RATIO - (by volume)

FIG. 15.—Effect of Lime/Gypsum Ratio by Volume and Sand/Gypsum Ratio by Volume on Compressive Strength of Gypsum Mortar

mortar suitable for the suggested gypsum blocks, and to avoid the use of cement mortars to save cement for better usage, several gypsum mixes were prepared with different percentages of sand and lime. Keratin was added in all mixes as 0.1% by weight of gypsum. The resulting compressive and tensile strengths after seven days were recorded for the different mortar mixes. The water to gypsum ratio by weight was varied for different mixes to attain excellent workability. The compressive strengths for the different mortar mixes are plotted in Fig. 15. Test results indicate that a mix proportion of gypsum:sand:lime by a volume of 1:1:0.2 and a ratio of water to gypsum by a weight of 0.70 would give a compressive strength after seven days of 1,107 psi (78 kg/cm^2; 7,634 kPa), and a corresponding tensile strength of about 255 psi (18 kg/cm^2), which is quite satisfactory for use as a mortar.

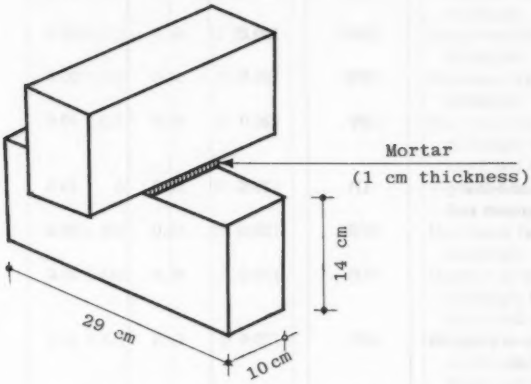

FIG. 16.—Bond Strength Test Samples

The average maximum bond strength between the gypsum blocks and the recommended type of mortar, tested on six bond samples as shown in Fig. 16, was found to be 64 psi (4.5 kg/cm^2; 441 kPa), which is satisfactory.

Group Action of Suggested Gypsum Blocks.—In an effort to study the group action of the developed gypsum blocks, a series of test walls were built using the suggested blocks and recommended mortar, and tested in compression and flexure. Six test walls were built using load-bearing gypsum blocks with plane connections, two to be tested in pure compression, one in pure flexure, and the rest in combined compression and flexure with ratios of applied compression to ultimate pure compression, (P/P_o), of 0.71, 0.41, and 0.28. Three test walls were also built using load-bearing gypsum block, with tongue-and-groove connections, with one to be tested in pure compression, one in pure flexure, and the third in combined compression and flexure with (P/P_o) of 0.50. A test wall was built using nonbearing cored gypsum blocks with sawdust filler and was tested in pure flexure. All of the ten aforementioned test walls were 3.94 in. (10 cm) thick, 23.62 in. (60 cm) wide, and 47.29 in. (120 cm) high. To

TABLE 4.—Test Results of Wall Samples Loaded

Type of wall blocks (1)	Wall sample number (2)	Average Overall Dimensions, in centimeters			P/P_o[a] (6)
		Height (3)	Width (4)	Thickness (5)	
Gypsum load-bearing blocks (plane connections)	P1	120.0	59.0	10.0	1
	P2	120.0	59.0	10.0	1
	P3	120.0	60.0	10.0	0.71
	P4	120.0	60.0	10.0	0.41
	P5	120.0	59.0	10.0	0.28
	P6	120.0	60.0	10.0	0
Gypsum load-bearing blocks (groove and tongue)	G1	120.0	60.0	10.0	1
	G2	120.0	60.0	10.0	0.5
	G3	120.0	60.0	10.0	0
Cored gypsum (nonbearing blocks)	C1	120.0	60.0	10.0	0
Traditional, red bricks	R1	120.0	60.0	12.0	1
	R2	120.0	60.0	12.0	0
Sand-lime bricks	S1	120.0	60.0	12.0	1

[a] P/P_o = ratio of applied compressive load to the ultimate pure compressive load.

provide for comparison, a test wall of sand-lime bricks and two test walls of traditional red bricks were built with the same dimensions as the gypsum test walls, except for the thickness which was 4.72 in. (12 cm), and traditional cement mortar used for their construction.

A full description of the different test walls and their corresponding recorded test results is given in Table 4, while the characteristics of the types of blocks used in building the test walls are given in Table 5.

A test setup shown in Fig. 17 was specially constructed in this investigation to be mounted on a 500-ton Amsler Compression Testing Machine to give a

in Combined Compression and Flexure

Maximum compressive load, P (in kilograms) (7)	Maximum bending moment, (in kilogram ·centimeters) (8)	Ultimate compressive stress, (in kilograms per square centimeters) (9)	Ultimate flexural stress, (in kilograms per square centimeters) (10)	Remarks (11)
18,500	0	31.4	0	Vertical crack through wall
21,000	0	35.0	0	Vertical crack in upper row only
14,000	28,675	23.33	28.68	Horizontal failure at midheight
8,100	32,250	13.33	32.35	Horizontal failure at midheight
5,500	27,750	9.17	28.22	Horizontal failure at midheight
0	4,625	0	4.62	Horizontal split at midheight between block and mortar
23,000	0	38.33	0	Vertical crack in upper row only
11,500	31,450	19.17	31.45	Horizontal failure at midheight
0	4,440	0	4.44	Horizontal split at midheight between block and mortar
0	4,625	0	4.63	Horizontal split at midheight between block and mortar
10,600	0	17.72	0	Vertical crack through wall
0	2,405	0	2.89	Horizontal split at midheight between block and mortar
18,500	0	25.69	0	Vertical crack through wall

simultaneous flexure load on the tested walls.

For walls tested under combined compression and flexure, the total predetermined compression load, (P), was applied first; then the flexural load was applied in increments up to ultimate failure.

An interaction diagram between flexural and compressive stresses was experimentally developed for load-bearing gypsum blocks with plane connections, and is shown in Fig. 18. Such an interaction diagram gives the different combinations of flexural and compressive stresses causing failure of the loaded gypsum wall.

The program on test walls indicated that the pure compressive strength of load-bearing gypsum walls is nearly twice that of the traditional red brick walls, and is greater by at least 30% than that of sand-lime brick walls.

TABLE 5.—Characteristics of Block Types Used in Tests[a]

Type of block (1)	Weight, in kilograms (2)	Average Overall Dimensions, in centimeters			Weight/volume, in kilograms per cubic meter (6)	Ultimate compressive strength, in kilograms per square centimeter (7)
		Length (3)	Width (4)	Height (5)		
Load-bearing gypsum block	14.45	29.0	10.0	29.0	1,718.1	48.0
Cored nonbearing gypsum block	6.50	29.0	10.0	29.0	772.8	15.5
Traditional red brick	2.62	24.0	12.0	6.0	1,516.2	37.3
Sand-lime brick	3.22	24.0	12.0	6.0	1,863.4	171.3

[a]Based on gross area of cored block.

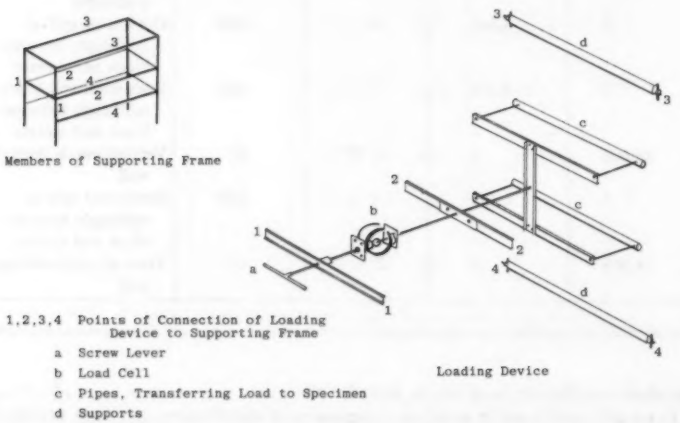
Members of Supporting Frame
1,2,3,4 Points of Connection of Loading Device to Supporting Frame
a Screw Lever
b Load Cell
c Pipes, Transferring Load to Specimen
d Supports
Loading Device

FIG. 17.—Schematic Sketch of Loading Test Setup and Supporting Frame for Flexural Loading on Walls

The pure flexural strengths of the different bearing and nonbearing gypsum walls were found to be nearly equal and greater by about 60% than the pure flexural strength of a corresponding traditional red brick wall. On the other

hand, gypsum walls with both plane and tongue-and-groove connections seemed to have no particular difference in behavior under load. Tongue-and-groove

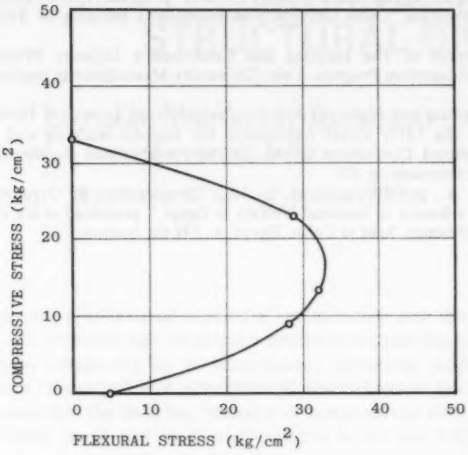

FIG. 18.—Experimental Compression-Flexure Interaction Diagram for Gypsum Load-Bearing Blocks with Plane Connections

blocks, however, required more care during construction and consumed a longer time and a larger amount of mortar than the blocks with plane flat sides.

Conclusions

Based on the foregoing tests, the following recommendations can be made.

1. Solid gypsum-sand blocks should be carefully considered for load-bearing walls and partitions carrying moderate loads at least equal to those traditionally supported by conventional sand-lime and red bricks.
2. Cored gypsum blocks with sawdust filler where light weight is important, or sand where cost predominates, should be similarly considered for nonbearing walls and partitions.

Acknowledgments

This extensive investigation was carried out at Cairo University in Egypt, as a joint research project with the Massachusetts Institute of Technology, of the United States, representing a part of the Technology Adaptation program, sponsored by the Agency for International Development of the United States Department of State. The contribution of S. L. Hanna in dealing with gypsum masonry blocks in his master's thesis is acknowledged. Thanks are extended to A. El-Erian, and the staff of the Materials Testing Laboratory for their valuable help.

APPENDIX.—REFERENCES

1. "The Housing and Construction Industry Project," progress report, Phase II, Technology Adaptation Program, Cairo University-Massachusetts Institute of Technology, Apr., 1978.
2. "Interim Report of The Housing and Construction Industry Project," Phase II, Technology Adaptation Program, Cairo University-Massachusetts Institute of Technology, 1978.
3. "Use of Gypsum and Volcanic Ash for Prefabricated Low-Cost Housing in Syria," presented at the 1977, World Association for Element-Building and Prefabrication, First International Conference on the Use of Prefabricated Building Elements, held at Hamburg, Germany, p. 65.
4. El-Erian, A. A., and El Agamawi, Y. M., "Development of Gypsum as a Building Material and a Source of National Welfare in Egypt," presented at the 1963 Afro-Asian Housing Conference, held at Cairo, Egypt, p. 138 (in Arabic).

JOURNAL OF THE STRUCTURAL DIVISION

LATERAL-TORSIONAL BUCKLING OF TAPERED I-BEAMS

By Thomas G. Brown,[1] A. M. ASCE

INTRODUCTION

With the current emphasis on structural optimization and the trend to limit states design, it is essential that we obtain a proper understanding of the instability (and the factors influencing it) of nonprismatic structural members. While a number of both theoretical and experimental investigations have been carried out, it is apparent that the buckling behavior of nonprismatic structural members under all possible loads and load combinations is not yet fully documented (11).

The behavior of tapered columns acted on by axial load or combined axial load and end moments has been the subject of a number of investigations (4,6,7,10,13,16). These have resulted in interaction curves similar to the ones used for the design of prismatic members (17). The lateral-torsional instability of doubly-symmetric, structural sections under the action of lateral load or end moments, or both, is a complex problem without the added inconvenience of a variable cross section (1,18). Timoshenko (18) first identified the problem and presented solutions to a number of cases of prismatic beams under various transverse loads. In addition, Timoshenko presented critical loads for narrow rectangular cantilevers in which the depth varied (18). Salvadori (16) used the Rayleigh Ritz method to evaluate critical end moments for a variety of moment gradients. A number of investigators (2,8,14) have used various methods to obtain critical loads or moments for a number of particular cases. Few have considered the point of application of the load other than at the centroid. Butler (4,5) has presented the results of a series of experimental programs none of which consider the case of pure lateral-torsional buckling under transverse load.

More recently, Kitipornchai (12) has presented solutions for the elastic stability of simply-supported tapered I-beams including comparisons with experimental

[1]Asst. Prof., Univ. of Petroleum & Minerals, P.O. Box 144, UPM Box 473, Dhahran, Saudi Arabia.

Note.—Discussion open until September 1, 1981. To extend the closing date one month, a written request must be filed with the Manager of Technical and Professional Publications, ASCE. Manuscript was submitted for review for possible publication on July 24, 1980. This paper is part of the Journal of the Structural Division, Proceedings of the American Society of Civil Engineers, ©ASCE, Vol. 107, No. ST4, April, 1981. ISSN 0044-8001/81/0004-0689/$01.00.

results. In this paper, critical loads for tapered beams, both simply-supported and cantilever, are determined using finite differences. Particular attention is paid to the location (with respect to the centroid) of the transverse load.

Lateral-Torsional Buckling

The characteristic eigenvalue equation for any structural stability problem may be developed from: (1) Equilibrium considerations; (2) imperfection equilibrium; and (3) energy considerations or dynamics.

The pre-buckling and post-buckling configurations of a doubly-symmetric I-section are shown in Fig. 1. The displacements of the centroid are denoted as u_c and v_c; the displacements of all other points on the section are given by

$$u = u_c - y\beta; \quad v = v_c + x\beta \quad \ldots\ldots\ldots\ldots\ldots\ldots\ldots\ldots\ldots\ldots (1)$$

The centroidal displacement along the axis of the beam is denoted as w_c, the displacement at all other points being given by

$$w = w_c - xu_c' - yv_c' + \phi_c\beta' \quad \ldots\ldots\ldots\ldots\ldots\ldots\ldots\ldots\ldots\ldots (2)$$

in which the prime denotes differentiation with respect to the longitudinal axis,

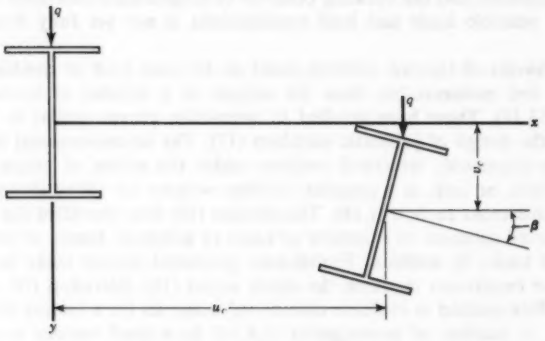

FIG. 1.—Coordinate System

z; and ϕ_c = the warping function. Using the foregoing displacement functions, the buckling strains become

$$\epsilon_{xx} = \frac{1}{2}\beta^2; \quad \epsilon_{yy} = \frac{1}{2}\beta^2; \quad \epsilon_{zz} = w_c' - xu_c'' - y\,v_c'' + \phi_c\beta''$$

$$+ \frac{1}{2}\left[(u_c' - y\beta')^2 + (v_c' + x\beta')^2\right]; \quad \epsilon_{xy} = 0; \quad \epsilon_{yz} = \frac{1}{2}\left[x\beta'\right.$$

$$\left. - \beta(u_c' - y\beta') + \beta'\frac{\partial\phi_c}{\partial y}\right]; \quad \epsilon_{zx} = \frac{1}{2}\left[-y\beta' + \beta(v_c' + x\beta') + \beta'\frac{\partial\phi_c}{\partial x}\right] \quad (3)$$

The total strain energy change during buckling can be divided into two

components: (1) The energy due to the buckling strains acting on the stress field immediately prior to buckling; and (2) the strain energy generated by the buckling strains themselves:

$$U = U_1 + U_2; \quad U = \int_{\text{vol}} \sigma^0_{ij} \epsilon_{ij} dv + \int_{\text{vol}} \sigma_{ij} \epsilon_{ij} dv \quad \ldots\ldots\ldots\ldots\ldots (4)$$

in which σ^0_{ij} denotes the stress tensor immediately prior to buckling.

For open thin-walled sections, the following integrals result as contributions to U_1:

$$\int_v \sigma^0_{zz} \epsilon_{zz} dv = \int_0^L \left\{ -P_0 w'_c - \frac{P_0}{2} (u'^2_c + v'^2_c + \rho^2_c \beta'^2) + M_0 \left[\frac{R_x}{I_x} \beta'' \right.\right.$$

$$\left.\left. - (u''_c - u'_c \beta') + \frac{k}{2I_x} \beta'^2 \right]\right\} dz; \quad \int_v (\sigma^0_{xx} \epsilon_{xx} + \sigma^0_{yy} \epsilon_{yy}) dv = \int_0^L \left[-\frac{1}{2} qa\beta^2 \right.$$

$$\left. + \frac{1}{4} \frac{M'_0 k}{I_x} \beta^2 \right] dz \ldots\}; \quad 2 \int_v \tau^0_{xy} \epsilon_{xy} dv = 0; \quad 2 \int_v (\tau^0_{xz} \epsilon_{xz} + \tau^0_{yz} \epsilon_{yz}) dv$$

$$= \int_0^L \left[M' u'_c \beta + \frac{1}{2} \beta\beta' \frac{k}{I_x} M'_0 + \beta' \frac{R_x}{I_y} M'_0 \right] dz \quad \ldots\ldots\ldots\ldots\ldots (5)$$

In addition

$$U_2 = \frac{1}{2} \int_v [E\epsilon^2_{zz} + 4G(\epsilon^2_{xz} + \epsilon^2_{yz})] dv = \frac{1}{2} \int_0^L EA \left[w'_c + \frac{1}{2} (u'^2_c + v'^2_c \right.$$

$$\left. + \rho^2_c \beta'^2)^2 \right] dz + \int_0^L [EI_x (u''_c + \beta' u'_c)^2 + EI_y u''^2_c + E\Gamma_c \beta''^2 - 2ER_y \beta'' u''_c$$

$$- Ek\beta'^2 (v''_c + \beta' u'_c) + GK\beta'^2 + GA\beta^2 u'^2_c + GI_x \beta^2 \beta'^2] dx \quad \ldots\ldots\ldots (6)$$

The total change in potential energy

$$V = U_1 + U_2 - W \quad \ldots\ldots\ldots\ldots\ldots\ldots\ldots\ldots\ldots\ldots\ldots (7)$$

then becomes, introducing Eqs. 5 and 6, and introducing the work term, W:

$$V = \frac{1}{2} \int_0^L \left\{ -P_o (u'^2_c + \rho^2_c \beta'^2) + 2M\beta u''_c + \frac{kM_0}{I_x} \beta'^2 - qa\beta^2 \right\} dz$$

$$+ \frac{1}{2} \int_0^L \{EI_y u''^2_c - 2ER_y \beta'' u''_c + GK\beta'^2 + E\Gamma_c \beta''^2 dz + \text{boundary terms} \quad (8)$$

In the preceding expression for potential energy, the terms associated with Euler buckling about the major (x) axis have been omitted and fourth order terms have been ignored.

Eq. 8 for the change in potential energy is developed with respect to the centroid of the cross section and this accounts for the minor differences between this equation and the corresponding equation in Ref. 1 and Eq. 10 of Masur and Milbradt (15).

Considering the variation of V, $\delta_{u_c} V = 0$, we get

$$(EI_y u_c'')'' - (ER_y \beta'')'' + (M\beta)'' + (P_0 u_c')' = 0 \quad \ldots\ldots\ldots\ldots\ldots\ldots (9)$$

and using the variation of $\delta_\beta V = 0$

$$(E\Gamma_c \beta'')'' - (ER_y u_c'')'' - (GK\beta')' + Mu_c'' - \left(\frac{M_0 k\beta'}{I_x}\right)'$$

$$+ (P_0 \rho_c^2 \beta')' - qa\beta = 0 \quad \ldots\ldots\ldots\ldots\ldots\ldots\ldots\ldots\ldots\ldots (10)$$

The result, then, is two simultaneous fourth order differential equations. Under certain conditions, however, these equations may be uncoupled; for example,

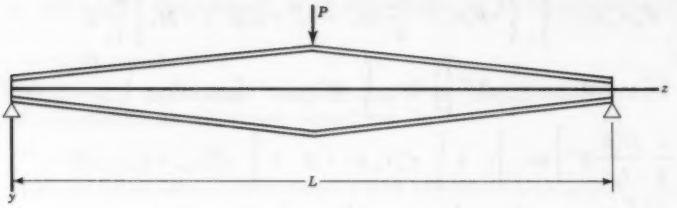

FIG. 2.—Simply—Supported Beam with Double Taper

the doubly symmetric section being considered and the absence of axial load, P_0, result in

$$P_0 = k = R_y = 0 \quad \ldots\ldots\ldots\ldots\ldots\ldots\ldots\ldots\ldots\ldots\ldots\ldots\ldots (11)$$

and the equations become

$$(EI_y u_c'')'' + (M\beta)'' = 0 \quad \ldots\ldots\ldots\ldots\ldots\ldots\ldots\ldots\ldots\ldots\ldots (12)$$

$$(E\Gamma_c \beta)'' - (GK\beta')' + Mu_c'' - qa\beta = 0 \quad \ldots\ldots\ldots\ldots\ldots\ldots\ldots (13)$$

Eq. 12 may be integrated twice and, with the introduction of appropriate boundary conditions, leads to the equation

$$EI_y u_c'' + M\beta = 0 \quad \ldots\ldots\ldots\ldots\ldots\ldots\ldots\ldots\ldots\ldots\ldots\ldots (14)$$

when introduced into Eq. 13 this gives one fourth order ordinary differential equation:

$$(E\Gamma_c \beta'')'' - (GK\beta')' - \frac{M^2\beta}{EI_y} - qa\beta = 0 \quad \ldots\ldots\ldots\ldots\ldots\ldots (15)$$

Depending on the beam type, M will be some function of z and the load. For the simply supported beam in Fig. 2

$$M = \frac{PL}{2}\left(1 - \frac{z}{L}\right) \quad \ldots\ldots\ldots\ldots\ldots\ldots\ldots\ldots\ldots\ldots\ldots\ldots (16)$$

Eigenvalues

Eq. 15 can be approximated using central finite differences (9), leading to a matrix eigenvalue equation of the form

$$[C]\{\beta\} - p[\beta]\{\beta\} - p^2[A]\{\beta\} = 0 \quad \ldots\ldots\ldots\ldots\ldots\ldots\ldots\ldots\ldots\ldots \quad (17)$$

This equation is of quadratic form and therefore does not lend itself to normal eigenvalue extraction techniques. It may, however, be solved directly if we introduce (3)

$$\{\bar{\beta}\} = p\{\beta\} \quad \ldots\ldots\ldots\ldots\ldots\ldots\ldots\ldots\ldots\ldots\ldots\ldots\ldots\ldots\ldots \quad (18)$$

Premultiplying Eq. 17 by $|A|^{-1}$ and combining Eqs. 17 and 18 results in the equation:

$$\begin{bmatrix} [0] & [I] \\ [A]^{-1}[C] & -[A]^{-1}[B] \end{bmatrix} \begin{Bmatrix} \beta \\ \bar{\beta} \end{Bmatrix} = p \begin{Bmatrix} \beta \\ \bar{\beta} \end{Bmatrix} \quad \ldots\ldots\ldots\ldots\ldots\ldots\ldots \quad (19)$$

from which eigenvalues can be extracted using any conventional eigenvalue program.

Critical Buckling Loads

Critical loads are obtained for the case of nonprismatic simply-supported beams and nonprismatic cantilevers. In all cases only the beam depth varies; the flange

TABLE 1.—Coefficients γ_1 for Simply-Supported Beams under Central Concentrated Loads

Taper ratio α (1)	Top Flange Load		Centroid Load		Bottom Flange Load	
	γ_1 (2)	$\gamma_1/\bar{\gamma}_1$ (3)	γ_1 (4)	$\gamma_1/\bar{\gamma}_1$ (5)	γ_1 (6)	$\gamma_1/\bar{\gamma}_1$ (7)
0.167	11.96	0.727	19.80	0.783	31.13	0.840
0.333	13.02	0.792	21.12	0.835	32.58	0.879
0.5	13.96	0.849	22.30	0.882	33.82	0.913
0.667	14.85	0.903	23.37	0.924	34.96	0.944
0.833	15.66	0.952	24.36	0.963	36.01	0.972
1.0	16.44 ($\bar{\gamma}_1$)	1.0	25.28 ($\bar{\gamma}_1$)	1.0	37.05 ($\bar{\gamma}_1$)	1.0

width and thickness and the web thickness remaining constant. The section used for all examples was an idealized I-section with a maximum depth of 24 in. (610 mm). Flange width and thickness were 6 in. (152 mm) and 0.5 in. (13 mm) respectively, and the web thickness was 0.375 in. (9.5 mm).

Critical loads are given in the form:

$$P_{cr} = \gamma_1 \frac{\sqrt{EI_{y0}GK_0}}{L^2} \quad \ldots\ldots\ldots\ldots\ldots\ldots\ldots\ldots\ldots\ldots\ldots \quad (20)$$

$$\text{or} \quad q_{cr} = \gamma_2 \frac{\sqrt{EI_{y0}GK_0}}{L^3} \quad \ldots\ldots\ldots\ldots\ldots\ldots\ldots\ldots\ldots\ldots\ldots \quad (21)$$

Table 1 summarizes the coefficients γ_1 for critical midspan concentrated loads for 20-ft (6.10-m) simply-supported beams (Fig. 2). The boundary conditions at $z = 0$ and $z = L$ were

$$u = u'' = \beta = \beta'' = 0 \quad \ldots \quad (22)$$

As expected, the top flange load results in significantly reduced critical loads as compared with the other load positions. There is not, however, the large reduction in critical load with the rather extreme case of an end depth of 4 in. (102 mm).

Table 2 summarizes the coefficients γ_2 for critical uniformly distributed loads, again acting on 20-ft (6.10-m) simply supported beams.

TABLE 2.—Coefficients γ_2 for Simply-Supported Beams under Uniform Load

Taper ratio α (1)	γ_2 (2)	$\gamma_2/\bar{\gamma}_2$ (3)
0.167	22.93	0.778
0.333	24.59	0.834
0.50	26.01	0.882
0.667	27.34	0.927
0.833	28.34	0.964
1.000	29.49 ($\bar{\gamma}_2$)	1.000

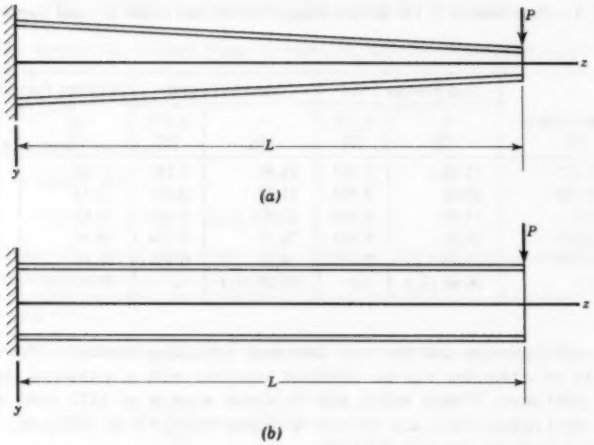

FIG. 3.—(*a*) Tapered Cantilever; (*b*) Prismatic Cantilever

For the cantilever beams shown in Fig. 3, the boundary conditions used were at $z = 0$:

$$u = u' = \beta = \beta' = 0 \quad \ldots \quad (23)$$

and at the free end, $z = L$

$$u'' = (EIu'')' = \beta'' = \beta''' = 0 \quad \ldots \quad (24)$$

Table 3 indicates that a reduction in the free end depth of a cantilever leads to an increase in the critical end load [Fig. 3(*a*)]. This is due to the very significant effect of the top-flange load. This is demonstrated by Table 4 which shows the effect of varying the point of application of the load from the centroid ($a/d = 0$) to the top flange ($a/d = 0.5$) of a prismatic cantilever [Fig. 3(*b*)].

TABLE 3.—Coefficient γ_1 for Cantilever Beams under End Concentrated Loads

Taper ratio α (1)	Top Flange Load		Centroidal Load	
	γ_1 (2)	$\gamma_1/\bar{\gamma}_1$ (3)	γ_1 (4)	$\gamma_1/\bar{\gamma}_1$ (5)
0.167	5.32	2.59	7.10	0.89
0.333	4.03	1.96	7.29	0.91
0.50	3.18	1.55	7.47	0.94
0.667	2.65	1.29	7.65	0.96
0.833	2.35	1.14	7.81	0.98
1.000	2.06 ($\bar{\gamma}_1$)	1.00	7.98 ($\bar{\gamma}_1$)	1.00

TABLE 4.—Coefficient γ_1 for Prismatic Cantilevers under End Concentrated Loads

Load location a/d (1)	γ_1 (2)
0	7.77
0.083	6.24
0.167	4.84
0.250	3.68
0.333	2.92
0.417	2.43
0.50	2.06

The critical load for the case of top flange loading is reduced to 26.5% of the corresponding load at the centroid.

Summary and Conclusions

Central finite differences are used to determine critical buckling loads for tapered beams. Using a direct solution by Buckingham of the quadratic characteristic equation, the effect of loads placed either above or below the centroid is included. This effect is shown to be significant in all types of beams but leads to an increase, with decreasing free end depth, of the critical load in cantilevers.

Acknowledgments

Thanks are due to Omar Al-Amoudi and Abdul-Rahman Khathlan who carried out all of the computational work and to John F. Doyle for advice on the mathematics.

Appendix I.—References

1. Bleich, F., *Buckling Strength of Metal Structures,* McGraw-Hill Book Co., Inc., New York, N.Y., 1952.
2. Boley, B. A., and Zimnoch, V. P., "Lateral Buckling of Nonuniform Beams," *Journal of Aeronautical Sciences,* Vol. 19, No. 8, Aug., 1952, p. 567.
3. Buckingham, R. A., *Numerical Methods,* Sir Isaac Pitman & Sons, London, England, 1957.
4. Butler, D. J., and Anderson, G. B., "The Elastic Buckling of Tapered Beam Columns," *Welding Journal,* Vol. 42, No. 1, Jan., 1963, p. 295.
5. Butler, D. J., "Elastic Buckling Tests on Laterally and Torsionally Braced Tapered I-Beams," *Welding Journal,* Vol. 45, No. 1, Jan., 1966, p. 415.
6. Culver, C. G., and Preg, S. M., "Elastic Stability of Tapered Beam—Columns," *Journal of the Structural Division,* ASCE, Vol. 94, No. ST2, Proc. Paper 5796, Feb., 1968, pp. 455–470.
7. Fogel, C. M., and Ketter, R. L., "Elastic Strength of Tapered Columns," *Journal of the Structural Division,* ASCE, Vol. 88, No. ST5, Proc. Paper 3301, Oct., 1962, pp. 67–106.
8. Gatewood, B. E., "Buckling Loads for Beams of Variable Cross-Section under Combined Loads," *Journal of Aeronautical Sciences,* Vol. 22, No. 4, Apr., 1955, p. 281.
9. Ghali, A., and Neville, A. M., *Structural Analysis—A Unified Classical and Matrix Approach,* Intext Paperback Press, Scranton, Pa., 1972.
10. Girijavallabhan, C. V., "Buckling Loads of Nonuniform Columns," *Journal of the Structural Division,* ASCE, Vol. 95, No. ST11, Proc. Paper 6908, Nov., 1969, pp. 2419–2431.
11. *Guide to Stability Design Criteria of Metal Structures,* Structural Stability Research Council, B. G. Johnston, ed., 3rd ed., John Wiley and Sons, Inc., New York, N.Y., 1976.
12. Kitipornchai, S., and Trahair, N. S., "Elastic Stability of Tapered I-Beams," *Journal of the Structural Division,* ASCE, Vol. 98, No. ST3, Proc. Paper 8775, Mar., 1972, pp. 713–728.
13. Lee, G. C., Morrell, M. L., and Ketter, R. L., "Design of Tapered Members," *Welding Research Council Bulletin, No. 173,* June, 1972.
14. Massey, C., and McGuire, P. J., "Lateral Stability of Nonuniform Cantilevers," *Journal of the Engineering Mechanics Division,* ASCE, Vol. 97, No. EM3, Proc. Paper 8172, June, 1971, pp. 673–686.
15. Masur, E. F., and Milbrodt, K. P., "Collapse Strength of Redundant Beams After Lateral Buckling," *Journal of Applied Mechanics,* American Society of Mechanical Engineers, Vol. 24, June, 1957, pp. 283–288.
16. Salvadori, M. G., "Lateral Buckling of Eccentrically Loaded I-Columns," *Transactions,* ASCE, Vol. 121, 1956, pp. 1163–1178.
17. *Specification for the Design, Fabrication and Erection of Structural Steel for Buildings (with Supplement #3),* American Institute of Steel Construction, New York, N.Y., 1969.
18. Timoshenko, S. P., and Gere, J. M., *Theory of Elastic Stability,* McGraw-Hill Book Co., Inc., New York, N.Y., 1961.

Appendix II.—Notation

The following symbols are used in this paper:

$[A], [B], [C]$ = matrices of finite difference coefficients;
a = vertical distance between point of application of transverse load and centroid;
d = depth of I-section;
E = modulus of elasticity;

G = shear modulus;
$[I]$ = identity matrix;
I_x, I_y = principle moments of inertia;
I_{x0}, I_{y0} = moment of inertia at deepest section;
K = St. Verant torsion constant;
k = $\int\int (x^2 - y^2) y dA$;
L = span;
M = total bending moment at any point in beam;
M_0 = moment due to eccentricity of axial load;
P = concentrated transverse load;
P_0 = axial load;
p = characteristic eigenvalue;
q = distributed transverse load;
R_x, R_y = $\int\int y \phi_c dA$, $\int\int x \phi_c dA$;
u, v, w = displacements of any point in beam;
u_c, v_c, w_c = displacements of centroid;
u_1, u_2 = strain energy;
V = total potential energy during buckling;
W = work done by external loads during buckling;
x, y, z = coordinates;
α = taper ratio;
β = angle of twist;
$\{\bar{\beta}\}$ = amended eigenvector (Eq. 18);
Γ_c = warping constant;
γ_1, γ_2 = nondimensional critical load parameters;
ϵ_{ij} = strain tensor;
ρ_c = polar radius of gyration;
σ_{ij} = additional stress tensor caused by buckling;
$\overset{o}{\sigma}_{ij}$ = stress tensor prior to buckling; and
$\phi_c(x, y)$ = warping coefficient.

JOURNAL OF THE
STRUCTURAL DIVISION

TECHNICAL NOTES

Note.—Discussion open until September 1, 1981. To extend the closing date one month, a written request must be filed with the Manager of Technical and Professional Publications, ASCE. This paper is part of the Journal of the Structural Division, Proceedings of the American Society of Civil Engineers, ©ASCE, Vol. 107, No. ST4, April, 1981.

Technical Notes

To provide a place within ASCE for publication of technical ideas that have not advanced, as yet, to the point where they warrant publication as a Proceedings paper in a *Journal*, the publication of Technical Notes was authorized by the Board of Direction on October 16–18, 1967, under the following guidelines:

1. An original manuscript and two copies are to be submitted to the Manager of Technical and Professional Publications, ASCE, 345 East 47th Street, New York, N.Y., 10017, along with a request by the author that it be considered as a Technical Note.
2. The two copies will be sent to an appropriate Technical Division or Council for review.
3. If the Division or Council approves the contribution for publication, it shall be returned to Society Headquarters with appropriate comments.
4. The technical publications staff will prepare the material for use in the earliest possible issue of the *Journal*, after proper coordination with the author.
5. Each Technical Note is not to exceed 4 pages in the *Journal*. As an approximation, each full manuscript page of text, tables, or figures is the equivalent of one-half a *Journal* page.
6. The Technical Notes will be grouped in a special section of each *Journal*.
7. Information retrieval abstracts and key words will be unnecessary for Technical Notes.
8. The final date on which a Discussion should reach the Society is given as a footnote with each Technical Note.
9. Technical Notes will not be included in *Transactions*.
10. Technical Notes will be included in ASCE's annual and cumulative subject and author indexes.

The manuscripts for Technical Notes must meet the following requirements:

1. Titles must have a length not exceeding 50 characters and spaces.
2. The author's full name, Society membership grade, and a footnote reference stating present employment must appear on the first page of the manuscript. Authors need not be Society members.
3. The manuscript is to be submitted as an original copy (with two duplicates) that is typed double-spaced on one side of 8-1/2-in. (220-mm) by 11-in. (280-mm) white bond paper.
4. All mathematics must be typewritten and special symbols must be properly identified. The letter symbols used must be defined where they first appear, in figures or text, and arranged alphabetically in an Appendix.—Notation.
5. Standard definitions and symbols must be used. Reference must be made to the lists published by the American National Standards Institute and to the *Authors' Guide to the Publications of ASCE*.
6. Tables must be typed double-spaced (an original ribbon copy and two duplicate copies) on one side of 8-1/2-in. (220-mm) by 11-in. (280-mm) paper. An explanation of each table must appear in the text.
7. Figures must be drawn in black ink on one side of 8-1/2-in. (220-mm) by 11-in. (280-mm) paper. Because figures will be reproduced with a width of between 3 in. (76 mm) to 4-1/2 in. (110 mm), the lettering must be large enough to be legible at this width. Photographs must be submitted as glossy prints. Explanations and descriptions must be made within the text for each figure.
8. References cited in text must be typed at the end of the Technical Note in alphabetical order in an Appendix.—References.
9. Dual units, i.e., U.S. Customary followed by SI (International System) units in parentheses, should be used throughout the paper.

WIND-EXCITED RESPONSE OF BUILDINGS IN HIGHER MODES

By Ahsan Kareem,[1] M. ASCE

INTRODUCTION

The wind-excited motion of tall buildings is generally found to be primarily in the fundamental sway modes. The higher modes of vibration have an insignificant contribution to the displacement response; however their influence on the higher derivatives of response, i.e., acceleration and jerk, is quite significant (2,4). The human biodynamic response to motion is generally influenced by the higher derivatives of displacement (4). Therefore, occupant comfort in tall buildings can be affected by underestimating the dynamic response as a consequence of neglecting the higher modes of vibration.

Simiu (5) has shown that the contribution of the higher modes to the root mean square (RMS) alongwind acceleration is on the order of 5%–20%. Fujimoto, Ohkuma, and Amano (1) utilized a four-mass aeroelastic model to study the dynamic response of a prototype building. They similarly concluded that the contribution of the higher modes to the RMS value of the acceleration response was 10% of the response in the fundamental mode; whereas the displacement response was not influenced by the higher modes.

For high wind speeds, the crosswind response of a uniform cross-sectional tall building is generally higher than the alongwind response (2,3). In this note, a simple method of computing the contribution of higher modes to the crosswind response is presented, and the results are compared with those of a detailed analysis.

ANALYSIS

It can be illustrated from a dimensional argument that the mean square acceleration for a lightly-damped structure with narrow-band response characteristics is proportional to $f_n S(f_n)/\xi_n$, in which f_n = the nth natural frequency; ξ_n = the structural damping ratio in the nth mode; and $S(f_n)$ = the power spectrum of the wind-loading function evaluated at the nth frequency.

The power spectrum of wind loads can be expressed as being proportional

[1]Asst. Prof. of Civ. Engrg., Cullen Coll. of Engrg., Univ. of Houston, Central Campus, Houston, Tex. 77004.

Note.—Discussion open until September 1, 1981. To extend the closing date one month, a written request must be filed with the Manager of Technical and Professional Publications, ASCE. Manuscript was submitted for review for possible publication on October 8, 1980. This paper is part of the Journal of the Structural Division, Proceedings of the American Society of Civil Engineers, ©ASCE, Vol. 107, No. ST4, April, 1981. ISSN 0044-8001/81/0004-0701/$01.00.

to $(f_n)^{-\alpha}$. The value of α depends on the approach wind characteristics and the building geometry (2). For the crosswind forcing function (3), the value of α is approximately equal to 5.5. The RMS acceleration response is given by

$$\sigma_{acc} \propto \sqrt{\frac{1}{\xi_n}\left(\frac{1}{f_n}\right)^{\alpha-1}} \quad \ldots\ldots\ldots\ldots\ldots\ldots\ldots\ldots\ldots\ldots\ldots\ldots (1)$$

in which σ_{acc} represents the RMS value of the acceleration response. The ratio between the nth and the first mode contribution to the acceleration response is, therefore, given by

$$\frac{(\sigma_{acc})_n}{(\sigma_{acc})_1} = \sqrt{\frac{\xi_1}{\xi_n}\left(\frac{f_1}{f_n}\right)^{\alpha-1}} \quad \ldots\ldots\ldots\ldots\ldots\ldots\ldots\ldots\ldots\ldots\ldots\ldots (2)$$

In the higher modes, the relatively high flexural and shear deformations of the structural system result in higher damping than occurs in the fundamental mode. Yokoo and Akiyama (6) established an approximate expression for the ratio of the damping values in the higher modes of vibration to the damping in the fundamental mode in terms of the associated frequencies

$$\frac{\xi_n}{\xi_1} = 1 + C\left(\frac{f_n}{f_1} - 1\right) \quad \ldots\ldots\ldots\ldots\ldots\ldots\ldots\ldots\ldots\ldots\ldots\ldots (3)$$

in which C = approximately equal to 0.38. Substituting Eq. 3 into Eq. 2

$$\frac{(\sigma_{acc})_n}{(\sigma_{acc})_1} = \sqrt{\frac{1}{\left[1 + C\left(\frac{f_n}{f_1} - 1\right)\right]}\left\{\frac{f_1}{f_n}\right\}^{\alpha-1}} \quad \ldots\ldots\ldots\ldots\ldots\ldots\ldots (4)$$

A more general expression for the ratio between the nth and the first mode contributions to various components of response is given by

$$\frac{(\sigma_r)_n}{(\sigma_r)_1} = \sqrt{\frac{1}{\left[1 + C\left(\frac{f_n}{f_1} - 1\right)\right]}\left\{\frac{f_1}{f_n}\right\}^{\alpha-2r+3}} \quad \ldots\ldots\ldots\ldots\ldots\ldots\ldots (5)$$

in which r represents various derivatives of the displacement response; e.g., jerk (the third derivative of displacement) is represented by r equal to three.

The wind-excited response of a tall building modeled as a multidegree-of-freedom system can be estimated using methods of random vibration theory (2). The mean square acceleration at the ith level is given by

$$\{\sigma^2_{acc_i}\} = \sum_{j=1}^{N} [\phi]\left[\int_0^\infty G_{y_{ij}}(f)\,df\right][\phi]^T \quad \ldots\ldots\ldots\ldots\ldots\ldots\ldots\ldots (6)$$

$$[G_y(f)] = \{[H_a(i2\pi f)]^*[\phi]^T[G_F(f)][\phi][H_a(i2\pi f)]\}, \text{ and} \quad \ldots\ldots (7)$$

in which $[H_a(i2\pi f)]$ = frequency response matrix; $[G_F(f)]$ = cross-power

spectral density matrix of the forcing function; [ϕ] = modal matrix; * = complex conjugate; and N = total number of modes.

It will be assumed that the cross terms in Eq. 7 are relatively small and that the forcing function varies slowly in the proximity of the building frequencies. The forcing function thus can be idealized by a white noise process. This reduces Eq. 6 to a simplified and approximate relationship

$$(\sigma^2_{acc}) = \sum_{n=1}^{N} \frac{\frac{\pi}{4} f_n S_{fn}(f_n)}{\xi_n m_n^2} \quad \ldots\ldots\ldots\ldots\ldots\ldots\ldots\ldots\ldots\ldots (8)$$

in which $S_{fn}(f_n)$, m_n = the generalized power spectrum of the forcing function, and the mass in the nth mode, respectively. A more general expression for the mean square value of various components of response is given by

$$(\sigma^2_r) = \sum_{n=1}^{N} \frac{\frac{\pi}{4} f_n S_{fn}(f_n)(2\pi f_n)^{2r}}{(2\pi f_n)^4 \xi_n m_n^2} \quad \ldots\ldots\ldots\ldots\ldots\ldots\ldots\ldots\ldots\ldots (9)$$

in which r represents various derivatives of the displacement response.

Example

A building 100 ft (31 m) square in plan, and 600 ft (183 m) tall was modeled as a five-degree-of-freedom system (2). The building characteristics are given in Table 1, and the kinematic model is shown in Fig. 1.

The contribution of the crosswind response in the higher modes was computed

TABLE 1.—Building Characteristics[a]

	Mode (n)				
	1	2	3	4	5
	Frequency, in hertz (f_n)				
	0.2	0.5	0.8	1.0	1.2
	Damping (ξ_n)				
	0.01	0.0157	0.0214	0.0252	0.029
Level	Mode Shapes				
(1)	(2)	(3)	(4)	(5)	(6)
1	1.0	−0.8	0.6	−0.4	0.2
2	0.8	−0.2	−0.2	1.0	−0.6
3	0.6	0.4	−0.8	−0.2	1.0
4	0.4	1.0	0.4	−0.6	−0.8
5	0.2	0.6	1.0	0.8	0.4

[a]Building density = 12 lb/cu ft (192 kg/m^3).

using Eq. 5 at level 1 for a reduced velocity of 5. The results are listed in Table 2. The displacement, acceleration, and jerk components of response were also computed using Eq. 9. The results are listed in Table 3, in which the numbers in the parentheses represent the contribution of each mode as a percentage of the first mode. The building response in the second mode is significantly affected by the acceleration and jerk components. This trend, however, tends to diminish in the succeeding higher modes. The estimates

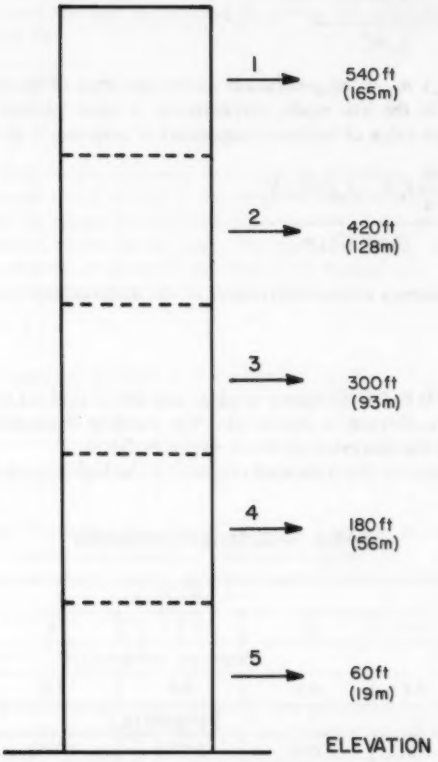

FIG. 1.—Kinematic Model

computed from Eq. 5 are lower than the values obtained from Eq. 9 for the second mode but tend to be higher for the succeeding modes (see Tables 2 and 3). This trend can be attributed to the changes in the value of α for the crosswind forcing function with an increase in the reduced frequency (2,3). For the example in this examination, the value of α near the first two frequencies is lower than 5.5; however for the third and higher frequencies, α tends to

exceed 5.5 value used in the present analysis. Therefore, by incorporating appropriate segmental values of α, one could achieve good estimates of response in the higher modes using Eq. 5, as compared with the detailed procedure. The use of the simple expression given by Eq. 5 for preliminary design purposes would allow early assessment of the structural requirements needed to resist

TABLE 2.—Contribution of Higher Modes/First Mode, as a percentage

Variable (1)	Mode (n) 2 (2)	3 (3)	4 (4)	5 (5)
Displacement	1.6	0.18	0.06	0.02
Acceleration	10.2	3.0	1.69	1.0
Jerk	25.4	12.0	8.4	4.9

TABLE 3.—Higher Modes Contribution, for Level 1[a]

Mode (n) 1 (1)	2 (2)	3 (3)	4 (4)	5 (5)
(a) RMS Displacement, in feet				
0.219	0.0042 (1.9)	0.0002 (0.09)	0.00004 (0.02)	0.000014 (0.006)
(b) RMS Acceleration, in feet per square second				
0.317	0.0412 (12.99)	0.0054 (1.7)	0.0017 (0.53)	0.00078 (0.024)
(c) RMS Jerk, in feet per cubic second				
0.401	0.1295 (32.3)	0.0272 (6.78)	0.011 (2.74)	0.0058 (1.45)

[a]Numbers in parentheses represent percentage of first mode.
Note: 1 ft = 0.305 m.

the oscillatory building response, and appraisal of the need for a more detailed multidegree-of-freedom analysis.

Conclusions

The results presented herein suggest that the strength and stability criteria for the design of a tall building can be sufficiently satisfied by a fundamental mode analysis since displacement response is completely dominated by the first mode. However, the assessment of serviceability and occupant comfort criteria requires the inclusion of higher modes of vibration in the dynamic analysis of tall buildings.

APPENDIX.—REFERENCES

1. Fujimoto, M., Ohkuma, T., and Amano, T., "Dynamic Model Tests of High-Rise Buildings in Wind Tunnel Flow and in Natural Winds," *Proceedings*, Fourth International Conference on Wind Effects on Buildings and Structures, 1975.
2. Kareem, A., "Wind-Excited Motion of Buildings," thesis presented to Colorado State University, at Fort Collins, Colo., in 1978, in partial fulfillment of the requirements for the degree of Doctor of Philosophy.
3. Kareem, A., "Determination of Fluctuating Wind Forces and Their Distribution on Buildings," presented at the October 27–31, 1980, ASCE, Annual Convention and Exposition, held at Hollywood, Florida.
4. Kareem, A., "Reduction of Wind-Excited Motion of High-Rise Buildings," *Third Engineering Mechanics Specialty Conference*, ASCE, 1979.
5. Simiu, E., "Equivalent Static Wind Loads for Tall Building Design," *Journal of the Structural Division*, ASCE, Vol. 102, No. ST4, Proc. Paper 12057, Apr., 1976, pp. 719–737.
6. Yokoo, Y., and Akiyama, H., "Lateral Vibration and Damping Due to Wind and Earthquake Effects," *Proceedings of the International Conference on Planning and Design of Tall Buildings*, Vol. 2, ASCE, 1972.

JOURNAL OF THE
STRUCTURAL DIVISION

DISCUSSION

Note.—This paper is part of the Journal of the Structural Division, Proceedings of the American Society of Civil Engineers, ©ASCE, Vol. 107, No. ST4, April, 1981. ISSN 0044-8001/81/0004-0709/$01.00.

Discussions

Discussions may be submitted on any Proceedings paper or technical note published in any *Journal* or on any paper presented at any Specialty Conference or other meeting, the *Proceedings* of which have been published by ASCE. Discussion of a paper/technical note is open to anyone who has significant comments or questions regarding the content of the paper/technical note. Discussions are accepted for a period of 4 months following the date of publication of a paper/technical note and they should be sent to the Manager of Technical and Professional Publications, ASCE, 345 East 47th Street, New York, N.Y. 10017. The discussion period may be extended by a written request from a discusser.

The original and three copies of the Discussion should be submitted on 8-1/2-in. (220-mm) by 11-in. (280-mm) white bond paper, typed double-spaced with wide margins. The length of a Discussion is restricted to two *Journal* pages (about four typewritten double-spaced pages of manuscript including figures and tables); the editors will delete matter extraneous to the subject under discussion. If a Discussion is over two pages long it will be returned for shortening. All Discussions will be reviewed by the editors and the Division's or Council's Publications Committees. In some cases, Discussions will be returned to discussers for rewriting, or they may be encouraged to submit a paper or technical note rather than a Discussion.

Standards for Discussions are the same as those for Proceedings Papers. A Discussion is subject to rejection if it contains matter readily found elsewhere, advocates special interests, is carelessly prepared, controverts established fact, is purely speculative, introduces personalities, or is foreign to the purposes of the Society. All Discussions should be written in the third person, and the discusser should use the term "the writer" when referring to himself. The author of the original paper/technical note is referred to as "the author."

Discussions have a specific format. The title of the original paper/technical note appears at the top of the first page with a superscript that corresponds to a footnote indicating the month, year, author(s), and number of the original paper/technical note. The discusser's full name should be indicated below the title (see Discussions herein as an example) together with his ASCE membership grade (if applicable).

The discusser's title, company affiliation, and business address should appear on the first page of the manuscript, along with the *Proceedings* paper number of the original paper/technical note, the date and name of the *Journal* in which it appeared, and the original author's name.

Note that the discusser's identification footnote should follow consecutively from the original paper/technical note. If the paper/technical note under discussion contained footnote numbers 1 and 2, the first Discussion would begin with footnote 3, and subsequent Discussions would continue in sequence.

Figures supplied by the discusser should be designated by letters, starting with A. This also applies separately to tables and references. In referring to a figure, table, or reference that appeared in the original paper/technical note use the same number used in the original.

It is suggested that potential discussers request a copy of the *ASCE Authors' Guide to the Publications of ASCE* for more detailed information on preparation and submission of manuscripts.

LIMIT DESIGN OF EXTENDED END-PLATE CONNECTIONS[a]

Closure by Allan P. Mann[5] and Linden J. Morris[6]

A difficulty that arises in comparing what at first appears to be similar research evidence from different sources is that there might in fact be significant differences in the purposes of the separate research projects. This in itself may be of little consequence provided other researchers and practicing engineers are made fully aware of the aims and limitations of the particular research projects being reviewed. For then the potential users of the research information can realistically evaluate what may be different recommendations for the same design problem. It is, therefore, important that the writers reiterate the aim of their own research and recommendations—which is to provide a design method for extended end-plate connections by which the beam moment reaches its plastic moment capacity while the connection sustains only *limited* distortions which neither inhibit the joint strength nor its rotation capacity. The recommendations are in the context of having four bolts grouped around the beam tension flange.

Connections proportioned by the writers' recommendations will have the capability of providing adequate rotation capacity while still sustaining the plastic moment capacity of the beam. This will allow the redistribution of moments in the frame as required for plastic analysis. On the other hand it appears, though not specifically stated in so many words, that the discusser bases his proposals on the performance of end-plates subject only to service loading, with an implied reserve of strength, i.e. 1.7 × maximum elastic conditions at working load. His test results (28) indicate that in most cases the plastic capacity of the beam was just reached. However, the M/M_p ratios achieved represent a necessary but insufficient requirement for connection design. Adequate rotation capacity is just as important, but very little evidence of the moment-rotation characteristics for the discusser's tests is given. Furthermore, it is stated (28) that the end-plate thicknesses produced by the discusser's method would frequently be accompanied by some reduction in connection rigidity and, under circumstances where deformations are critical, the influence of such increased flexibility may need to be reviewed. It should also be remembered that the discusser's research at present covers only the case where the column flange is stiff or adequately stiffened, though neither term is defined, whereas the writers' procedure covers other practical cases where the flange thickness is less than or approximately equal to the end-plate thickness. The research

[a]March, 1979, by Allan P. Mann and Linden J. Morris (Proc. Paper 14460).

[5]Research Fellow, Dept. of Engrg., Univ. of Manchester, Simon Engrg. Labs., Oxford Rd., Manchester, M139PL England.

[6]Lect., Dept. of Engrg., Univ. of Manchester, Simon Engrg. Labs., Oxford Rd., Manchester, M139PL England.

by Packer and Morris (14) showed that it was the combined deformation of the column flange and end-plate that governed whether or not the moment-rotation characteristic of a connection was satisfactory. Fig. 13 shows the effect of different column flange thicknesses on a connection's moment-rotation behavior. If only the attainment of strength was considered then it could be said that specimens *J*1, *J*2, and *J*3 were all satisfactory having achieved moment ratios, M/M_p, of 1.21, 1.09, and 0.98; however when rotation is also a requirement

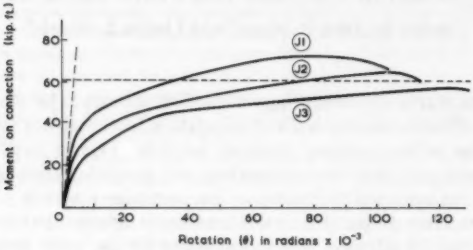

FIG. 13.—Moment-Rotation Characteristics of Connections *J*1 to *J*3

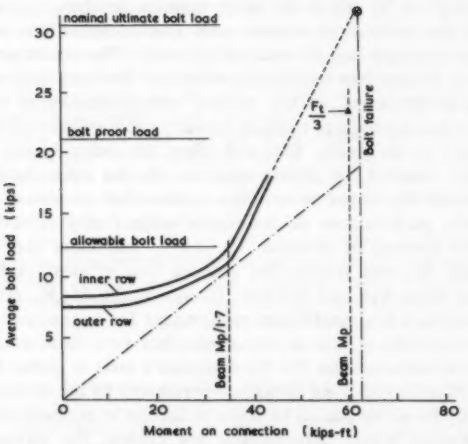

FIG. 14.—Average Tension Bolt Behavior for *J*5

then only *J*1 has produced the necessary behavior implicit in the writers' method. Similar curves can be produced for decreasing end-plate thicknesses. Indeed, the discusser refers to tests by Beall (22) which seem to confirm that the connection moment capacity decreased with a reduction in end-plate thickness. By reducing the column flange or end-plate thickness below that recommended, the effective "moment" capacity of the bolt group, and thus that of the connection, decreases for a given rotation requirement.

The discusser emphasizes that prying force is not a critical factor and need not be considered in design. Certainly the writers would agree with that statement if only allowable stress conditions were being considered. Figs. 14 and 15 support this argument as any prying action is nominal at working load level. But the writers would contend that the behavior of the bolts between service and limiting plastic loads has an important bearing on the design of the bolts even in allowable stress design where there is an implied reserve of strength of 1.7 × working load conditions. The diagrams show that there is a definite enhancement in the predicted direct bolt load ($F_t/4$) which if not allowed for in design could result in bolt failure. As Agerskov noted in a previous discussion (32) in the case of specimen *J5* (Fig. 14) the apparent prying force is some 70% in excess of the direct bolt load ($F_t/4$). But specimen *J5* represents the case when the connection does not in fact comply with the writers' recommendations, i.e., column flange requires stiffening. Specimen *J4* (Fig. 15) represents a stiffened

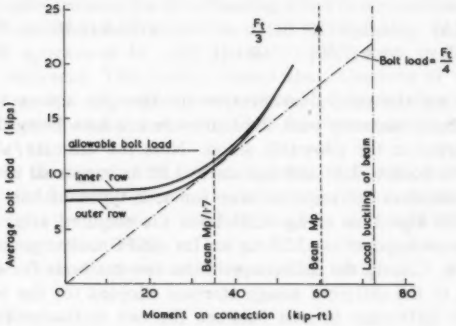

FIG. 15.—Average Tension Bolt Load Behavior for *J4*

J5 and accordingly the measured bolt forces show that the prying force had been reduced to about 33% the estimate of the prying force assumed in the design procedure. The value of 33% was chosen as representing a realistic upper limit on the increased bolt force due to prying action for connections designed by the writers' method. This results in a *simple* design rule for selecting bolt size.

The discusser agrees that the inner row of bolts will attract more of the direct load and concludes that these bolts could become somewhat overstressed at service loading. The discusser then suggests that the possible development of prying action (!) would be resisted wholly by the understressed outer row of bolts. This does not negate the problem of the overstressed inner bolts! Indeed, these inner bolts in a splice connection have been known to fail due to the flexibility of that portion of the end-plate that projects beyond the tension flange. As explained in the original paper, in the context of beam-to-column connections, the lower bolts carry a larger share of the direct force (F_t) but as prying action increases the upper bolts attract more of the prying force until at limiting plastic load level the total force (direct plus prying) in both

the inner and outer rows tend to become equal. This is demonstrated by the measured bolt forces indicated in Figs. 14 and 15 for the specimens *J5* and *J4*. Clearly, if the prying forces are taken into account in proportioning the bolts then there should be no problem with overstressing the bolts.

The problem of not having any bolt failures is that it is difficult to assess the reserve of strength left in the bolts, i.e., is it 1% or 101%? It is always helpful to the researcher to have the occasional bolt failure in order to judge the performance of the bolts. The discusser suggests that the reason for the apparent difference in the required bolt area is attributable to the neglect of prying forces, some 33%, in the discusser's method. Nevertheless, there are significant differences in the bolt characteristics and design loads specified by the national codes, which need to be examined, i.e.:

	Allowable stress	Proof stress	Yield stress	Ultimate stress
A325 (USA)	44.0 (1.00)	—	74.8 (1.70)	93.0 (2.11)
HSFG (UK)	35.4 (1.00)	60.1 (1.70)	—	85.9 (2.43)

These values are the equivalent stresses (in kips per square inch) based on the nominal shank diameter with the figures in brackets being the ratio of the appropriate stress to the allowable stress. Note the ultimate/allowable stress ratio for HSFG bolts is 2.43 and not about 2.00 as suggested by the discusser. If one now considers the required area for both types of bolt for a factored load of say 200 kips then using A325 bolts the required area would need to be 2.67 sq in. as opposed to 3.33 sq in. for HSFG bolts, giving a difference in area of 25%. Clearly the difference in the two methods for designing bolts is mainly due to the different design stresses adopted for the bolts producing only some 8% difference in area between the two methods. The 33% prying force advocated by the writers is absorbed by the inherent reserve of strength (43%) between proof and ultimate stresses of the HSFG bolt leaving an additional margin of safety against instant bolt fracture at plastic limit load level.

The discusser also comments that his method gives end-plate thicknesses which are approx 90% of the values obtained from the writers' recommendations. In Ref. 28 the discusser compares the end-plate thicknesses, determined for different design criteria, for 36-ksi steel, knowing the A_f/A_w ratio of the beam sections. In the range of universal beam sections, equivalent to WF sections, for which the writers advocate the use of their method the modified split-tee method virtually gives the same values as the split-tee method. Therefore, a direct comparison can be made between the split-tee method and the tee-stub model used by the writers. The difference in the end-plate thicknesses can be accounted for by the definition of the effective span p_e. The discusser achieves a smaller value of p_e by assuming the application of the bolt load to be $D/4$ nearer to the beam web, he justifies this as a result of extensive finite analyses (29). The location of the bolt load will always be a debatable point. Some United Kingdom commercial interests advocate that the value of $D/4$ should be $(3/4)\ D$ or even D because it results in thinner end-plates and presumably lower costs. Unfortunately such thinner end-plates carry the penalty of increased deformations within the connection and the subsequent loss of moment capacity

as stated earlier. Packer and Morris (14) illustrated that the local influence of the bolt head can be misleading when considering the general flexural behavior of a plate element. The difference in end-plate thicknesses approximates to about a 5% drop in the "moment" capacity of the bolts.

By using smaller bolts and thinner end-plates there would be a tendency for increased connection deformations causing relaxation on the tension side of the beam and a lowering of the moment capacity of the bolt group. This is confirmed by the discusser who states that when even thinner end-plates than those proposed by the modified split-tee methods are used in tests, then the moment capacity reduces significantly. Such a reduction in moment capacity for a decrease in end-plate thickness was illustrated by the writers in a recent paper (33) in connection with lack of fit in flush end-plate joints.

Incidentally the test connections used by the discusser have smaller cross centers of holes than would be the normal practical dimension used in the United Kingdom (about $5D$). This automatically results in thinner end-plates becoming acceptable because the cross bending effect in the end-plates is reduced. When the two methods are examined in detail for the range of beam section indicated, there appears to be only about 10% difference in both bolt area and end-plate thickness. This really reflects the objectives of the individual research programs, i.e., the discusser is interested in the elastic capacity of a beam while the writers have concentrated on the plastic capacity with adequate rotation.

As regards the discusser's last two paragraphs concerning current work the writers cannot comment on the rather nebulous description of the work, except to say that it might be unrealistic to assume a fully *active* yield line extending down to the compression flange. The writers await the discusser's findings and will comment in more detail at the appropriate time.

Appendix.—References

32. Agerskov, H., "Analysis of Bolted Connections Subject to Prying" *Journal of the Structural Division*, ASCE, Vol. 105, No. ST9, Proc. Paper 14795, Sept., 1979, pp. 1851–1855.
33. Mann, A. P., and Morris, L. J., "Lack of Fit in End-Plate Connections" presented at the April 14–18, 1980, ASCE Convention and Exposition, held at Portland, Oregon (Preprint 80-179).

DOME EFFECT IN RC SLABS: RIGID-PLASTIC ANALYSIS[a]

Discussion by Paul Regan[2]

The writer read the paper with considerable interest and it seems that in practical terms the central issue is the effect of unloading (or strain reduction) on the stress block in the concrete compression zone.

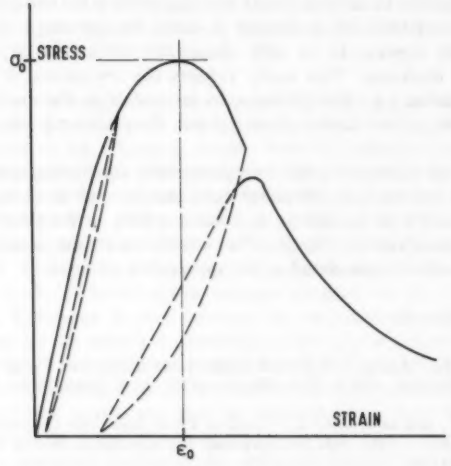

FIG. 7.—Typical Stress-Strain Relationship for Concrete

It is of course true that, when the position of the neutral axis moves towards the extreme compressed fiber material near the neutral axis undergoes a reduction of strain. The same thing occurs in an ordinary under-reinforced beam once the steel yields and, in this case, seems not to worry anyone. What is not clear is whether the strain reduction has any significant effect on the compressive force and it seems that this question is confused by the application of rigid-plastic theory.

Fig. 7 shows a typical stress-strain relationship for concrete and includes two unloading lines: one from a stage before the peak stress and one from

[a]June, 1980, by Mikael W. Braestrup (Proc. Paper 15501).

[2]Reader in Civ. Engrg., The Polytechnic of Central London, 35 Marylebone Rd., London NW1 5LS, England.

beyond it. Fig. 8 presents the strain "histories" of material at various levels in a compression zone whose depth is halved while the peak strain doubles in a regime in which the product "peak strain × depth" remains constant.

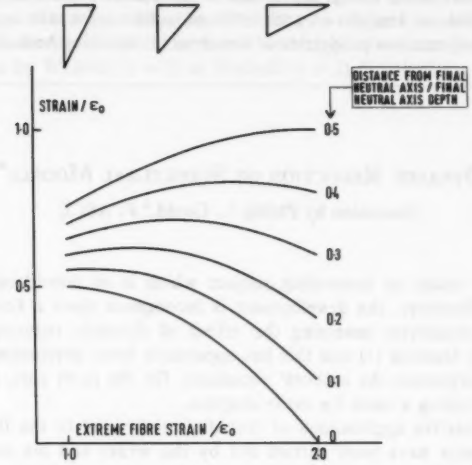

FIG. 8.—Development of Strains in Compression Zone

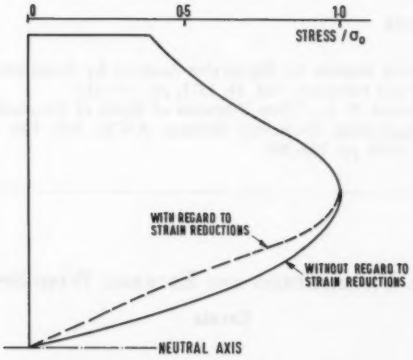

FIG. 9.—Final Stress Distribution in Compression Zone

Finally Fig. 9 shows the stress distributions for this compression zone at the final stage as derived on the basis of Figs. 7 and 8 and also as obtained directly from the envelope of Fig. 7 without regard to strain reductions. The differences between the two lines can be seen to be small. The reason is that the area where there is any appreciable strain decrement is one in which the strains have never been particularly high.

While the foregoing example is an arbitrary one it would seem to represent the essential features of arching action rather better than a rigid-plastic approach according to which yield of the concrete occurs over half the depth of the member without there being any strain or deflection. The writer thinks that to be successful, an analysis of arch or dome action must take a realistic view of the load/deformation properties of concrete in the rising branch.

Dynamic Reduction of Structural Models[a]

Discussion by Phillip L. Gould,[2] F. ASCE

The author treats an interesting subject which is of considerable practical importance. However, the development is incomplete since a firm theoretical basis for quantitatively assessing the effect of dynamic reduction has been established by Geradin (5) and this has apparently been overlooked. The latter reference incorporates the authors' equations, for the most part, and goes far beyond in providing a basis for error analysis.

Some quantitative applications of Geradin's technique to the finite element analysis of shells have been carried out by the writer and his co-workers. It was shown that the use of high-order approximations can detrimentally effect the calculation of eigenvalues when kinematic condensation is employed.

Appendix.—References

5. Geradin, M., "Error Bounds for Eigenvalue Analysis by Elimination of Variables," *Journal of Sound and Vibration*, Vol. 19, 1971, pp. 111–132.
6. Sen, S. K. and Gould, P. L., "Free Vibration of Shells of Revolution Using FEM," *Journal of the Engineering Mechanics Division*, ASCE, Vol. 100, No. EM2, Proc. Paper 9629, Apr., 1974, pp. 283–303.

Weibull Distributions and Extreme Wind Speeds[b]

Errata

The following corrections should be made in the original paper:

Page 2366, Eq. 3: should read $[-\ln (1 - F)]$ instead of $[-\ln (1 - F)$

Page 2371, Table 2: the heading "Wind Speed" of Col. 7 and the heading

[a]October, 1980, by Charles A. Miller (Proc. Paper 15775).

[2]Prof. and Chmn., Dept. of Civ. Engrg., School of Engrg. and Applied Science, Washington Univ., Campus Box 1130, St. Louis, Mo. 63130.

[b]December, 1980, by Emil Simiu and James J. Filliben (Proc. Paper 15909).

"Data Sets" of Col. 8 should be deleted; Cols. 7 and 8 should have the common heading "Wind Speed Data Sets."

Page 2371, Table 2, Cols. 4, 6, and 8: the numbers in the first, third, fifth, and seventh lines should be deleted; the numbers in the second and sixth lines are percentages of sets best fitted by Weibull ($\gamma = 1$) or Extreme Value Type I distributions; the numbers in the fourth and eighth lines are percentages of sets best fitted by Weibull ($\gamma = 2$) or Weibull ($\gamma > 2$) distributions.

TECHNICAL PAPERS

Original papers should be submitted in triplicate to the Manager of Technical and Professional Publications, ASCE, 345 East 47th Street, New York, N.Y. 10017. Authors must indicate the Technical Division or Council, Technical Committee, Subcommittee, and Task Committee (if any) to which the paper should be referred. Those who are planning to submit material will expedite the review and publication procedures by complying with the following basic requirements:

1. Titles must have a length not exceeding 50 characters and spaces.

2. The manuscript (an original ribbon copy and two duplicate copies) should be double-spaced on one side of 8-1/2-in. (220-mm) by 11-in. (280-mm) paper. Three copies of all figures and tables must be included.

3. Generally, the maximum length of a paper is 10,000 word-equivalents. As an *approximation*, each full manuscript page of text, tables or figures is the equivalent of 300 words. If a particular subject cannot be adequately presented within the 10,000-word limit, the paper should be accompanied by a rationale for the overlength. This will permit rapid review and approval by the Division or Council Publications and Executive Committees and the Society's Committee on Publications. Valuable contributions to the Society's publications are not intended to be discouraged by this procedure.

4. The author's full name, Society membership grade, and a footnote stating present employment must appear on the first page of the paper. Authors need not be Society members.

5. All mathematics must be typewritten and special symbols must be identified properly. The letter symbols used should be defined where they first appear, in figures, tables, or text, and arranged alphabetically in an appendix at the end of the paper titled Appendix.—Notation.

6. Standard definitions and symbols should be used. Reference should be made to the lists published by the American National Standards Institute and to the *Authors' Guide to the Publications of ASCE*.

7. Figures should be drawn in black ink, at a size that, with a 50% reduction, would have a published width in the *Journals* of from 3 in. (76 mm) to 4-1/2 in. (110 mm). The lettering must be legible at the reduced size. Photographs should be submitted as glossy prints. Explanations and descriptions must be placed in text rather than within the figure.

8. Tables should be typed (an original ribbon copy and two duplicates) on one side of 8-1/2-in. (220-mm) by 11-in. (280-mm) paper. An explanation of each table must appear in the text.

9. References cited in text should be arranged in alphabetical order in an appendix at the end of the paper, or preceding the Appendix.—Notation, as an Appendix.—References.

10. A list of key words and an information retrieval abstract of 175 words should be provided with each paper.

11. A summary of approximately 40 words must accompany the paper.

12. A set of conclusions must end the paper.

13. Dual units, i.e., U.S. Customary followed by SI (International System) units in parentheses, should be used throughout the paper.

14. A practical applications section should be included also, if appropriate.